UNIVERSITA' DEGLI STUDI DI PADOVA

DIPARTIMENTO DI PEDIATRIA

SCUOLA DI DOTTORATO DI RICERCA IN MEDICINA DELLO SVILUPPO E SCIENZE DELLA PROGRAMMAZIONE
INDIRIZZO EMATOONCOLOGIA E IMMUNOLOGIA
XXIII CICLO

TITOLO TESI

2-DEOXYGLUCOSE EFFECTS AND CANCER STEM CELL DISTRIBUTION ARE AFFECTED BY HYPOXIA IN GLIOBLASTOMA MULTIFORME

Direttore della Scuola : Ch.mo Prof. Giuseppe Basso

Supervisore : Dr. Francesca Pistollato

Dottorando: Sara Abbadi

31 Gennaio 2011

To my beloved uncle

Table of Contents

SUMMARY

Glioblastoma multiforme (GBM) is the highest grade glioma and the most common and aggressive form of primary adult brain tumors, classified as grade IV astrocytoma. The term "multiforme" in GBM describes the heterogeneous nature of these tumors, also characterized by diffuse infiltration into surrounding tissue. These features prevent complete surgical resection. Despite the use of surgery, radiation and chemotherapy, the median survival for patients with GBM is only 14.6 months. The poor prognosis for GBM patients is due to a high incidence of recurrence and limited responses to approved therapies [1]. Treatment-refractory property is thought to be due to a subpopulation of cells, called brain tumor stem cells or brain tumor initiating cells [2]. To overcome this problem, strategies combining chemotherapy and drugs that target different mechanism of action are under current research [3]. One of the most used oral alkylating agents for the treatment of GBM is temozolomide (TMZ). However, controversial data indicate that although TMZ seems to induce a dose- and time-dependent decline of the tumor stem cell subpopulation [4], other works indicate that TMZ does not seem to affect stem cells [5], which are considered the most chemoresistant cell population in the tumor bulk [6-9]. Thus, it is becoming pivotal to identify the phenotypic features of the resistant tumor cells and define their localization in the GBM tumor mass in order to distinguish and more effectively target them.

Structural and functional integrity of brain function profoundly depends on a regular oxygen and glucose supply. Glucose metabolism in tumor cells occurs mainly through anaerobic glycolysis, even when tumor-derived cells are cultured under normoxic conditions, indicating that pseudo-anaerobic glycolysis is constitutively upregulated through stable genetic changes [10]. This phenomenon was first reported by Otto Heinrich Warburg in the 1920s [11]. Following Warburg's initial observation, the interest of the scientific community toward the metabolic property of cancer cells, varied in the course of the years, especially after the widespread of the newer molecular techniques. The application of the imaging technique positron emission tomography (PET) using the glucose analogue tracer ^{18}fluorodeoxyglucose (fdG) showed that most primary and metastatic human cancers had significantly increased glucose uptake, which is largely dependent on the rate of glycolysis, indicating that it continues to confer a proliferative

advantage for the tumor [12-14]. Control over glycolytic flux primarily resides at the transporter and phosphorylation steps [15-17], although it can also be regulated at many downstream steps in the glycolytic pathway [18, 19]. The proliferative advantage of the glycolytic phenotype is not immediately apparent, since anaerobic metabolism of glucose produces only 2 ATP per glucose, whereas complete oxidation produces 38 ATP per glucose. Moreover, the metabolic products of glycolysis, such as hydrogen ions (H^+), causes acidification of the extracellular space, which might result in cellular toxicity [20]. So why do tumor cells undergo glycolysis which is inefficient and potentially toxic? It has been suggested that cancer cells up regulated glycolysis is neither random nor accidental. Rather, it represents an evolved solution to common environmental growth constraints during carcinogenesis [10]. Tumors, particularly highly proliferative glioblastomas, characterized by a hypoxic microenvironment, modify their vascular niches in order to maintain the cancer stem cell pool [21]. These data provide further evidence that cancer development is not only a process that involve epigenetic or genetic events, but that also depends on the microenvironment. One of the aspects we investigated is the role of the hypoxic region, a common feature of solid tumors, in the maintenance of the brain tumor mass. Oxygen is an essential regulator of cellular metabolism, survival and proliferation. The oxygenation level within a tumor is not consistent and behaves in a cycling nature [22, 23]. This phenomenon is a result of several tumor characteristics such as chaotic vasculature, poor oxygen diffusion across the expanding tumor and irregular blood flow leading to an enhanced metastatic potential of the tumor [24]. Under these conditions a signaling pathway involving a key oxygen response regulator termed the hypoxia-inducible factor 1α (HIF1α) is switched on. HIF1α is a transcription factor that, in hypoxia, drives the induction or repression of a myriad of genes controlling multiple cell functions such as angiogenesis, metabolism, invasion/metastasis and apoptosis/survival [25]. Thus, the level of oxygen in a tumor cell dictates their molecular response through the modulation of gene expression. For this research project we sought to define how microenvironmental and intratumoral hypoxia affects cell metabolism and cancer stem cell distribution in GBM. Particularly, in the first part of this study we investigated the effects mediated by 2-deoxyglucose (2-DG), a glucose analogue and a very well described competitive inhibitor of glycolysis on primary GBM-derived cells maintained under hypoxia. In the second part, by exploiting image guided surgery to sample multiple intratumoral areas, in collaboration with the neurosurgery department, we identified the presence of a cellular

heterogeneity in correlation to the oxygen tension gradient within the GBM mass. These results led us to define a novel concentric model of GBM stem cell niche.

SOMMARIO

Il glioblastoma multiforme (GBM) è il più alto grado di glioma e la forma più comune e aggressiva tra i tumori primari cerebrali nell'adulto, classificato come astrocitoma di grado IV. Il termine "multiforme" in GBM descrive la natura eterogenea di questi tumori, anche caratterizzata da diffusa infiltrazione nel tessuto circostante. Queste caratteristiche rendono l'asportazione completa del tumore impossibile. Nonostante l'uso della chirurgia, la radioterapia e la chemioterapia, la sopravvivenza media per i pazienti con GBM è di soli 14,6 mesi. La bassa sopravvivenza dei pazienti colpiti da questo tumore è dovuta ad una elevata incidenza di recidiva e scarsa risposta alle terapie convenzionali [1]. Si pensa che la refrattarietà al trattamento sia dovuta ad una sottopopolazione di cellule, chiamate cellule staminali tumorali o cellule iniziatrici del tumore cerebrale [2]. Per superare questo problema, attualmente sono in fase di ricerca diverse strategie che combinano la chemioterapia con farmaci che colpiscono diversi meccanismi di azione [3]. Uno degli agenti alchilanti più utilizzati nel trattamento del glioblastoma multiforme è il temozolomide (TMZ). Tuttavia, a questo riguardo esistono dati controversi: alcuni studi hanno dimostrato, infatti, il trattamento con TMZ sembra indurre una diminuzione delle cellule staminali del tumore in una maniera dose-e tempo-dipendente [4], al contrario altri lavori hanno dimostrato che il TMZ non sembra influenzare le cellule staminali [5]. Per questa ragione queste cellule vengono considerate le più chemio-resistenti all'interno della massa tumorale [6-9]. Quindi sta diventando di fondamentale importanza identificare le caratteristiche fenotipiche delle cellule tumorali resistenti e definire la loro localizzazione all'interno della massa tumorale, al fine di distinguerle dalla controparte sana ed eliminarle più efficacemente.

L'integrità strutturale e funzionale delle funzioni cerebrali dipende profondamente da un normale apporto di ossigeno e glucosio. Il glucosio nelle cellule tumorali viene metabolizzato principalmente attraverso la glicolisi anaerobica e questo processo si mantiene anche quando le cellule tumorali vengono messe in coltura in condizioni normossiche. Questo indica che la glicolisi pseudo-anaerobica è costitutivamente upregolata attraverso mutazioni genetiche [10]. Tale fenomeno è stato descritto per la prima volta da Otto Heinrich Warburg nel 1920 [11]. A seguito di questa iniziale osservazione, l'interesse della comunità scientifica verso le proprietà metaboliche delle cellule tumorali è stata variabile nel corso degli anni, soprattutto dopo la

diffusione delle nuove tecniche molecolari. L'applicazione della tecnica PET (Positron Emission Tomography), che utilizza il tracciante analogo del glucosio ^{18}fluorodeossiglucosio (FDG), ha dimostrato un notevole aumento nell'assorbimento del glucosio, che dipende in larga misura dal tasso di glicolisi, nella maggior parte dei tumori primari e metastatici umani. Questo risultato sta ad indicare che la glicolisi continua a conferire un vantaggio proliferativo per il tumore [12-14]. Il controllo sul flusso glicolitico risiede principalmente a livello del trasportatore del glucosio e nei primi passaggi di fosforilazione [15-17], ma può anche essere regolato in molte fasi più a valle della via glicolitica [18, 19]. Il vantaggio proliferativo del fenotipo glicolitico non è immediatamente evidente, poiché il metabolismo anaerobico del glucosio produce solo 2 ATP per glucosio, mentre l'ossidazione completa produce 38 ATP per glucosio. Inoltre, i prodotti metabolici della glicolisi, come ad esempio gli ioni idrogeno (H^+), provocano l'acidificazione dello spazio extracellulare, cosa che potrebbe comportare tossicità cellulare [20]. Allora perché le cellule tumorali utilizzano preferibilmente la glicolisi, che è inefficiente e potenzialmente tossica? È stato suggerito che l'upregolazione della via glicolitica, da parte delle cellule tumorali, non sia né casuale né accidentale. Piuttosto, essa rappresenta una soluzione evolutasi durante lo sviluppo del tumore in risposta a vincoli microambientali [10]. I tumori altamente proliferativi, come ad esempio il glioblastomi, sono caratterizzati da un microambiente ipossico. Le cellule tumorali, presenti in questo microambiente ipossico, modificano le loro nicchie vascolari al fine di mantenere il pool delle cellule staminali tumorali [21]. Questi dati indicano che lo sviluppo del cancro non è solo un processo che coinvolge solamente eventi epigenetici o genetici, ma dipende anche dal microambiente.

Uno degli aspetti che stiamo indagando è il ruolo dell'ipossia, una caratteristica comune dei tumori solidi, nel mantenimento della massa tumorale cerebrale. L'ossigeno è un regolatore fondamentale del metabolismo cellulare, la sopravvivenza e la proliferazione. Il livello di ossigenazione all'interno del tumore non è costante [22, 23]. Questo fenomeno è il risultato di diverse caratteristiche del tumore, come la presenza di una rete vascolare aberrante, una povera diffusione dell'ossigeno attraverso il tumore in espansione e un irregolare flusso di sangue. Tutti questi fattori aumentano le capacità metastatiche del tumore [24]. In queste condizioni ipossiche viene attivato un pathway che coinvolge un regolatore chiave della risposta ai livelli di ossigeno presenti nella cellula, chiamato hypoxia inducible factor 1α (HIF1α). HIF1α è un fattore di trascrizione che, in presenza di ipossia, promuove l'induzione o la repressione di una miriade di

geni che controllano funzioni cellulari multiple, come l'angiogenesi, il metabolismo, l'invasione/metastasi e l'apoptosi/sopravvivenza [25]. Pertanto, il livello di ossigeno nelle cellule tumorali controlla particolari risposte cellulari consequenzialmente alla modulazione dell'espressione genica.

Durante questo progetto di ricerca abbiamo cercato di definire come l'ipossia microambientale e intratumorale influenzasse il metabolismo e la distribuzione delle cellule staminali tumorali nel GBM. In particolare, nella prima parte dello studio abbiamo analizzato gli effetti mediati dal 2-deoxyglucosio (2-DG), un analogo del glucosio e noto inibitore competitivo della glicolisi su cellule primarie di GBM mantenute in ipossia. Nella seconda parte, mediante l'uso della chirurgia guidata per immagini, grazie alla collaborazione con la neurochirurgia di Padova, abbiamo campionato regioni diverse intratumorali ed abbiamo identificato la presenza di una certa eterogeneità cellulare in correlazione al gradiente di ossigeno all'interno della massa dei GBM. Questi risultati ci hanno permesso di definire un nuovo modello concentrico di nicchia delle cellule staminali del GBM.

INTRODUCTION

Brain tumors and particularly glioblastoma multiforme (GBM) are highly proliferative tumors. According to their degree of malignancy and morphological features gliomas have been classified into four grades by the World Health Organization (WHO). Low Grade Gliomas (I and II) are characterized by the presence of well differentiated cells ; they bear histological similarity to astrocytes and oligodendrocytes. High Grade Glioma (III and IV) (HGG) cells are more anaplastic, resembling immature astrocytes, or oligodendrocytes, or a mixture of both [26]. Glioblastoma Multiforme (GBM) is a grade IV tumor and the most invasive and aggressive of HGGs. Hallmark features of this tumor are: uncontrolled cellular proliferation, diffuse infiltration, propensity for necrosis, robust angiogenesis, intense resistance to apoptosis and genomic instability. Grade IV tumors are highly chemo- and radioresistance leading to tumor recurrence within few month post surgery, with a median survival duration after diagnosis that varies from 6 month to 2 years. This is largely due to the inability of current treatment strategies to hamper the highly invasive nature of this disease [26].

It has been recently shown that solid tumors, amongst which also GBM, are characterized by the presence of a hypoxic microenvironment. Oxygen (O_2) is an essential nutrient that serves as a key substrate in cellular metabolism and bioenergetics. Oxygen tensions present in the adult tissues are considerably different from the inhaled ambient oxygen tensions of 21% (160 mm Hg). It decreases after it enters the lungs and as it travels in the blood throughout the body. By the time it reaches organs and tissues, the partial pressure oxygen (pO_2) levels have dropped to 2%–9% (14–65 mm Hg) [27]. In tumors, insufficient oxygen availability or hypoxia is a result of a disorganized vasculature and inadequate blood supply. In order to cope with this stress, evolutionarily conserved responses are engaged and key genes involving cell survival and angiogenesis are upregulated [28]. Recent literature shows that this hypoxic microenvironment correlates with tumor aggressiveness and progression through multiple mechanisms including modifying angiogenesis, metabolic switch, invasion [29-31] and over-activity of hypoxia inducible factor-1α (HIF-1α) [32] which is implicated in the maintenance of a de-differentiated (i.e. stem) tumor cell phenotype [31].

Hypoxia-inducible factors (HIFs) are transcription factors that belong to the subfamily of the basic-helix-loop-helix (bHLH) family of transcription factors. HIF-1 is a heterodimer composed of an alpha and a beta subunit. While the alpha subunit responds to changes in oxygen availability in the cellular microenvironment, the beta subunit is a constitutively-expressed aryl hydrocarbon receptor nuclear translocator, known also as ARNT. In the presence of oxygen HIF-1α is hydroxylated on proline 402 and 564 by three specific oxygen-dependent proline-hydroxylases (PHD 1–3) and sent to degradation by the proteasome. The presence of iron, oxygen and 2-oxoglutarate are necessary for full enzymatic hydroxylation of HIF-1α by the PHDs [33] (Figure1).

HIF-1α has also been found to contribute to a differentiation defect in malignant gliomas [34], even following exogenous bone morphogenetic protein2 (BMP2) treatment, known to induce glial commitment in GBM [35-37]. These evidences shed new light on the differentiation therapy of solid tumors by HIF-1α targeting. Hypoxia has a role in normal physiological responses, such as carotid body growth and generation of new neural crest derived glomus cells [38], and angiogenesis [39]. It is implicated in the regulation of several developmentally important signaling pathways, such as Notch [40] and BMP pathways [36], as well as glucose metabolism [41]. Moreover, hypoxia, through HIF1, alters cancer cells metabolism by increasing tumor anaerobic glycolysis and reducing mitochondrial activity [11] (Figure 2).

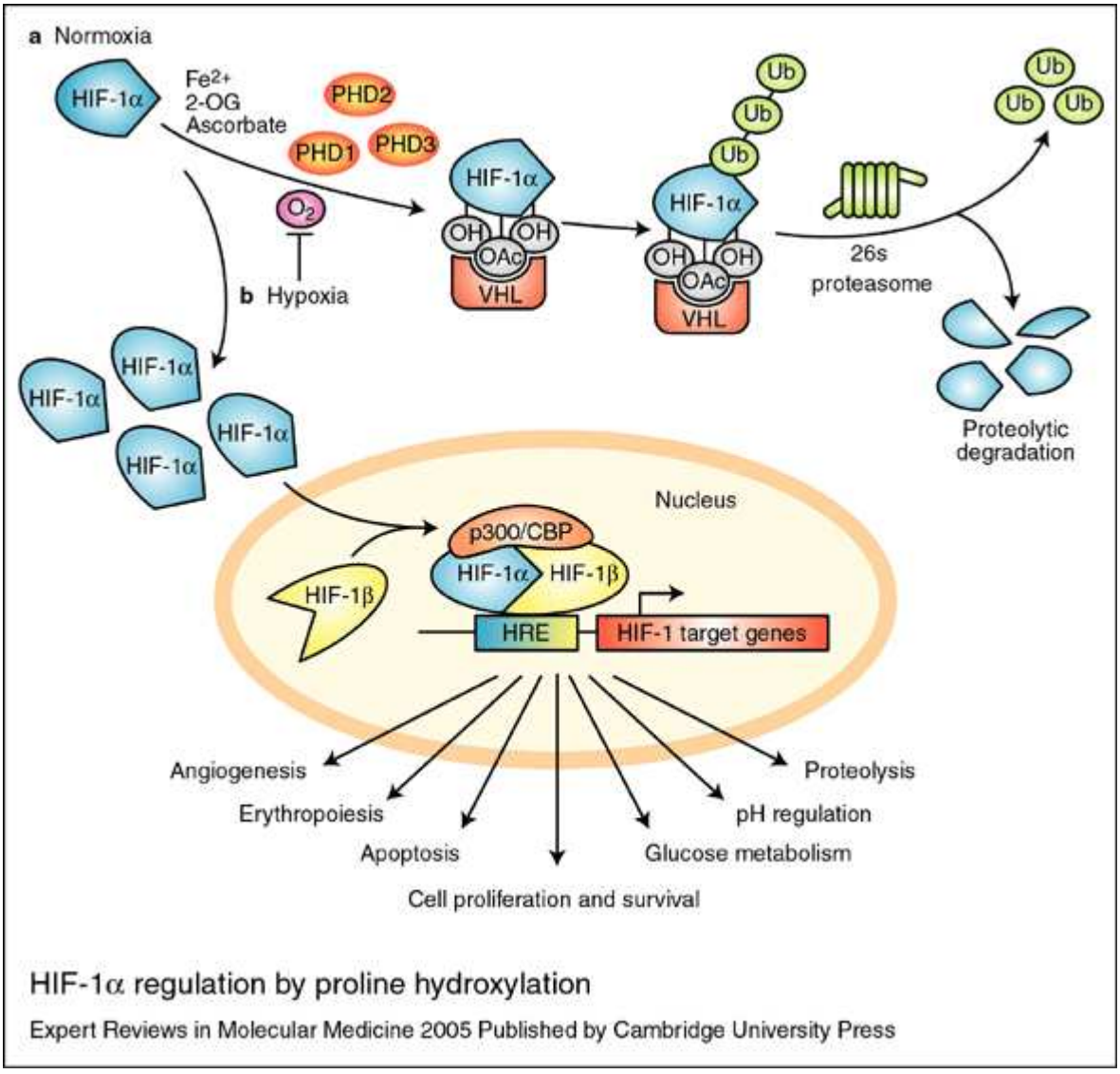

Figure 1. HIF-1α regulation by proline hydroxylation. (a) In normoxia, hypoxia-inducible factor (HIF)-1α is hydroxylated by proline hydroxylases (PHD1, 2 and 3) in the presence of O_2, Fe^{2+}, 2-oxoglutarate (2-OG) and ascorbate. Hydroxylated HIF-1α (OH) is recognised by pVHL (the product of the von Hippel–Lindau tumor suppressor gene), which, together with a multisubunit ubiquitin ligase complex, tags HIF-1α with polyubiquitin; this allows recognition by the proteasome and subsequent degradation. Acetylation of HIF-1α (OAc) also promotes pVHL binding. (b) In response to hypoxia, proline hydroxylation is inhibited. VHL is no longer able to bind and target HIF-1α for proteasomal degradation, which leads to HIF-1α accumulation and translocation to the nucleus. There, HIF-1α dimerises with HIF-1β, binds to hypoxia-response elements (HREs) within the promoters of target genes and recruits transcriptional co-activators such as p300/CBP for full transcriptional activity. A range of cell functions are regulated by the target genes, as indicated. Abbreviation: CBP, CREB-binding protein; Ub, ubiquitin. (Figure taken from, Veronica A. Carroll and Margaret Ashcroft. HIF-1α regulation by proline hydroxylation. Accession information: 2005, Vol. 7; Issue 6; 15 April).

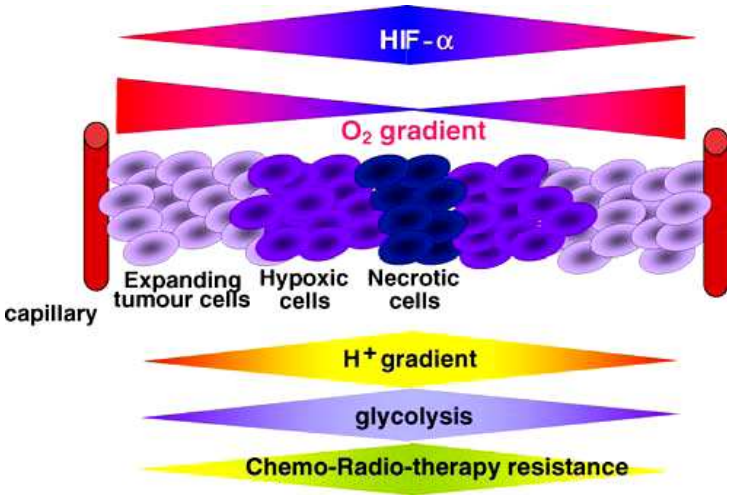

Figure 2. The characteristics of a hypoxic tumor mass. Blood capillaries carry oxygen to tissues, but since oxygen has a diffusion limit, its concentration decreases as the distance from capillaries increases. Macroscopic examination of solid tumors reveals the presence of expanding tumor cells in proximity to capillaries and a central region of necrotic cells. This gradient of cell viability parallels that of a decreasing gradient of oxygen, which is accompanied by an increase in HIF-1α levels, a decrease in the extracellular pH and an increase in the resistance to radio- and chemo-therapy. (Figure taken from, M. Christiane Brahimi-Horn & Johanna Chiche & Jacques Pouysségur. Hypoxia and cancer. 2007, J Mol Med).

Particularly, succinate dehydrogenase (SDH), the enzyme complex II bound to the inner mitochondrial membrane that converts succinate to fumarate via FAD reduction to FADH2, has been found inactive in some solid tumors [42]. This has been described as a key event leading to the accumulation of intra-cytoplasmic succinate and reactive oxygen species (ROS) causative of the ‘‘pseudo-hypoxic’’ effect, a major tumor-related hallmark, characterized by the activation of HIF even under normoxia [43, 44]. As intratumoral hypoxia increases glycolytic activity in many types of cancer, including GBM, limiting glucose uptake or glucose metabolism is a promising therapeutic approach for cancer treatment [45, 46] in order to reduce tumor growth as shown in animal models [45].

The hyper glycolytic phenotype of cancer cells was first described by Otto Heinrich Warburg in the 1920s. Warburg's work had a significant and lasting input on thinking about the biochemistry of tumors, awarding him in 1931 with the Nobel Prize in Physiology and Medicine for his discovery of the nature and mode of action of the respiratory enzyme. The concept that cancer cells switch to glycolysis has become widely accepted by the scientific community, even if it is not seen as the cause of cancer. This phenomenon is now known as the Warburg effect, where cancer cells shift their metabolism from oxidative to glycolytic (Figure3). However, the proliferative advantage of the glycolytic phenotype is not immediately apparent. Indeed, anaerobic metabolism of glucose produces only 2 ATP per glucose, whereas complete oxidation

produces 38 ATP per glucose. Moreover, the metabolic products of glycolysis, such as hydrogen ions (H^+), causes acidification of the extracellular space, which might result in cellular toxicity [20]. So why do tumor cells undergo glycolysis which is inefficient and potentially toxic? One potential explanation for the use of glycolysis by tumor cells and more in general by all proliferating cells, is that glycolysis facilitates the uptake and incorporation of nutrients into the biomass (e.g., nucleotides, amino acids, and lipids) needed to produce a new cell [47]. Moreover, many glycolytic enzymes have direct anti-apoptotic actions [48]; lactic acid promotes angiogenesis and interstitial matrix breakdown, facilitating metastasis [10]; and decreased mitochondrial function is associated with inhibition of mitochondrial apoptosis [49].

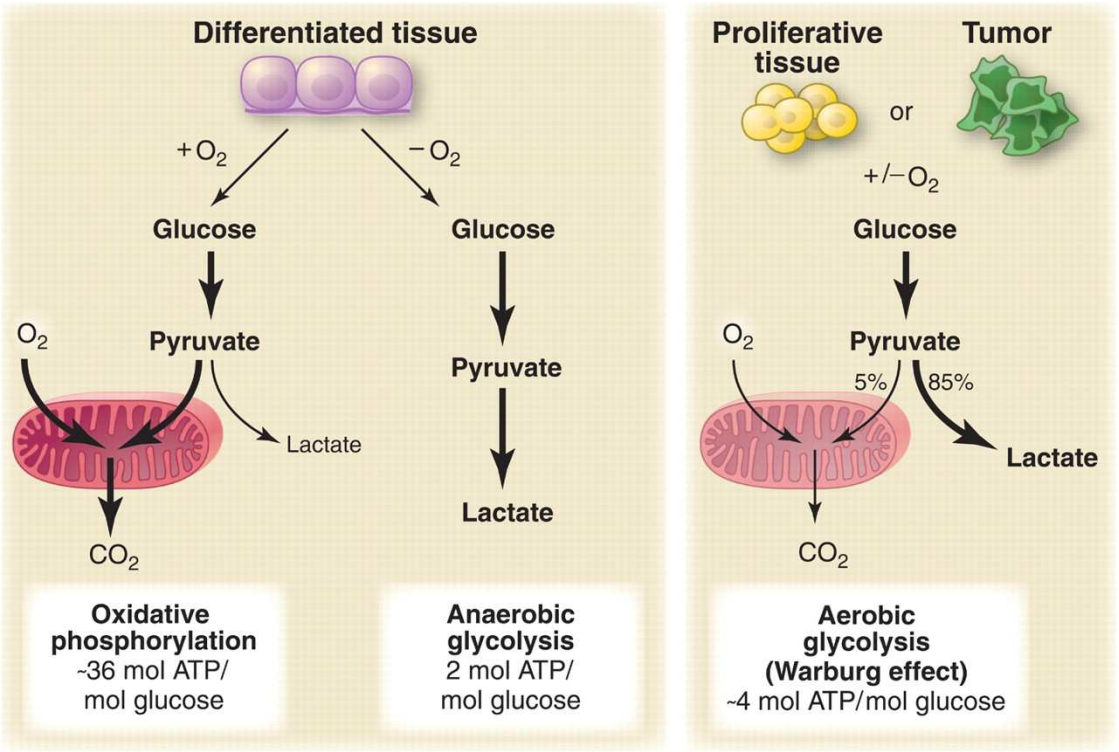

Figure 3. Schematic representation of the differences between oxidative phosphorylation, anaerobic glycolysis, and aerobic glycolysis (Warburg effect). In the presence of oxygen, nonproliferating (differentiated) tissues first metabolize glucose to pyruvate via glycolysis and then completely oxidize most of that pyruvate in the mitochondria to CO_2 during the process of oxidative phosphorylation. Because oxygen is required as the final electron acceptor to completely oxidize the glucose, oxygen is essential for this process. When oxygen is limiting, cells can redirect the pyruvate generated by glycolysis away from mitochondrial oxidative phosphorylation by generating lactate (anaerobic glycolysis). This generation of lactate during anaerobic glycolysis allows glycolysis to continue (by cycling NADH back to NAD^+), but results in minimal ATP production when compared with oxidative phosphorylation. Warburg observed that cancer cells tend to convert most glucose to lactate regardless of whether oxygen is present (aerobic glycolysis). This property is shared by normal proliferative tissues. Mitochondria remain functional and some oxidative phosphorylation continues in both cancer cells and normal proliferating cells. (Figure taken from, Matthew G. Vander Heiden, Lewis C. Cantley, Craig B. Thompson. Understanding the Warburg Effect: The Metabolic Requirements of Cell Proliferation. Science 2009, Vol. 324 22 MAY).

In addition, numerous key enzymes in glycolysis, oxidative phosphorylation, the pentose phosphate pathway, and glutamine metabolism are directly controlled by signaling pathways, involving known oncogenes and tumor suppressor genes. Activation of growth factor receptors leads to both tyrosine kinase signaling and phosphoinositide 3-kinase (PI3K) activation [REF?]. PI3K activation stimulates glucose uptake and flux through the early part of glycolysis. Tyrosine kinase signaling negatively regulates flux through the late steps of glycolysis, making glycolytic intermediates available for macromolecular synthesis as well as supporting NADPH production. The oncogene MYC drives glutamine metabolism, which also supports NADPH production. Tumor suppressor protein LKB1, AMP-activated protein kinase (AMPK) signaling and p53 decrease metabolic flux through glycolysis in response to cell stress. Decreased glycolytic flux in response to LKB/AMPK or p53 may be an adaptive response to shut off proliferative metabolism during periods of low energy availability or oxidative stress [47].

Glucose can also be used to drive the synthesis of glycogen. Studies performed in 1925 proved that tumors presented notable glycogen content [50, 51]. One of the enzymes involved in glycogen synthesis is glycogen synthase, which can be inactivated through phosphorylation by glycogen synthase kinase-3 (GSK3), a multi-functional regulatory enzyme [52]. One of the characteristics of cancer cells is a reduced GSK3 activity through activation of PI3K/Akt pathway [52] leading to increased glycogen synthesis. This result further supports the hypothesis that cancer cells may store glycogen in abnormal quantities. Interestingly, it was found some years ago that raising the extracellular concentration of glucose increased the glycogen content of ascites cancer cells, while their glycogenolysis was relatively active [53], and that glycogen phosphorylase is overexpressed under hypoxia [54]. This additional glucose reserve would therefore constitute a growth advantage to cancer cells when their microenvironment is impoverished in oxygen and glucose due to deficient vascularisation [55]. Taken together, all these findings suggest that it is important to address cancer diagnostics and treatments with an effective metabolic point of view.

Currently, there are several drugs under development or in clinical trials that are designed to specifically target the altered metabolic pathways of tumors (Figure 4) [56].

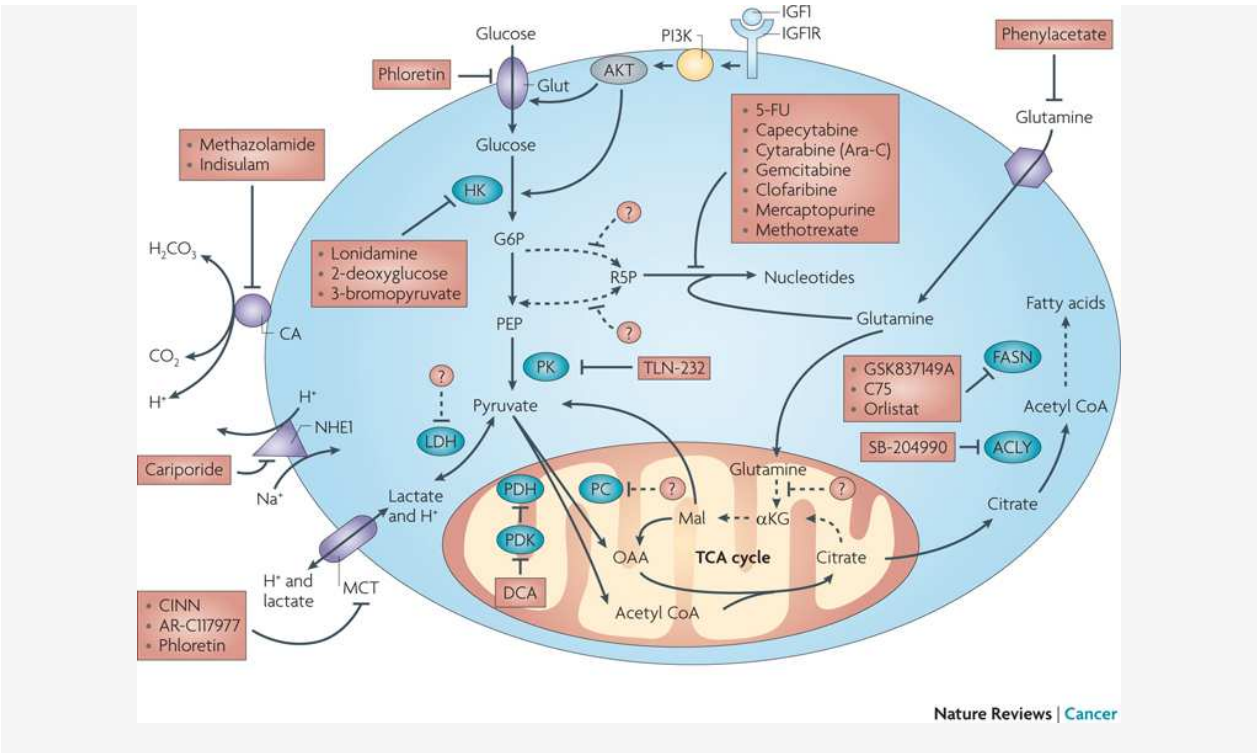

Figure 4. Metabolic pathways and enzymes against which compounds are already in the clinic. Dashed lines indicate possible areas of inhibition for which suitable compounds have not yet been tested. 5-FU, 5-fluorouracil; αKG, α-ketoglutarate; ACLY, ATP citrate lyase; CA, carbonic anhydrase; CINN, α-cyano-4-hydroxycinnamate; DCA, dichloroacetate; FASN, fatty acid synthase; G6P, glucose-6-phosphate; Glut, glucose transporter; HK, hexokinase; IGF1, insulin-like growth factor 1; IGF1R, IGF1 receptor; LDH, lactate dehydrogenase; Mal, malate; MCT, monocarboxylate transporter; NHE1, Na^+/H^+ exchanger 1; OAA, oxaloacetate; PDH, pyruvate dehydrogenase; PDK, pyruvate dehydrogenase kinase; PEP, phosphoenol pyruvate; PK, pyruvate kinase; R5P, ribose 5-phosphate; TCA, tricarboxylic acid cycle. (Figure taken from, Daniel A. Tennant, Raúl V. Durán, Eyal Gottlieb. Targeting metabolic transformation for cancer therapy. Nature Reviews Cancer**.** 2010**,** 267-277).

2- Deoxyglucose (2-DG) is a glucose analog, currently in phase I/II of clinical trials, which has the 2-hydroxyl group replaced by hydrogen (Figure 5), so that it cannot undergo further glycolysis.

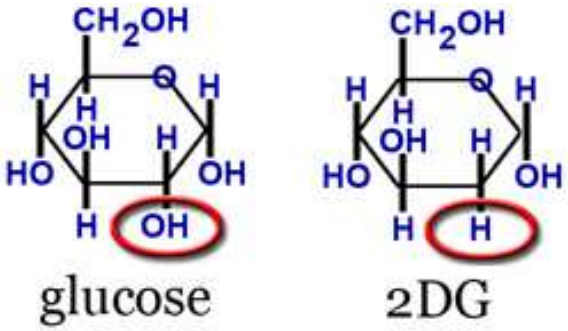

Figure 5: 2-Deoxyglucose (2-DG) is a glucose molecule which has the 2-hydroxyl group replaced by hydrogen. (Figure modified from, R L Aft, F W Zhang and D Gius. Evaluation of 2-deoxy-D-glucose as a chemotherapeutic agent: mechanism of cell death. British Journal of Cancer 2002, 87, 805–812).

Inhibition of glycolysis by phosphorylated 2-DG, 2-DG-6-phosphate, is thought to occur via inhibition of hexokinase and phosphohexoisomerase [57, 58]. 2-DG is effective in several mouse tumor models, particularly in combination therapy [59]. Indeed, metformin, a widely used antidiabetic agent, has been seen to exert antitumoral and antiproliferative action in prostate cancer cells, especially when used in combination with 2-DG [59]. Moreover, earlier studies have shown that 2-DG significantly enhances the cytotoxic effects of anticancer agents like topoisomerase inhibitors and a radiomimetic drug (bleomycin) in established human tumor cell lines. Also, it has been shown that 2-DG can be used as a modulator of radiation response [60, 61]. These studies demonstrate that targeting carbohydrate metabolism may be an effective therapeutic approach for cancer treatment.

2DG-6-phosphate cannot be further metabolised and hence it accumulates until it is de-phosphorylated by a specific phosphorylase [58]. One of the phosphorylases that could be involved in 2-DG dephosphorylation is glucose-6-phosphatase (G6Pase). This enzyme is a multifunctional system that catalyzes the final step in both the glycogenolytic and the gluconeogenic pathways, cleaving phosphate from glucose-6-phosphate to liberate free glucose into the circulation. It thus regulates both circulating concentrations of glucose and the storage of excess glucose as glycogen. G6Pase complex is found in microsomes and is composed by a catalytic subunit, facing the endoplasmic reticulum (ER) lumen, and 3 transporters (T1–3), one to move G6P into the lumen and two to allow the efflux of glucose and phosphate out into the cytoplasm. Defects in the enzyme cause glycogen storage disease type I (von Gierke disease). Glucose-6-phosphatase-alpha (G6PC) isoform is expressed mainly in liver and kidney [62]. Astrocytes are found to express the ubiquitously isoform glucose-6-phosphatase beta (G6PC3), suggesting a role of astrocytes in providing an endogenous source of brain glucose [63]. Additionally, previous studies on U87MG cells, a very well known GBM cell line, have shown that, targeting the microsomal G6PC with chlorogenic acid (CHL) decreased the invasive phenotype of these cells [64]. CHL has been proven in animal studies *in vitro* to inhibit the hydrolysis of the enzyme glucose-6-phosphatase in an irreversible fashion, thus reducing the absorption of new glucose.

In this study we investigated how 2-DG affects primary GBM-derived cells growth, comparing GBM cells that have been maintained under hypoxia (2% oxygen) and cells that had been acutely exposed to higher oxygen tension (environmental 20% oxygen). We aimed to understand

whether the presence of a hypoxic niche counteracted or *viceversa* improved the metabolic inhibition mediated by 2-DG. Moreover, gliomas are characterized by a high capacity to invade throughout normal brain tissue. This infiltrative nature is the hallmark of poor prognosis and a major obstacle for the clinical treatment of these tumors [65]. For these reasons, we tested how 2-DG was affecting cell invasion and migration by using an *in vitro* model. Considering the potentially crucial role played by G6Pase in preventing or mitigating 2-DG effects, we looked at the expression level of G6Pase in our GBM cell cultures and we also tested the effects of a G6Pase inhibition by using the CHL. Moreover, in order to study the effect of 2-DG in a more physiological microenvironment, we performed *in vivo* experiments by stereotactically injecting GBM derived cells into the right striatum of six week-old male nude mice, which had been subsequently treated with 2-DG or saline, via intraperitoneal daily injection. Both our *in vitro* and the *in vivo* data suggest that 2-DG might be used as a suitable molecule to impact GBM cells growth and migration, particularly when combined to inhibition of G6Pase activity.

Another aspect that has been investigated during my PhD program is GBM stem cells distribution within the tumor. Indeed, the discovery of a stem cell population within the tumor mass (cancer stem cells, CSCs) has changed the knowledge of tumor cell biology, leading to the definition of a cell hierarchy within the tumor [6]. Importantly, CSCs seem to persist in tumors as a distinct population and may be responsible of relapse and resistance to treatments following surgical resection [6]. Thus, there is intra-tumoral heterogeneity that has to be taken into account for designing effective treatments. CSCs have been positively identified and successfully isolated from a variety of tumors such as acute/chronic myeloid leukemia, breast/lung cancer, gastrointestinal and brain tumors. As normal stem cells, CSCs have been defined to have the capacity to self-renew as well as to undergo differentiation and give rise to the variety of non-tumorigenic cells found in the tumor [66]. However, if in normal tissues the pathways of self-renewal and differentiation are tightly controlled, in tumors, probably due to continuing mutagenesis, stem cells display aberrant growth and differentiation capacity. GBM CSCs are detected by the expression of normal neural stem cells markers such as CD133 and nestin found in human central nervous system (CNS) precursors. They can also differentiate into all neuronal lineages expressing the markers of mature neurons, astrocytes and oligodendrocytes. The main

property of the CSCs is to reconstitute the original tumor upon the transplantation in immuno-compromised mice. There are different hypothesis on the origin of CSCs: they may arise from normal tissue-resident stem cells; likewise, they may derive from mature cells that acquired ability to self-renew as a result of oncogenic mutations. Defining the regulation of normal stem cell self-renewal and differentiation mechanisms is of fundamental importance for understanding how initial malignant transformation, disease metastasis and progression occur. This knowledge will help to develop individualized therapeutic strategies targeting the subsets harboring the CSC function [6].

GBM are currently treated by surgical removal, followed by radiotherapy and mostly alkylating agents based chemotherapy. Nevertheless, CSCs may contribute to therapy resistance, initiation and the maintenance of GBM [7, 9], which might lead to reconsider the traditional therapeutic approaches.

One of the most used oral alkylating agents for the treatment of GBM is temozolomide (TMZ), which is currently regarded as a tolerable and effective drug. TMZ is a monofunctional methylating agent which is spontaneously activated in aqueous solution into the dacarbazine metabolite 5-(3-methyl-1-triazeno) imidazole-4-carboxamide (Figure 6).

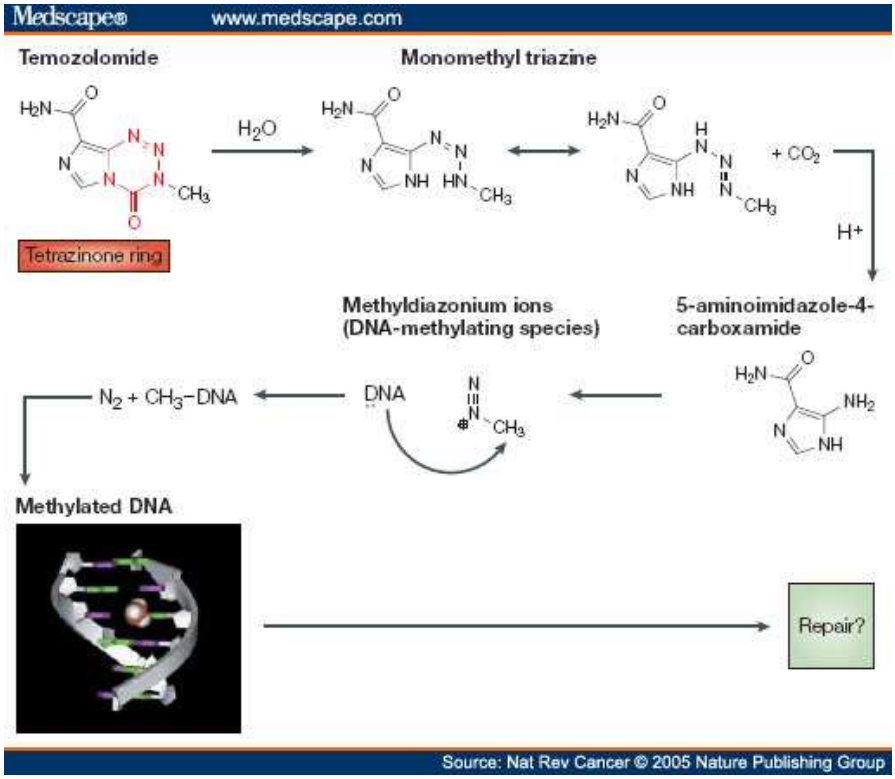

Figure 6: Structure of Temozolomide an its mechanism of action.
(http://img.medscape.com/fullsize/migrated/502/816/nrc502816.fig2.jpg)

In GBMs, TMZ is used in combination with radiotherapy. It exerts its anticancer property by adding methyl adducts to DNA, which eventually leads to apopotosis. Tumor cells can resist apoptosis by expressing wild-type O6-methylguanine-DNA-methyltransferase (MGMT), a DNA-repair protein that excises toxic methyl lesions from the O^6 position of guanine residues, allowing DNA repair. Treatment of cells with O^6-benzylguanine (6-BG) can overcome WT-MGMT-mediated resistance. This drug binds directly to MGMT, inactivating its ability to repair DNA [4].

Clinical trials have been performed to assess the activity of TMZ, alone or in combination, on brain metastatic solid tumors and leukaemias. However, developing concerns regarding the use of TMZ exist. Indeed, controversial data indicate that although TMZ seems to induce a dose- and time-dependent decline of the tumor stem cell subpopulation [4], other works indicate that TMZ does not seem to affect stem cells [5], which are considered the most chemoresistant cell population in the tumor bulk [6-9]. Thus, it is becoming pivotal to identify the phenotypic features of the resistant tumor cells and define their localization in the GBM tumor mass in order to distinguish and more effectively target them. The DNA repair protein MGMT has been found

expressed in a subgroup of GBM, conferring resistance to TMZ [67, 68], and importantly MGMT mRNA has been shown to be more highly expressed in $CD133^+$ cells [5]. Nonetheless, current studies on MGMT expression are conducted on analyses of promoter methylation and this does not always correlate with MGMT protein expression profile [69]. It has been shown that hypoxic tumor correlates with resistance to chemotherapics, thus suggesting that a better understanding of the tumor microenvironment may be essential to improve current anticancer strategies [70]. Recent data suggest that HIF-2α and multiple HIF-regulated genes are preferentially expressed in glioma stem cells in comparison with non stem tumor cells and normal neural progenitors [71]. Moreover, hypoxia promotes preferential expansion of $CD133^+$ glioma stem cells [72] and it also correlates with the dedifferentiation state in neuroblastoma [31]. These findings confirm a potential mutual relation between tumor immatureness and the hypoxic gradient within the tumor niche. Current investigations on primary cultures of brain tumors are generally conducted on random portions (i.e., regionally undetermined) of surgically resected tumor samples. It has recently been reported the existence of two types of cancer stem cells within different regions of the same human GBM [73]. Moreover, recent works have shown that within brain tumors CSCs reside in two niches, a perivascular location and the surrounding necrotic and/or less vascularized (i.e. hypoxic) tissue [21, 74]. According to our previous data [36], it has been reported that restricted oxygen conditions increase the CSC fraction and promote acquisition of a stem-like state [22, 36].

We investigated the phenotypic profile of the regions concentrically localized within the GBM tumor mass in relation to the oxygen tension gradient. We exploited radiological imaging and image guided surgery to sample multiple intratumoral areas in order to define potential phenotypic heterogeneity and differential expression of molecular signaling pathways in correlation to the oxygen tension gradient within the GBM tumor mass. We analyzed the peripheral, the intermediate area, and the central core of nine GBM biopsies by collecting multiple histological samples. Our data indicate the existence of a strong correlation between the concentric hypoxic gradient of the tumor mass, the GBM stem cells distribution, MGMT expression, and the consequential resistance to TMZ, leading us the define a novel concentric model of tumor stem cell niche. This novel model may be useful to define the real localization of the chemo-resistant GBM tumor cells in order to design more effective treatment strategies.

MAIN AIMS OF THE STUDY

Given the important role played by the hypoxic microenvironment in regulating GBM cell growth and metabolism, in this study we aimed to investigate whether primary GBM-derived cells maintained under hypoxia (2% O_2) were less sensitive compared to tumor cells acutely exposed to higher oxygen tension (environmental 20% O_2) to the effects induced by 2-deoxyglucose (2-DG), a glucose analogue and a very well described competitive inhibitor of glycolysis. As GBM stem cells share many properties with normal neural stem cells, we performed the analyses in parallel also on normal human subventricular zone derived stem cells (SVZ cells).

Additionally, in the effort to define the intra-tumoral localization of cancer stem cells within the GBM mass, and given the described correlation between hypoxia and GBM stem cells maintenance, we sought to understand whether the intratumoral hypoxic gradient affected GBM stem cell intra-tumoral distribution and their drug resistance property.

RESULTS

Part of the results obtained for part I have been collected during my third year of doctorate in the Brain Tumor Stem Cell Laboratory, Department of Neurosurgery at Johns Hopkins University School of Medicine, Baltimore, MD, where I worked as a visiting PhD student with Dr. Alfredo Quinones-Hinojosa, MD. Part of the results in part I have been published (Pistollato F, **Abbadi S**, Rampazzo E, Viola G, Della Puppa A, Cavallini L, Frasson C, Persano L, Panchision DM, Basso G. Hypoxia and succinate antagonize 2-deoxyglucose effects on glioblastoma. Biochem Pharmacol. 2010 Nov 15;80(10):1517-27. Epub 2010 Aug 10). Results described in part II have also been published (Pistollato F, **Abbadi S**, Rampazzo E, Persano L, Della Puppa A, Frasson C, Sarto E, Scienza R, D'avella D, Basso G. Intratumoral hypoxic gradient drives stem cells distribution and MGMT expression in Glioblastoma. Stem Cells. 2010 May;28(5):851-62).

RESULTS (PART I)

1.1. Characterization of phenotypic profile and differentiation properties of three GBM-derived cell cultures.

In this study we used primary cultures of adult GBM tumors to study the interaction between oxygen levels and the effects elicited by 2-DG, thereby inducing a block of glycolysis. We first characterized the phenotypic identity of our GBM cell cultures maintained under hypoxia (2% O_2) in order to establish their multipotency property. Indeed, a characteristic of GBMs is the presence of a subset of cells with a multilineage phenotype. These cells have remarkable phenotypic similarities to neural progenitors and express neural and mesenchymal markers before differentiation [75]. Thus, multipotency is a very important characteristic of tumor stem-like cells. Our primary cultures were established by plating GBM-derived cells on either fibronectin (not shown) or laminin- coated flasks (Fig. 7A left) or by briefly maintaining cells in suspension and then plating on laminin-coated flasks (Fig. 7A right). To verify the multipotency of our cell lines we investigated whether three of our primary-cultured gliomas (denominated

GBM612, GBM626 and GBM651) expressed the neural stem cell marker nestin, an intermediate filament protein expressed in undifferentiated CNS cells during development and cancer. Moreover, a defining property of stem cells is their ability to generate differentiated progeny. To test whether our GBM cells were capable to undergo astroglial or neuronal differentiation, we looked at the expression of glial fibrillary acidic protein (GFAP) and neuron-specific class III β-tubulin (Tuj1) upon growth factor withdrawal [76]. Our results showed that, in the undifferentiated groups, all three cell lines expressed high levels of nestin and only few cells expressed GFAP (Fig. 7B). Upon differentiation, GBM626 and GBM612 had a strong increase in the expression of GFAP, and the morphology of these cells was more characteristic of astrocytes with several cytoplasmic projections. GBM651 had only a slight increase of GFAP (Fig. 7B). All three cell lines expressed high levels of Tuj1 after differentiation (Fig. 8). Together these data indicate that GBM undifferentiated cells ($nestin^{+}$), despite some varibailities, are generally able to differentiate toward both glial and neuronal lineage.

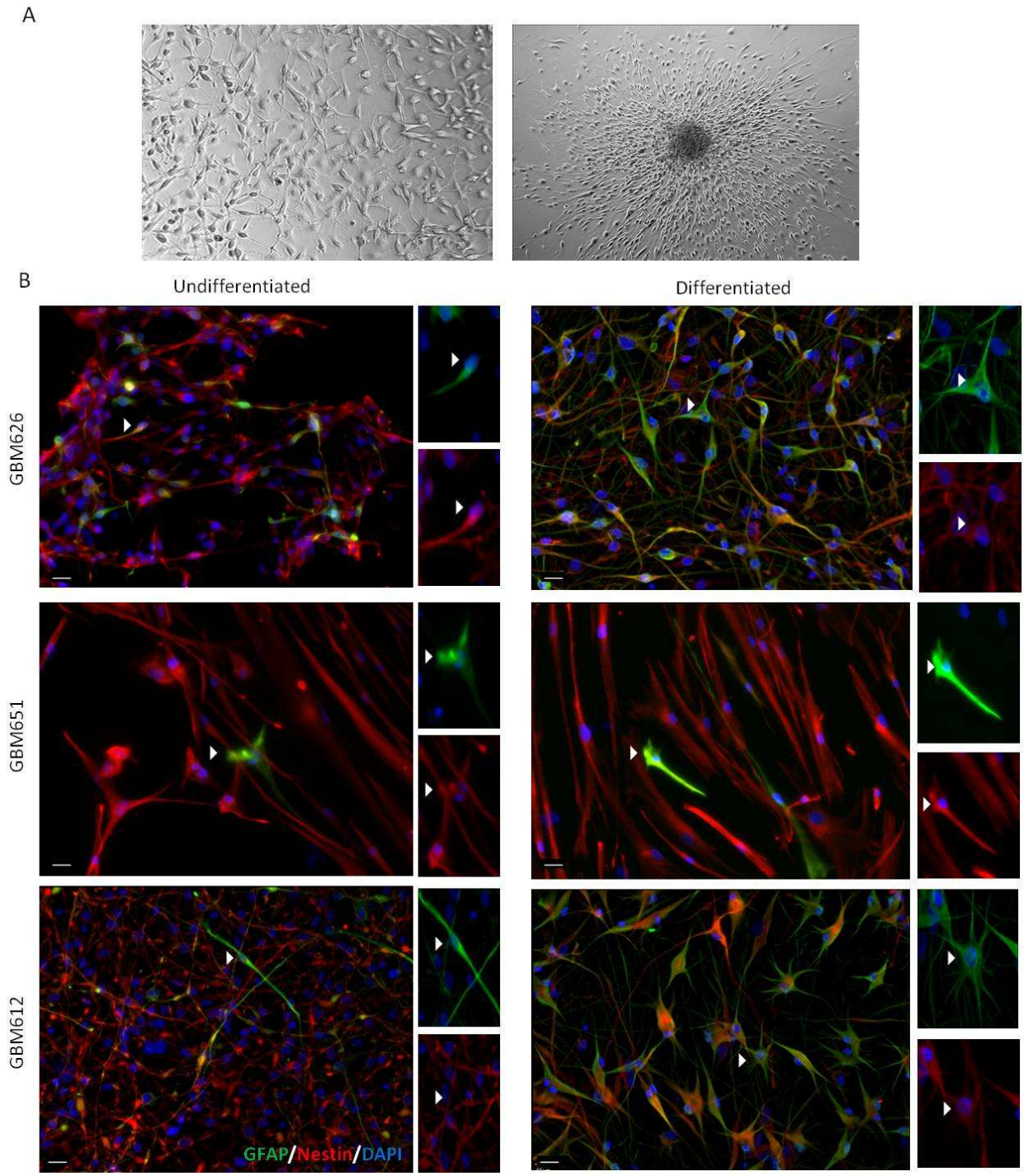

Figure 7. GBM-derived cells express neural stem cell marker and are multipotent. (A) Representative pictures of primary cultures (GBM626) established by plating the GBM cells on a laminin- coated flask (left) or briefly maintained in suspension and then plated on a laminin-coated flask (right).(B). Immuocytochemistry (ICC) of undifferentiated and differentiated GBM612, 626 and 651. In the undifferentiated groups, all three cell lines expressed high levels of nestin and only few cells were expressing GFAP. Upon differentiation, GBM626 and GBM612, had a strong increase in the expression of GFAP, and the morphology of these cells is more characteristic of astrocytes with several cytoplasmic projections. GBM651 had a slight increase of GFAP (arrowheads). GFAP – green, Nestin - red, DAPI – blue. n=3. Scale Bar: 10 μm.

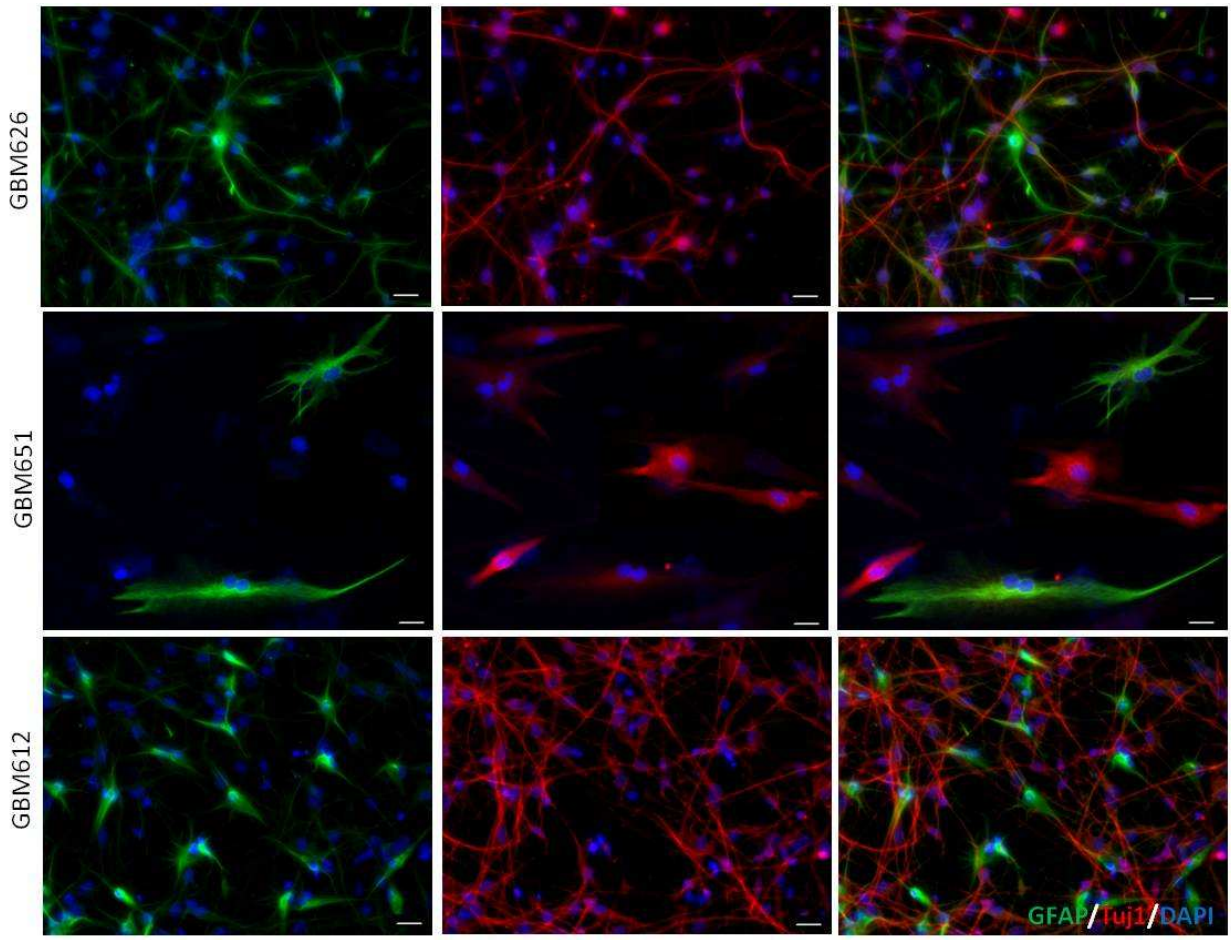

Figure 8. GBM-derived cell differentiation. Immuocytochemistry of differentiated cells. Immunostaining for GFAP and Tuj1 in the three different glioma cell lines (GBM626, 651 and 612). All cell lines expressed high levels of Tuj1 after differentiation. GFAP – green, Tuj1 - red, DAPI – blue. n=3. Scale Bar: 10 μm.

1.2. 2-DG induces loss of GBM cell adhesive properties and decreases cell proliferation.

It has been suggested that hypoxia is one of the major regulatory factors in the brain tumor niche, since it positively correlates with brain tumor aggressiveness, supporting the idea that hypoxia may confer a growth advantage to brain tumor stem cells [30, 31, 34, 36]. Under hypoxia cancer cell metabolism is pushed toward increased anaerobic glycolysis, which has been extensively described as a hallmark of tumor cell biology [11]. We evaluated cells grown in 2% oxygen, which represents the condition typically found in hypoxic solid tumors [77], versus cells that were acutely exposed to higher oxygen tension (20% oxygen). We found that addition of 25mM 2-DG for 18 h, under the two oxygen tensions, induced loss of cell adhesive properties compared

to GBM cells grown without 2-DG (Fig. 9A, 10A and B). Simply decreasing the glucose medium concentration from 25mMto 2.5mM, without adding 2-DG (Fig. 10C) did not cause change of cell morphology. By adding both 2-DG and glucose in the medium (i.e. 25mM 2-DG + 25mM glucose, Fig. 10C, or 12.5mM 2-DG + 12.5mM glucose, not shown), we found that loss of cell adherence was prevented and cells showed a flat phenotype with more extensions compared to cells grown in the absence of 2-DG. As GBM stem cells share many properties with normal neural stem cells, we performed the analyses in parallel also on normal human subventricular zone derived stem cells (SVZ cells). Measurement of extracellular lactate was generally high in tumor cell culture medium (Fig. 9B) compared to non-tumor SVZ-derived cells (Fig. 9C), consistent with GBM cell metabolic dependence on anaerobic glycolysis. Addition of 2-DG under both oxygen tensions led to a strong extracellular lactate decrease in both GBM and SVZ-derived cells (Fig. 9B and C). Moreover, 2-DG lowered GBM cells growth (Fig. 9D), especially in cells acutely exposed to high oxygen, while SVZ cells did not undergo morphological changes (Fig. 11) and underwent proliferation reduction only when acutely exposed to high oxygen tension (Fig. 9E). Analysis of GBM cell viability by trypan blue revealed no significant differences among conditions (not shown), while methyltetrazolium reduction (MTT) (Fig. 9F), indicative of extra-mitochondrial NADH and NADPH [78] occurred. Also, intracellular ATP content in GBM cells, which was found higher at 20% oxygen tension consequentially to stimulated mitochondrial activity, was decreased following addition of 2-DG (Fig. 9G).

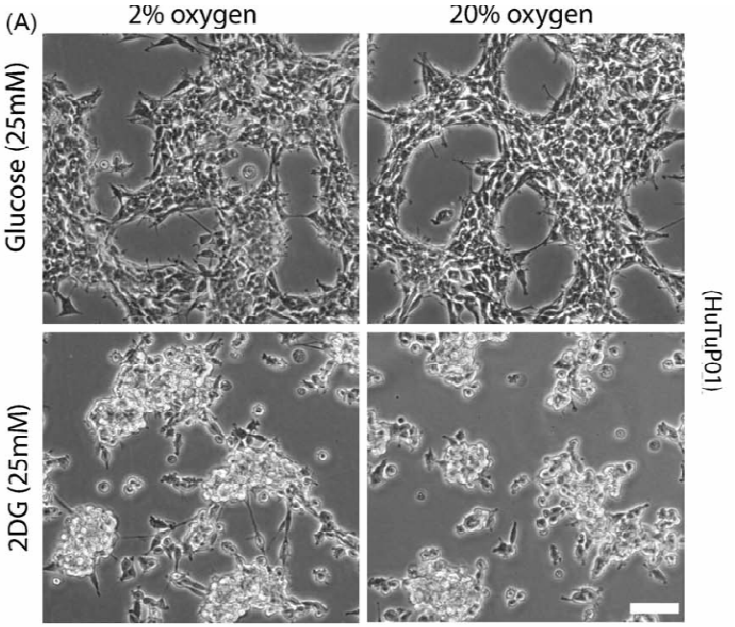

Figure 9A. Glycolysis block by 2-DG reduces extracellular lactate and lowers proliferation in GBM derived cells. (A) Representative pictures of GBM-derived cells (HuTuP01), plated at medium density (49 cells/mm2) and expanded 1 day (18 h) in 2% or 20% oxygen in the presence of 25 mM glucose or of 25 mM 2-DG (in low glucose medium, containing 2.5 mM glucose). Pictures acquired with an IX50 Olympus inverted microscope; 10x magnification. Bar = 100 mm.

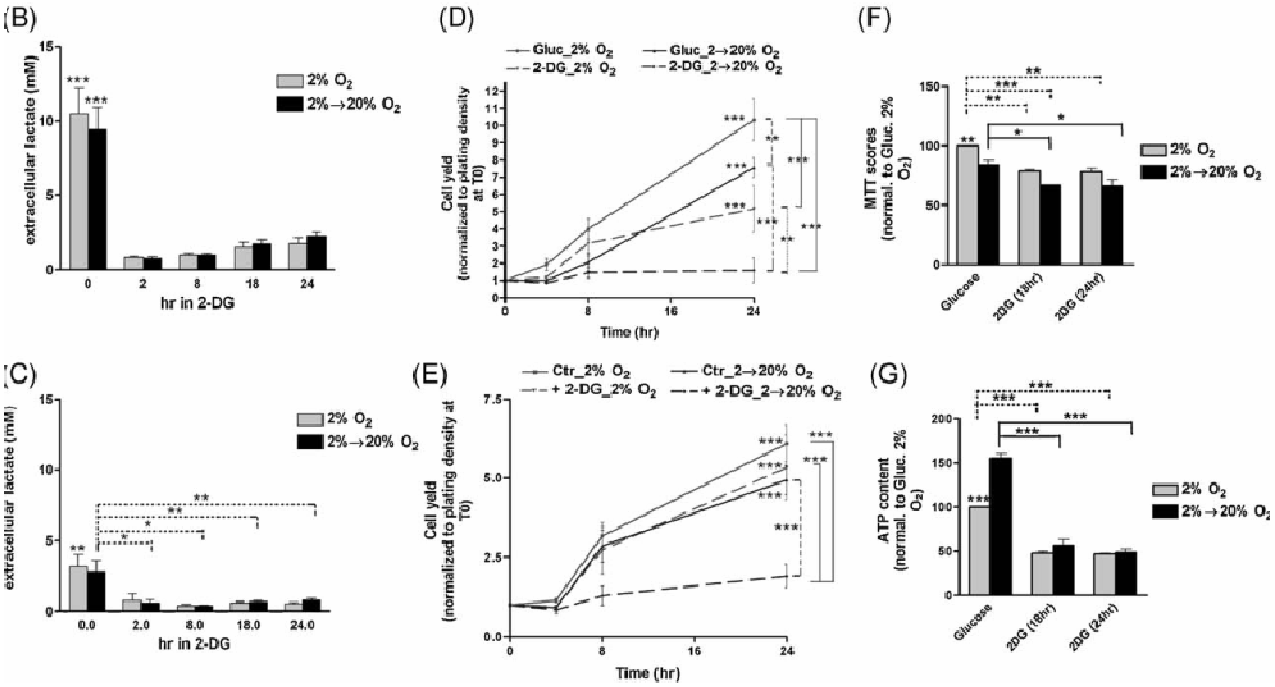

Figure 9B. Glycolysis block by 2-DG reduces extracellular lactate and lowers proliferation in GBM derived cells. (B and C) Extracellular lactate measurement following 2-DG addition, comparing 2 different GBM cell cultures (B) and 3 SVZ-derived cell cultures (C), cultured under 2% oxygen or 20% oxygen at the indicated times.***p < 0.001 above 0 h time point bars indicates statistically significant differences with all the other time points. (D and E) Cell growth kinetics: GBM cells (D) and SVZ cells (E) were plated at medium density (T0 = 49 cells/mm2); cells were either maintained in glucose (solid line) or in 2-DG (dashed line) for 4, 8 and 24 h at either

2% (light gray) or transferred to 20% oxygen (dark gray). Final cell counts/mm2 were normalized to plating density at T0. Mean of 4 different tumors ±S.E.M., n = 3 for each tumor. Mean of 3 different SVZ cell cultures ±S.E.M., n = 3 for each cell culture. (F) Analysis of metabolic activity by MTT assay; cells were cultured under 2% oxygen or 20% oxygen and 2-DG was added for 18 or 24 h, values were normalized to cells cultured with glucose at 2% O2. (G) Intracellular ATP content in GBM cells cultured as described in (F), values normalized to cells cultured with glucose at 2% O2.

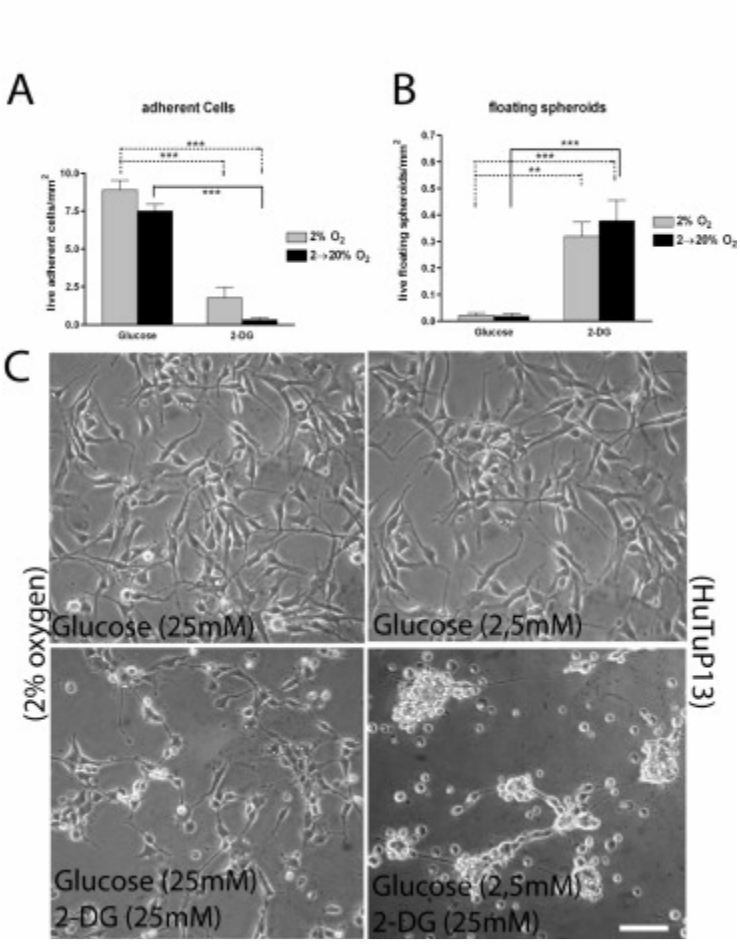

Figure 10. Reducing glucose concentration in the media does not affect cell morphology. Addition of 25mM2-DG for 18 h, under the two oxygen tensions, induced loss of cell adhesive properties compared to GBM cells grown without 2-DG (A). Simply decreasing the glucose medium concentration from25mMto 2.5mM, with out adding 2-DG did not cause change of cell morphology (C). By adding both 2-DG and glucose in the medium (i.e. 25mM 2-DG + 25mM glucose),we found that loss of cell adherence was prevented and cells showed a flat phenotype with more extensions compared to cells grown in the absence of 2- DG (C). S.E.M., n = 3. Values normalized to cells cultured with glucose at 2% O2. Pictures acquired with an IX50 Olympus inverted microscope; 10X magnification. Bar = 100 mm.

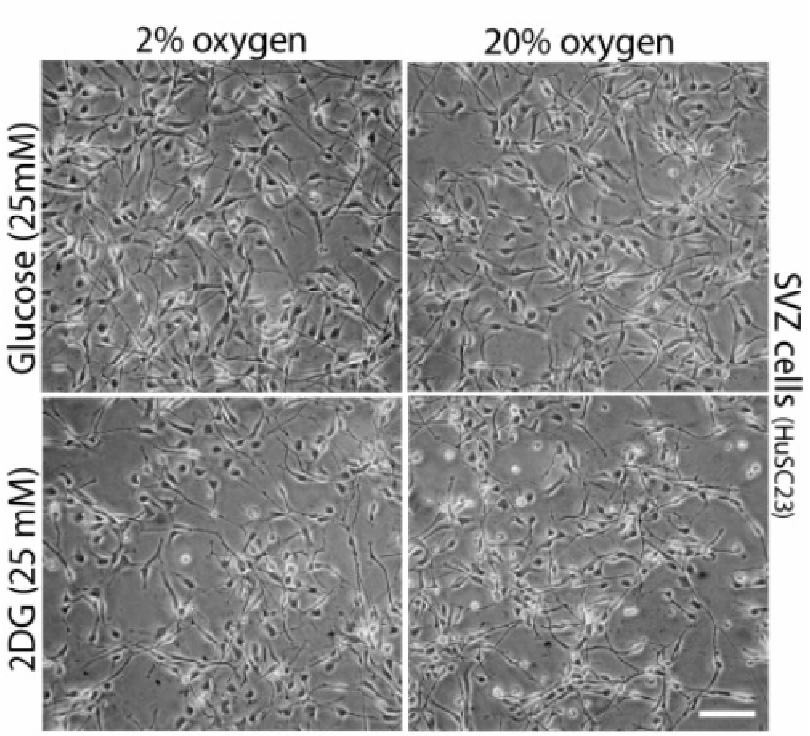

Figure 11. 2-DG treatment does not affect SVZ derived cells. SVZ cells did not undergo morphological changes Pictures acquired with an IX50 Olympus inverted microscope; 10X magnification. Bar = 100 mm.

1.3. 2-DG increases succinate dehydrogenase and pyruvate dehydrogenase activity.

We sought to investigate if 2-DG, besides determining a glycolytic block, was able to perturb mitochondrial metabolism. Thus, we analyzed succinate dehydrogenase (SDH) activity. It is known that SDH activation is impaired in several solid tumors, inducing the accumulation of succinate and ROS into the cytoplasm and causing strong HIF-1α stabilization even in the absence of hypoxia [42]. Surprisingly, we found that addition of 2-DG increased SDH activity in GBM-derived cells, especially at 20% oxygen (Fig. 12A and B). Addition of cell permeable succinate either in presence or absence of 2-DG did not modify SDH activation state (data not shown). Notably, in SVZ-derived cells SDH activity did not change after addition of 2-DG (data not shown), confirming differences in metabolic response between non-tumor and tumor cells. Additionally, we analyzed the phosphorylation state of pyruvate dehydrogenase E1a (pPDH E1a) in order to test if addition of 2-DG induced an increase of mitochondrial metabolism. The PDH complex contributes to transforming pyruvate into acetyl-CoA, which is used in the citric acid cycle to carry out cellular respiration. The activation state of PDH is controlled by the enzyme pyruvate dehydrogenase kinase (PDK), which inhibits PDH activity by phosphorylating it using ATP [79]. We found that GBM cells maintained at 2% oxygen had a higher level of pPDH

compared to cells acutely exposed to 20% oxygen (see T0 at 2% and T0 at 20% oxygen in Fig. 12C), indicating inactivation of the complex and increased lactate production level under hypoxia, as confirmed in Fig. 9B. After the addition of 2-DG, a transient increase of pPDH level occurred, which decreased after 18 h (Fig. 12C) and 24 h (data not shown). Importantly, total PDH level did not significantly change following addition of 2-DG (Fig. 12C). These results, together with the observation of an increase in SDH activation after the addition of 2-DG (Fig. 12A and B) indicate a transient recovery of mitochondrial activity following addition of 2-DG. As intracellular succinate level and ROS production are associated to SDH activity and defects of electron transfer in the respiratory chain are bound to enhanced ROS production [80], we evaluated the possible effects of 2-DG on ROS production. We found that hypoxic GBM-derived cells, which resulted to contain a variable but generally high percentage of ROS, underwent transient superoxide anion (O_2^-) reduction after the addition of 2-DG for 18 h (Fig. 12D). Importantly, by adding succinate to GBM cells ROS levels were higher under both oxygen tensions and this effect was repressed by the addition of 2-DG (Fig. 12E).

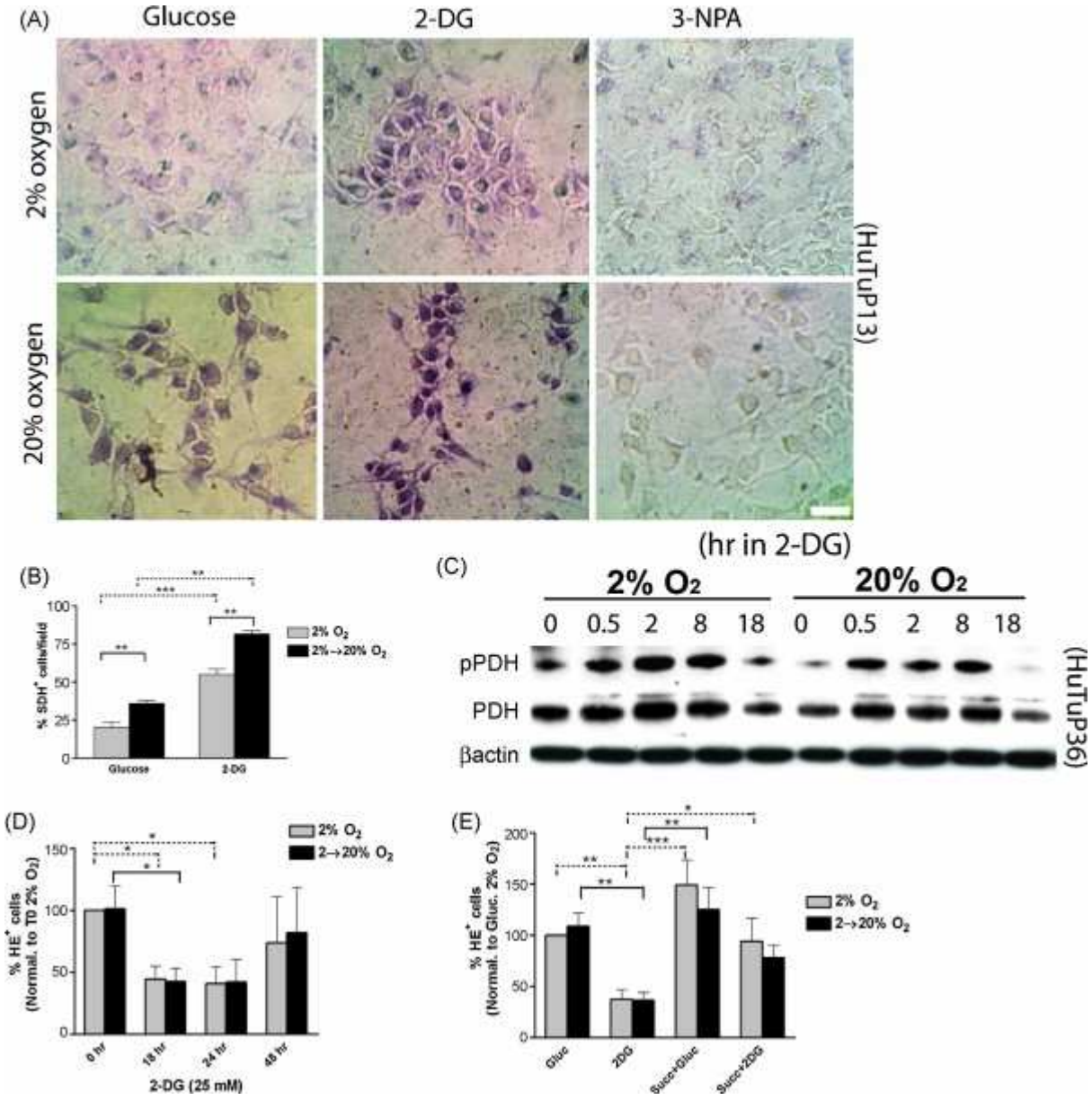

Figure 12. Block of glycolysis with 2-DG increases SDH and PDH activity. (A) Representative citochemical analysis (HuTuP13) of SDH activity by using NBT reduction methodology. Cells were incubated for 48 h in presence of glucose, 2-DGor 3-NPA known to irreversibly inactivate SDH (negative control). (B) Bar graph showing mean percentage of SDH+ cells (blue–violet cells) counted from 40_ magnification pictures (picture area = 0.02 cm2), bar = 20 mm. 3 different tumors have been used, n = 2 for each tumor. (C and D) Representative Western blot analyses (HuTuP36) of pPDHE1a and total PDH along with β-actin to control for protein loading. (C) Cells were cultured for 0.5,2,8or18 hwith2-DG, either left at 2% oxygen or acutely exposed to 20% oxygen; the analysis was confirmed using3 different tumors, n = 3 for each tumor. (Dand E) Histograms showing percentages of cells with intracellular superoxide anion ($O2^{-}$) measured by using hydroethidine (HE), mean ±S.E.M. from 3 different tumors, n = 2 for each tumor.

Conversely, significant variations of ROS content under the same conditions were not observed in SVZ-derived cells (Fig. 13).

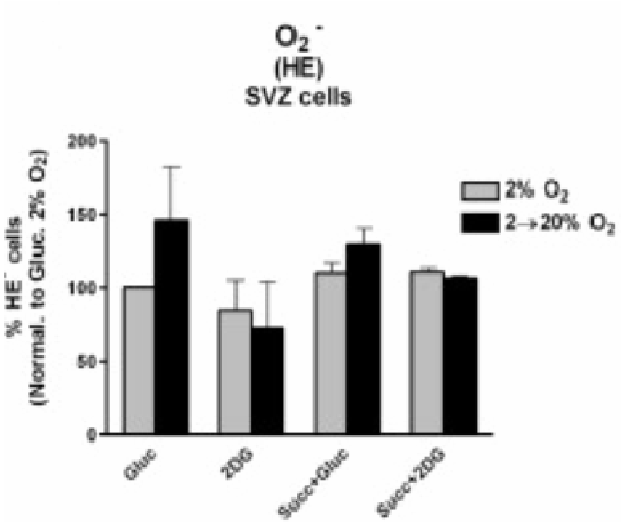

Figure 13: 2-DG treatment does not affect ROS release in SVZ derived cells. No significant variations of ROS content was observed in SVZ-derived cells treated with 2-DG. Two different SVZ cell cultures have been analyzed, n = 3 for each culture.

The decrease in ROS may also relate to higher reduced glutathione (GSH) level. GSH is maintained in cells by reduced nicotinamide adenine dinucleotide phosphate (NADPH), which is primarily generated when glucose is metabolized by pentose phosphate pathway. By measuring total GSH level we could not find any significant change following addition of 2-DG (Fig.14). This suggests that ROS level reduction is primarily connected to higher SDH activity (i.e. lower succinate level) rather than improved cytoplasmic radical scavenging.

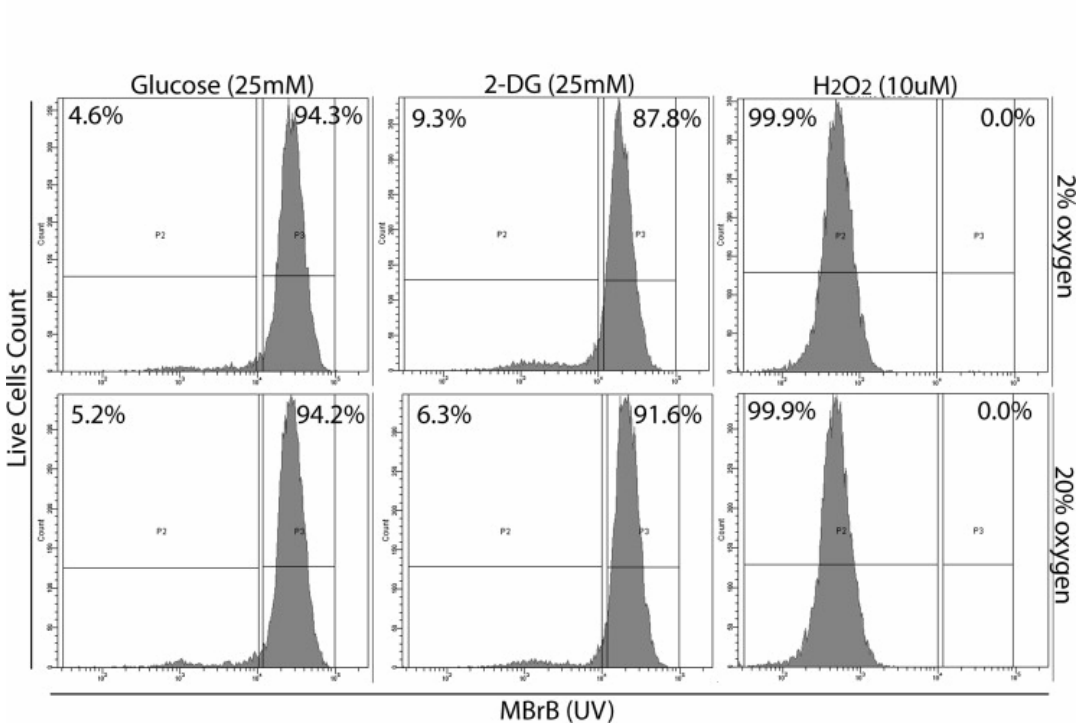

Figure 14. Total GSH levels are not affected by 2-DG. Addition of 2-DG did not induce any significant change in the total GSH levels compared to the control groups.

1.4. 2-DG promotes HIF-1α degradation in GBM cells and addition of succinate prevents this effect

It has been previously reported in a fibrosarcoma cell line that the hypoxic accumulation of HIF-1α, an endogenous hypoxia marker, strongly depends on glucose availability, as shown by modulation with 2-DG [81]. Nevertheless, the molecular mechanism causing this phenomenon has not been elucidated. HIF-1α is known to be chemically stabilized by hypoxia independent factors, such as mitochondrial ROS [82], $CoCl_2$, Fe^{2+} and cytoplasmic succinate [42], all known to be cofactors and inhibitors of proline hydroxylases (PHDs) [83], which target HIF-1α degradation through proteasome. Importantly, we found that HIF-1α protein level was reduced by 2-DG under hypoxia, in some cases below detection level (Fig. 15A). Higher-molecular-weight isoform of HIF- 1α, indicative of poly-ubiquitylated isoform [43], eventually occurred (Fig. 15A). In SVZ-derived cells HIF-1α was rapidly reduced following addition of 2-DG but its recovery was visible after 18 h (Fig. 16).

HIF-2α has been described as a promising target for anti-GBM therapies as it has been found highly expressed in glioma stem cells [71]. We found that, oppositely to HIF-1α, HIF-2α level was not significantly decreased by addition of 2-DG neither in GBM cells (Fig. 15A), nor in SVZ derived cells (not shown).

To explain HIF-1α degradation, we tested expression of proline hydroxylase-2 (PHD2), the best described proline hydroxylase involved in HIF-1α protein hydroxylation. We found that after addition of 2-DG, PHD2 protein increased under hypoxia (Fig. 15A) reaching the level observed in cells exposed to 20% oxygen. We hypothesized that 2-DG-mediated PHD2 protein increase was dependent on *de novo* protein synthesis. Analyses of QRT-PCR revealed that HIF-1α transcript did not change after addition of 2-DG (Fig. 15B), while expression of PHD2 transcript was decreased by 2-DG (Fig. 15C), leading to exclude *de novo* PHD2 synthesis. Importantly, this is related to the observed degradation of HIF-1α, as HIF-1α is known to control PHD2 transcription [58].

Importantly, by silencing HIF-1α with lentiviral vectors we previously showed that GBM derived cells acquired a more differentiated phenotype, with increased endogenous BMP signaling, and eventually underwent cell death after 5–7 days, as already reported [36, 37]. Importantly, further addition of 2-DG did not promote any difference in HIF-1α silenced cells (data not shown).

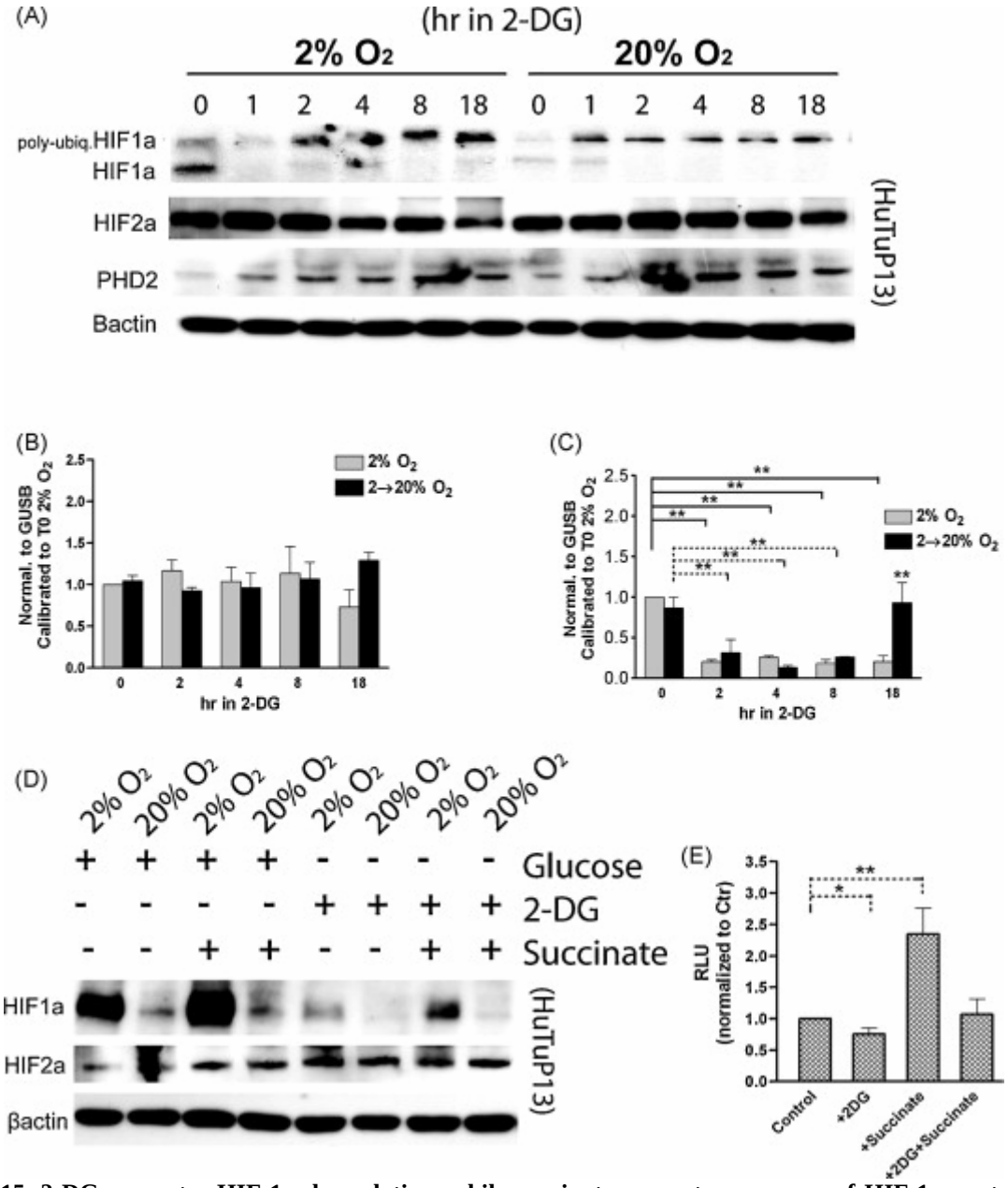

Figure 15. 2-DG promotes HIF-1α degradation, while succinate promotes recovery of HIF-1α protein level and transcriptional activity in GBM-derived cells. (A) Representative Western blot analyses (HuTuP13) of HIF-1α, HIF-2α and PHD2, along with β-actin to control for protein loading. GBM-derived cells were initially expanded in 2%, then 2-DG was added for 0, 1, 2, 4, 8, 18 h, maintaining cells at 2% or exposing them to 20% O2. The analyses were confirmed using 3 different tumors, n = 3 for each tumor. (B and C) QRTPCR analyses of HIF-1α and PHD2 normalized to GUSB and then calibrated to 2% O2 0 h (DDCt method), mean ±S.E.M. comparing 3 different GBM, n = 3 for each tumor. (D) Representative Western blot analyses (HuTuP13) of HIF-1α and HIF-2α along with β-actin to control for protein loading, in GBM-derived cells cultured for 18 h with glucose, 2-DG or diethyl-succinate (5 mM), combined as indicated; to confirm the data 3 different tumors have been used, n = 2 for each tumor. (E) HRE-luciferase assay: GBM cells were transiently transfected either with a HRE-firefly luciferase reporter construct or with a mutated HRE version of the same construct to evaluate aspecific effects. Along with these vectors, also a Renilla luciferase vector has been transfected in order to normalize luciferase detection. Normalization of the data, expressed in RLU (relative light unit), to the mutated HRE vector was done and then values were calibrated to untreated cells (Control). Two different GBM have been analyzed, n = 3 for each tumor.

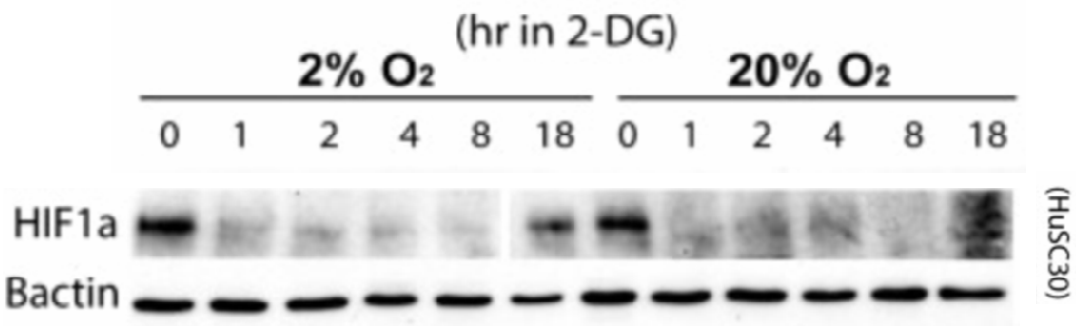

Figure 16. Addition of 2-DG affects HIF-1α stability also in SVZ derived cells. In SVZ-derived cells HIF-1α was rapidly reduced following addition of 2-DG but its recovery was visible after 18 h. Two different SVZ cell cultures have been analyzed, n = 3 for each culture.

As HIF-1α stability is related to accumulation of intracytoplasmic succinate consequential to impaired SDH activity [42], we hypothesized that 2-DG dependent HIF-1α degradation may be caused by the observed increase of SDH activity (Fig. 12A and B). To prove this hypothesis we evaluated if addition of succinate in combination with 2-DG, promoted a recovery of HIF-1α protein level in GBM-derived cells. We found that HIF-1α stability was recovered in 2-DG/succinate cultured cells (Fig. 15D). Analysis of HIF-2α did not reveal any significant change among conditions (Fig. 15D). We investigated if 2-DG, besides modulating HIF-1α protein stability, promoted also inhibition of HIF-1α transcriptional activity, by using a hypoxia responsive element (HRE)-luciferase reporter construct. We found a modest reduction of HIF-1α transcriptional activity under hypoxia following 8 h of 2-DG treatment compared to untreated GBM cells (Fig. 15E). Notably, by adding succinate together with 2-DG this reduction did not occur, and addition of succinate alone doubled HIF-1α transcriptional activity (Fig. 15E).

1.5. Hypoxia inhibits the pro-apoptotic effect caused by 2-DG in GBM derived cells.

We sought to investigate whether these changes of GBM metabolic profile and the observed reduction of HIF-1α protein level correlated to block of cell cycle and induction of apoptosis. It has already been reported that downregulation of HIF-1α suppresses tumorigenicity of renal cell carcinoma through induction of apoptosis [84] and attenuates glioma growth in vivo [85]. Analysis of cell cycle revealed that addition of 2-DG in GBM cells acutely exposed to high oxygen tension induced a modest but not significant decrease of S phase and a slight increase of apoptotic cells (sub G1 fraction), but these effects were not observed in hypoxia (Fig. 17A). Analysis of apoptosis by using annexin-V/propidium iodide staining (annexin-V/PI) indicated

that addition of 2-DG significantly induced early apoptosis (annexin-V^+/PI^- cells) especially when GBM cells were exposed for 24 and 48 h to high oxygen tension (Fig. 17B). Oppositely, addition of 2-DG on SVZ-derived cells did not promote significant cell cycle changes and/or induction of apoptosis (not shown). Apoptosis often implicates disruption of mitochondrial membrane potential (ΔΨmt). We found that addition of 2-DG for 24 and 48 h caused reduction of ΔΨmt especially when cells were exposed to 20% oxygen (Fig. 17C). Moreover, we found that anti-apoptotic proteins (Bcl-2 and Bcl-XL), involved in mitochondria controlled apoptosis, were down-regulated more rapidly by addition of 2DG under 20% oxygen, while PARP cleavage, which is a marker of cells undergoing apoptosis [86], occurred earlier under the same conditions (Fig. 17D). Importantly, even though decrease of Bcl-2 and Bcl-XL proteins occurred even after 18 h after addition of 2-DG, percentage of early apoptotic cells (annexin-V^+/PI^- cells) increased significantly only after 48 h (Fig. 17B). In normal SVZ-derived cells these apoptosis-related proteins were not affected at early time points, but only after prolonged 2-DG stimulus (Fig. 18). Analysis of $p21^{cip1}$, which is related to cell cycle arrest and induction of differentiation or to cell death [87], revealed that GBM cells exposed to 20% oxygen, independently from addition of 2-DG, had a higher p21cip1 level compared to cells maintained under hypoxia, confirming our previous report [36] (Fig. 17D). Under hypoxia addition of 2-DG slowly up-regulated $p21^{cip1}$ (Fig. 17D) to level comparable to the one observed at 20% oxygen. In SVZ derived cells $p21^{cip1}$ did not change following addition of 2-DG (Fig. 18).

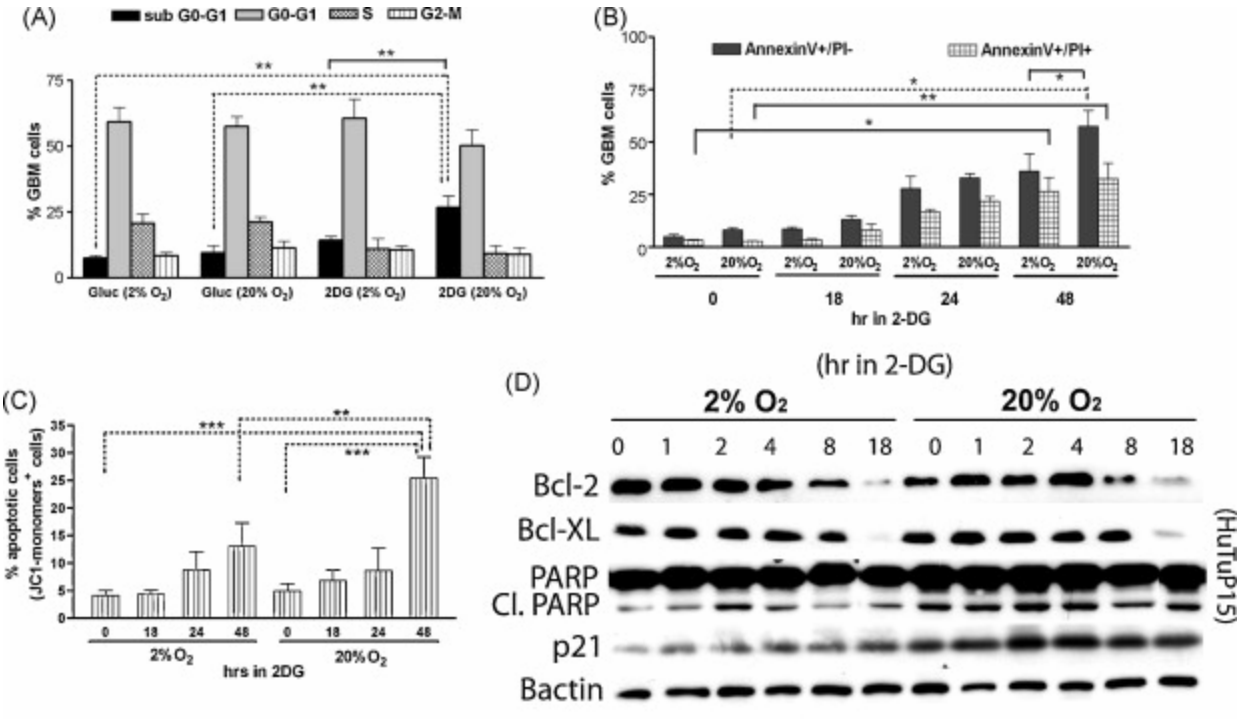

Figure 17. Hypoxia inhibits the pro-apoptotic effect caused by 2-DG in GBM-derived cells. (A) Histogram showing percentages of different cell cycle phases in live gated cells based on BrdU and 7-AAD incorporation. . Mean of 3 tumors ±S.E.M., n = 2 for each tumor. (B) Annexin-V/Propidium Iodide (Annexin-V/PI) staining of GBM-derived cells expanded for 0, 18, 24 or 48 h in the presence of 2-DG, either at 2% or 20% oxygen. Bar graph represents percentages of early apoptotic cells (annexin-V+/PI$^-$ cells) and late apoptotic cells (annexin-V+/PI+ cells); mean of 3 tumors ±S.E.M., n = 3 for each tumor. (C) Analysis of mitochondrial membrane potential by using JC-1: histogram shows % of low ΔΨmt in live gated cells (based on physical parameters, side scatter and forward scatter), mean of 2 tumors ±S.E.M., n = 3 for each tumor. (D) Representative Western blot analyses (HuTuP15) of Bcl-2, Bcl-XL, PARP, p21^{cip1} along with β-actin to control for protein loading, in GBM cells cultured for 0, 1, 2, 4, 8, 18 h in presence of 2-DG, either at 2% or 20% oxygen. The analyses were confirmed using 3 different tumors, n = 3 for each tumor.

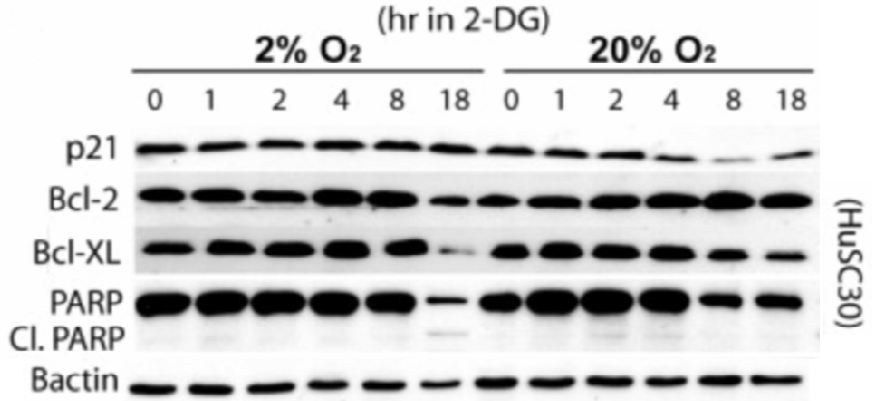

Figure 18. 2-DG treatment does not induce cell death in SVZ derived cells. In SVZ cells, Bcl-2, Bcl-XL, PARP cleavage and p21 levels were not significantly affected by 2-DG neither at 2% nor at 20% oxygen. Two different SVZ cell cultures have been analyzed, n = 3 for each culture.

1.6. 2-DG induces neuronal commitment and addition of succinate antagonizes this effect by reducing GBM differentiation.

HIF-1α expression has been related to the maintenance of a more immature phenotype in ductal breast carcinoma and neuroblastoma [30, 31], a phenomenon that has been recently described also in malignant gliomas [34, 36]. As we found that addition of 2-DG within the first 18 h induced increase of $p21^{cip1}$, with apoptosis significantly occurring after 48 h (Fig. 17B–D), together with HIF-1α poly-ubiquitylation and degradation even under hypoxia (Fig. 15A), we evaluated if these events correlated to the acquisition of a more differentiated phenotype in live remaining GBM cells. Flow cytometric analysis of cell surface marker CD133, revealed that addition of 2-DG promoted a decrease of $CD133^+$ cells percentage, especially at 20% oxygen (Fig. 19A). Normal SVZ-derived cells contained a lower percentage of $CD133^+$ cells compared to GBM-derived cells, and addition of 2-DG analogously induced a slight decrease of $CD133^+$ cells (Fig. 20). Importantly, we found that addition of succinate under hypoxia increased $CD133^+$ cells in GBM (Fig. 19A), and this did not occur in SVZ-derived cells (Fig. 18). Addition of both 2-DG and succinate slightly prevented 2-DG-mediated decrease of tumor $CD133^+$ cells exposed to 20% oxygen (Fig. 19A). Another described GBM stem cell marker is CD90 [88], which we found to be highly expressed in all our GBM cell cultures. Nevertheless, only a slight decrease of $CD90^+$ cells was observed after addition of 2-DG and succinate did not reverse this effect (Fig. 21). Immunocytochemical analysis on adherent remaining cells of nestin (Fig. 19B and E), indicative of undifferentiated precursors, glial fibrillary acidic protein (GFAP) (Fig. 19C and E), a marker of astroglia and their progenitors, and βIII-tubulin (Fig. 19D and F), expressed in neurons and their committed progenitors, revealed that addition of 2-DG under hypoxia promoted specifically neuronal differentiation (i.e. higher $\beta III\text{-tubulin}^+$ cells percentage), rather than glial commitment, with decrease in $nestin^+$ cells. In GBM cells acutely exposed to 20% oxygen a higher basal neuronal and glial commitment was visible and under this condition the addition of 2-DG did not further increase differentiation. Opposite to 2-DG effects, addition of succinate raised fraction of $nestin^+$ cells (Fig. 19B and E), lowering the percentage of $GFAP^+$ and $\beta III\text{-tubulin}^+$ cells (Fig. 19C–F). Finally, addition of succinate together with 2-DG prevented 2-DG mediated differentiation of GBM-derived cells (Fig. 19B–D). Altogether these data suggest that addition of 2-DG promotes induction of GBM cell differentiation and lately cell death under

20% oxygen, while maintaining cells at 2% oxygen partially inhibits these effects, preserving tumor stem cells survival, despite HIF-1α degradation occurs.

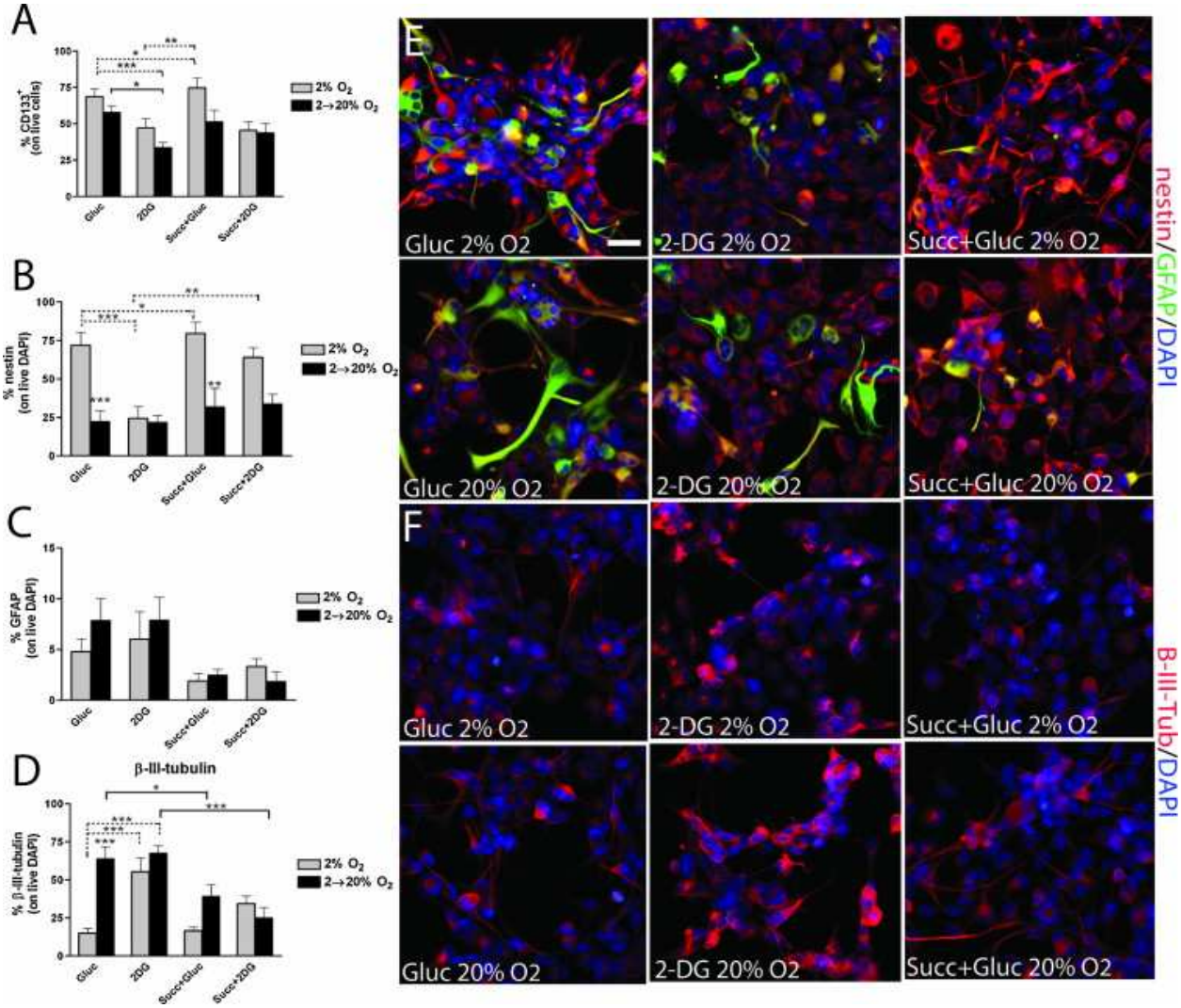

Figure 19. 2-DG induces neuronal commitment and addition of succinate antagonizes this effect by reducing GBM differentiation. (A) Histogram showing percentages of CD133+, mean of 4 tumors ±S.E.M., n = 3 for each tumor. (B–D) Histograms showing, respectively, nestin, GFAP and b-III-tubulin quantitations relative to total DAPI+ cells. Mean of 3 tumors ±S.E.M., n = 2 for each tumor. (E and F) Representative immunocytochemical images (HuTuP10) of nestin (red)/GFAP (green) (E) and β-III-tubulin (red) (F). GBM cells were plated at medium density (49 cells/mm2), expanded 18 h in 2% or 20% oxygen in the presence of glucose, 2-DG and/or succinate. 20_ magnification, bar = 40 mm.

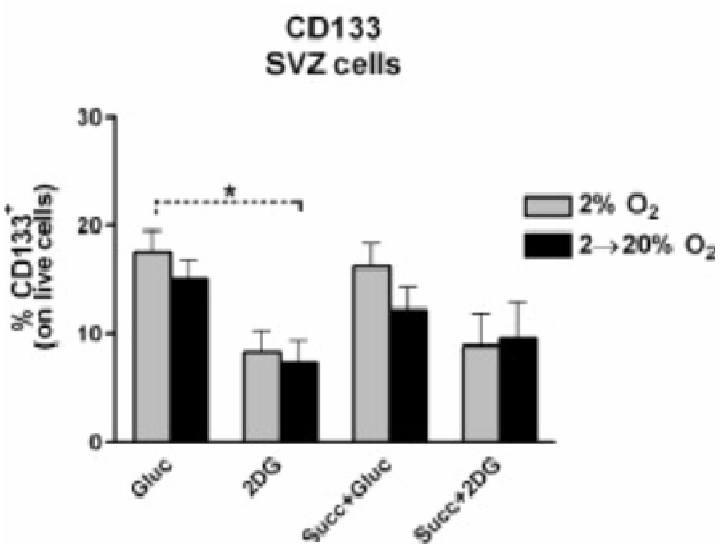

Figure 20. Addition of 2-DG induced a significant decrease in the expression levels of CD133 only when SVZ derived cells where cultured at 20% oxygen. Two different SVZ cell cultures have been analyzed, n = 3 for each culture.

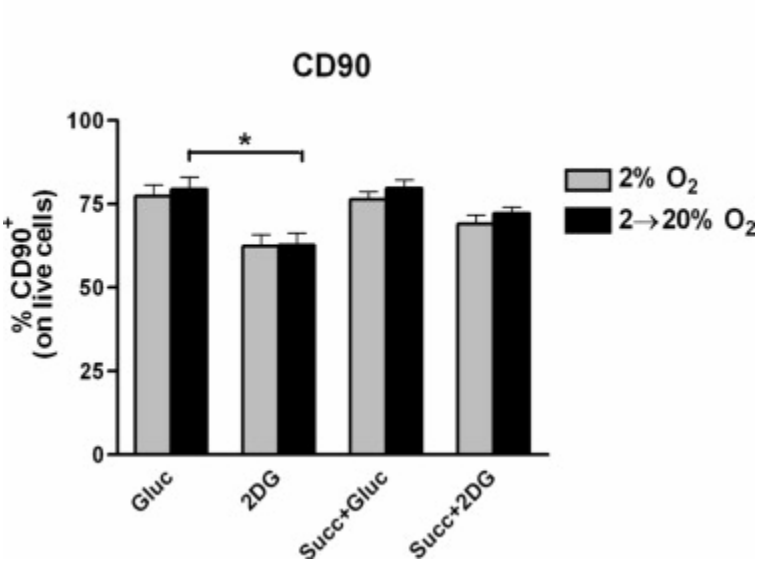

Figure 21. Only a slight decrease of $CD90^+$ cells was observed after addition of 2-DG and succinate did not reverse this effect. Three different GBM cell cultures have been analyzed, n = 3 for each culture.

1.7. GBM-derived cells recovered from 2-DG treatment display a higher proliferating phenotype .

We sought to investigate whether GBM cells were able to recover and proliferate following addition of 2-DG. Thus, after 18 hr in presence of 2-DG, GBM cells were left to recover for additional 72 hr in presence of glucose supplemented medium and constantly maintained under

hypoxia. Comparing three GBM cultures we found that while 2-DG promoted reduction of proliferation, according to figure 9, surprisingly, when cells were allowed to recover from 2-DG exposure, they were more proliferative compared to the control group, suggesting a possible mechanism of survival that has been activated in these resistant cells (Fig. 22).

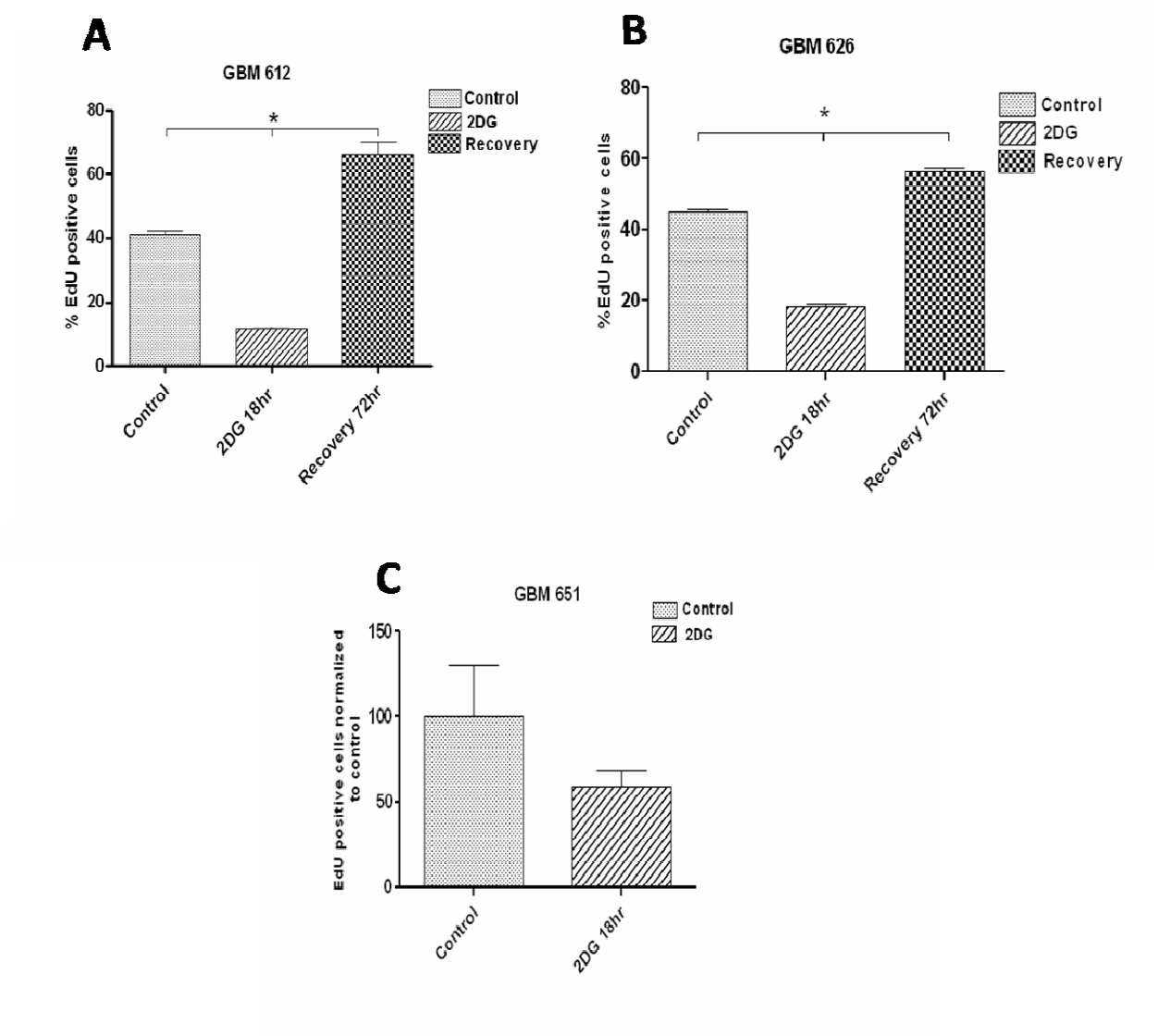

Figure 22.GBM-derived cells recovered from 2-DG treatment display a higher proliferating phenotype. (A-C). Cells were cultured at 2% for 18h. Glucose or 2-DG was added at 25mM for control or experimental conditions respectively. Cells from the recovery group were removed from 2-DG exposure (by changing the media with 2-DG to glucose supplemented media for 72hr). Results are expressed as mean ± SEM. *< p 0.05 respective to control at 2%.

1.8. 2-DG decreases GBM cells invasiveness but the cells recovered from 2-DG treatment display a stronger invasive ability.

GBM tumors rarely metastasize outside of the CNS, possibly due to a combination of the blood–brain barrier's (BBB) resistance to extravasation and a lack of suitable cell adhesion molecules on the surface of GBM cells to facilitate homing to target tissues [89]. However, GBM tumors are characterized by diffuse local invasion, which involves processes shared with metastasis, including increased motility, altered adhesion, and remodeling of extracellular matrix (ECM). Invasive tumor cells are probably one of the major factors in GBM recurrence following surgery, radiotherapy and chemotherapy. It is found that highly migratory and invasive GBMs overexpress certain members of the matrix metalloproteinases (MMPs), a family of proteolytic enzymes implicated in tumor cell metastasis, leading to increased invasiveness [90]. Our results showed that all three cell lines have a slight tendency to invade more at 2% oxygen tension than at 20% oxygen, which is indicative of a more aggressive phenotype. Importantly, addition of 2-DG strongly reduced the ability of the cells to invade in both oxygen tension (Fig. 23). As observed in cell proliferation experiments, the GBM612 cell line appeared to be more sensitive to the effects of 2-DG than GBM651 and 626 cell lines. Cells that were cultured in the absence of both, 2-DG and glucose, were still able to pass through the boyden chamber, suggesting a specific role of 2-DG in decreasing cells ability to invade (Fig. 23). Cells allowed to recover from 2-DG exposure showed also an increase in invasion when compared to the control group, suggesting the acquisition of a more aggressive phenotype acquired by these surviving cells (Fig. 24).

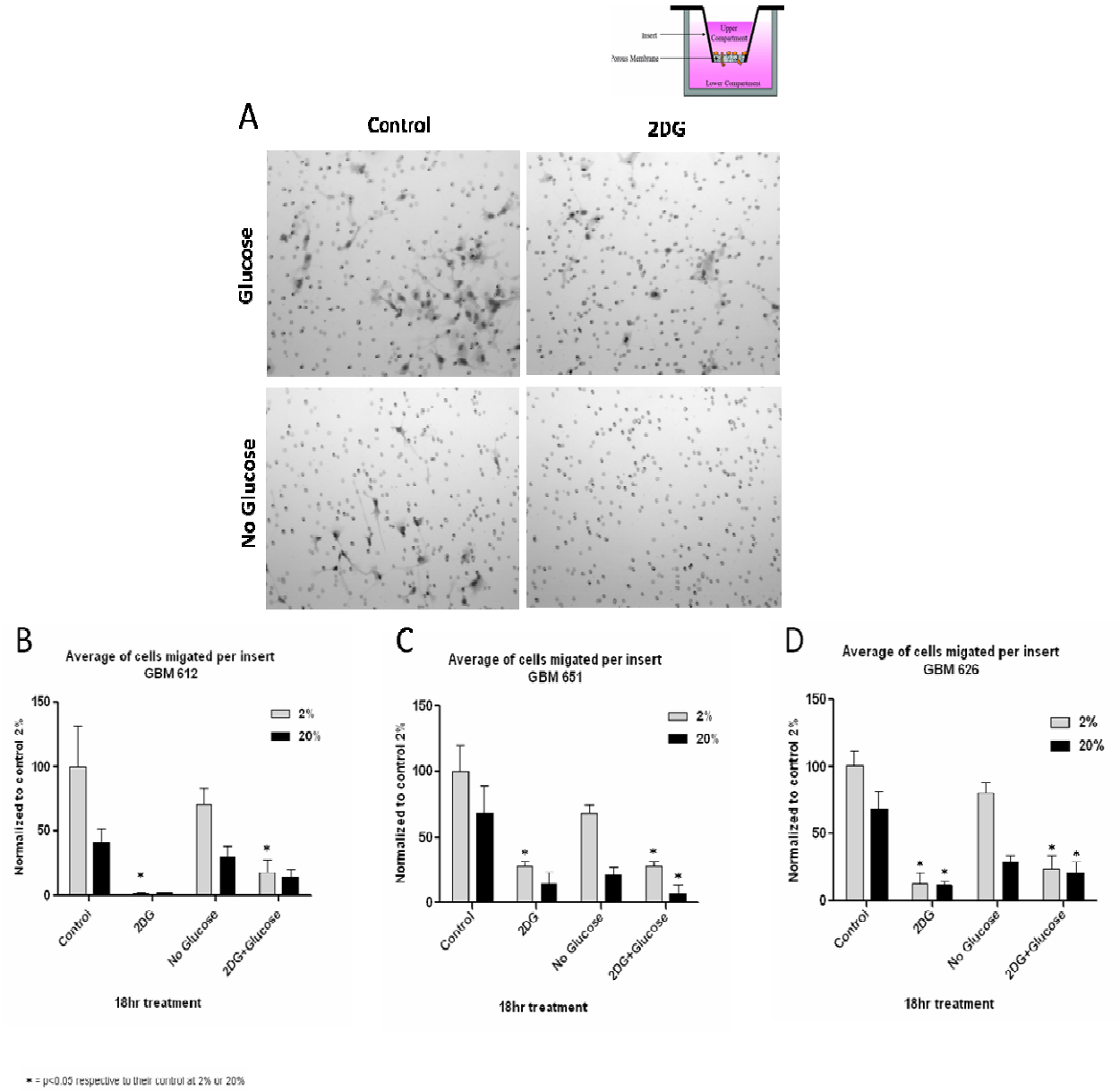

Figure 23. 2-DG affects invasive behavior of GBM cells. Cells were cultured at 2% or 20% oxygen for 18h with glucose or 2-DG at 25mM for control or experimental conditions respectively in Boyden chambers. (A). Representative images of GBM612 cells invaded through the Boyden chamber membrane at 2% oxygen. A decreased number of invading cells was observed after the addition of 2-DG. (B-D), Bar graphs showing the invasive behavior of the three cell lines (GBM612, GBM651 and GBM626). n=3. Results are expressed as mean ± SEM. *< p 0.05 respective to their control at 2% and 20% oxygen.

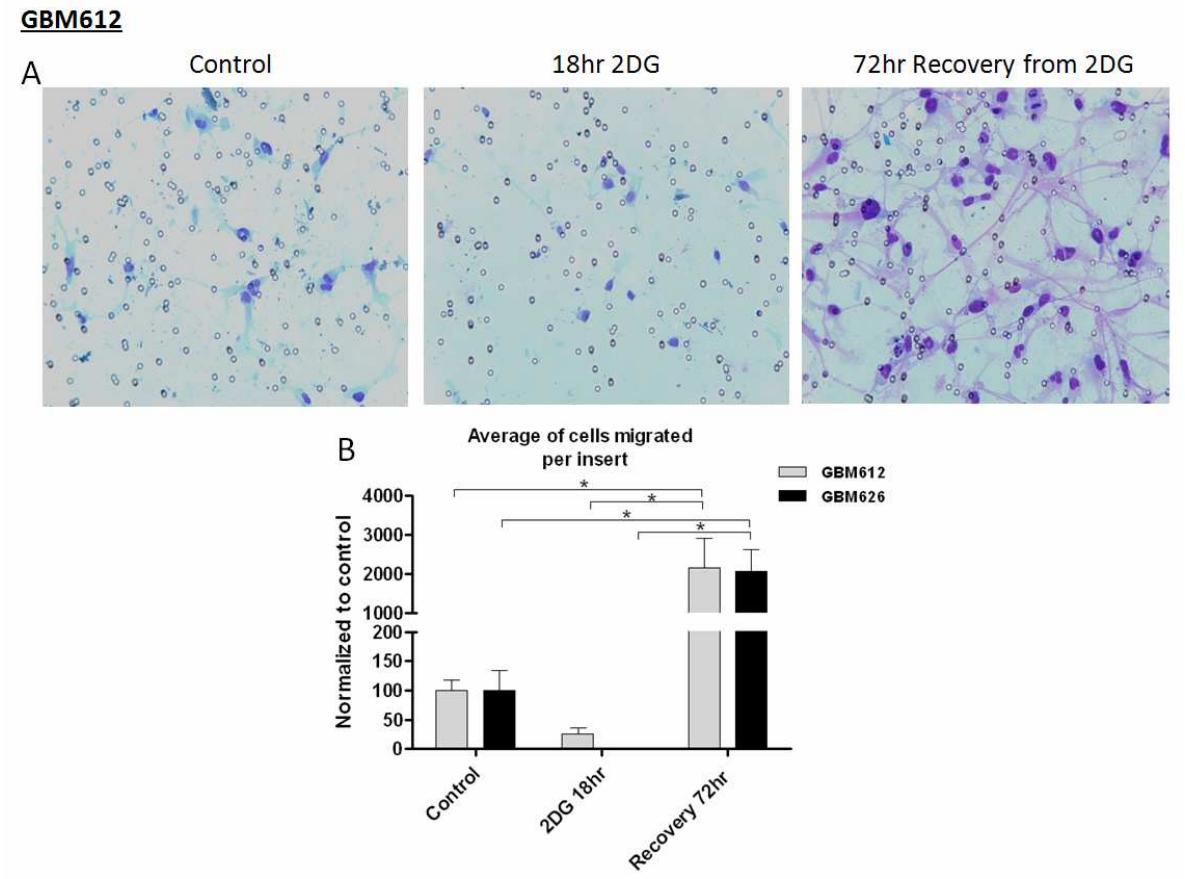

Figure 24. GBM cells recovered from 2-DG treatment display a stronger invasiveness. Cells cultured at 2% oxygen were either exposed to 2-DG for 18h at 25mM or allowed to recover for 72hr from 2-DG, and compared to control group. (A) Representative images of GBM612 cells invading through the Boyden chamber membrane at 2% oxygen. (B) Bar graphs showing the migration GBM612 and GBM626 at 2% oxygen. Results are expressed as mean ± SEM. n=3. *< p 0.05 respective to control at 2%.

1.9. Addition of 2-DG does not affect GBM cell ability to uptake glucose.

In the brain, the principal glucose transporters are the GLUT1 and GLUT3 isoforms, which have high affinities for glucose and thus influence the rate of glucose uptake by their membrane concentration [91]. In cancer cells, the primary metabolic characteristic is an increased uptake of glucose and its anaerobic metabolism. Therefore, glucose is a vital energy source of tumors [92]. To determine whether glucose uptake is influenced by 2-DG treatment, glucose uptake was measured using the fluorescent deoxyglucose analogue 6-(N-(7-nitrobenz-2-oxa-1,3-diazol-4-yl)amino)-6-deoxyglucose (6-NBDG). The uptake of glucose was inhibited by cytochalasin-B, a competitive inhibitor of the glucose transport. Results showed that our GBM-derived cell cultures had a high glucose uptake rate. Interestingly, reducing glycolysis through the addition of

2-DG did not affect the glucose transporter and hence the cells ability to uptake glucose (Fig. 25).

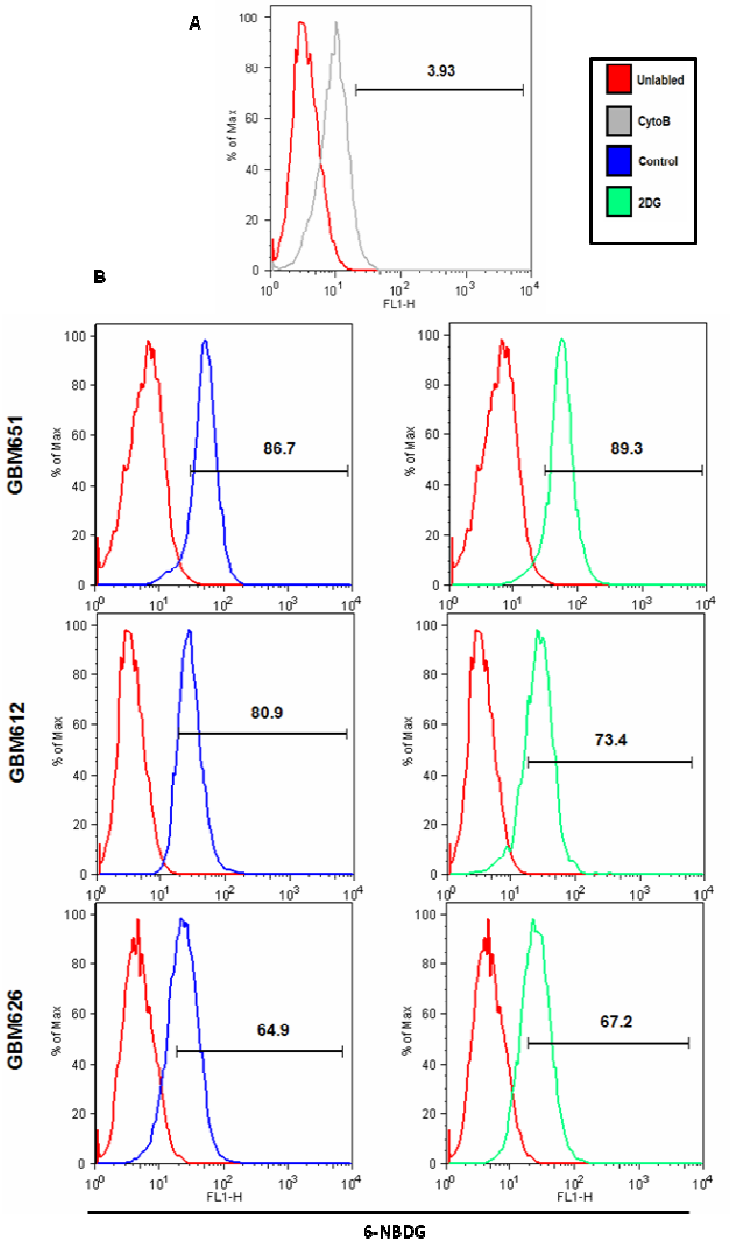

Figure 25. 2-DG does not affect GBM cell ability to uptake glucose. (A). Representative images of histograms obtained from unlabeled GBM612 and treated with cytochalasin-B. (B). Percentage of cells uptaking 6-NBDG in the three cell lines GBM612, GBM651 and GBM626. In all three cell lines the addition of 2-DG for 18 hr did not affect the ability of the cell to uptake glucose. In the control condition cells were cultured in the presence of 25mM glucose. n=3.

1.10. 2-DG treatment promotes an increase in the expression level of Glucose-6-phosphatase.

Both glucose and 2-DG are phosphorylated by hexokinase; however, in contrast to glucose 6-phosphate, 2DG-6-phosphate cannot be further metabolized and hence it accumulates until it is de-phosphorylated by a specific phosphorylase [58]. One of the phosphorylases that could be involved in 2-DG dephosphorylation is glucose-6-phosphatase (G6Pase). This enzyme is a multifunctional system that catalyzes the final step in both the glycogenolytic and the gluconeogenic pathways, cleaving phosphate from glucose-6-phosphate to liberate free glucose into the circulation. It thus regulates both circulating concentrations of glucose and the storage of excess glucose as glycogen. G6Pase complex is found in microsomes, and is composed by a catalytic subunit, facing the endoplasmic reticulum (ER) lumen, and 3 transporters (T1–3), one to move G6P into the lumen and two to allow the efflux of glucose and inorganic phosphate (Pi) out into the cytoplasm. Defects in the enzyme cause glycogen storage disease type I (von Gierke disease). Glucose-6-phosphatase-alpha (G6PC) isoform is expressed mainly in liver and kidney [62]. Astocytes are found to express the ubiquitously isoform glucose-6-phosphatase beta (G6PC3), suggesting a role of astrocytes in providing an endogenous source of brain glucose [63]. Silencing the microsomal glucose-6-phosphate transporter (G6PT) in U87 cell line, induced necrosis and late apoptosis [64]. Moreover, the gene expression of G6PT in glioma cells was reduced after treatment with concavalin A, a cytoskeleton disrupting agent, or the silencing of membrane type 1 MMP (MT1-MMP) [93-95]. G6PT has also been linked to metabolic adaptation to hypoxia in cancer cells, through the activation of HIF-1α [96]. These results suggest a role for glucose-6-phosphatase in important cellular processes different from glucose metabolism i,e, cell death and cell invasion.

In order to elucidate the role of this enzyme in our cell cultures we decided to evaluate the expression level of both G6PC and G6PC3 in the presence and absence of 2-DG. G6PC and G6PC3 expression levels in GBM derived cells (GMB612, 626 and 651) were compared to normal adult brain (NAB) and fetal brain tissue (FB). We found a generally higher G6PC3 expression level in cells simply exposed to 20% oxygen (Fig. 26A-C, control). This might be explained considering that mature astrocytes are known to express G6PC3 [63] and we previously reported that increase in astroglial differentiation occurs in GBM cells exposed to higher oxygen tension [Pistollato F. Stem cells 2009]. Also, addition of 2-DG promoted a modest

increase in the expression level of G6PC3 in GBM626 but not in GBM612 and 651 (Fig. 26A-C). There were no differences in the expression level of G6PC3 between GBM612 and normal adult brain, while fetal brain had a lower expression level compared to these two groups (Fig. 26D).

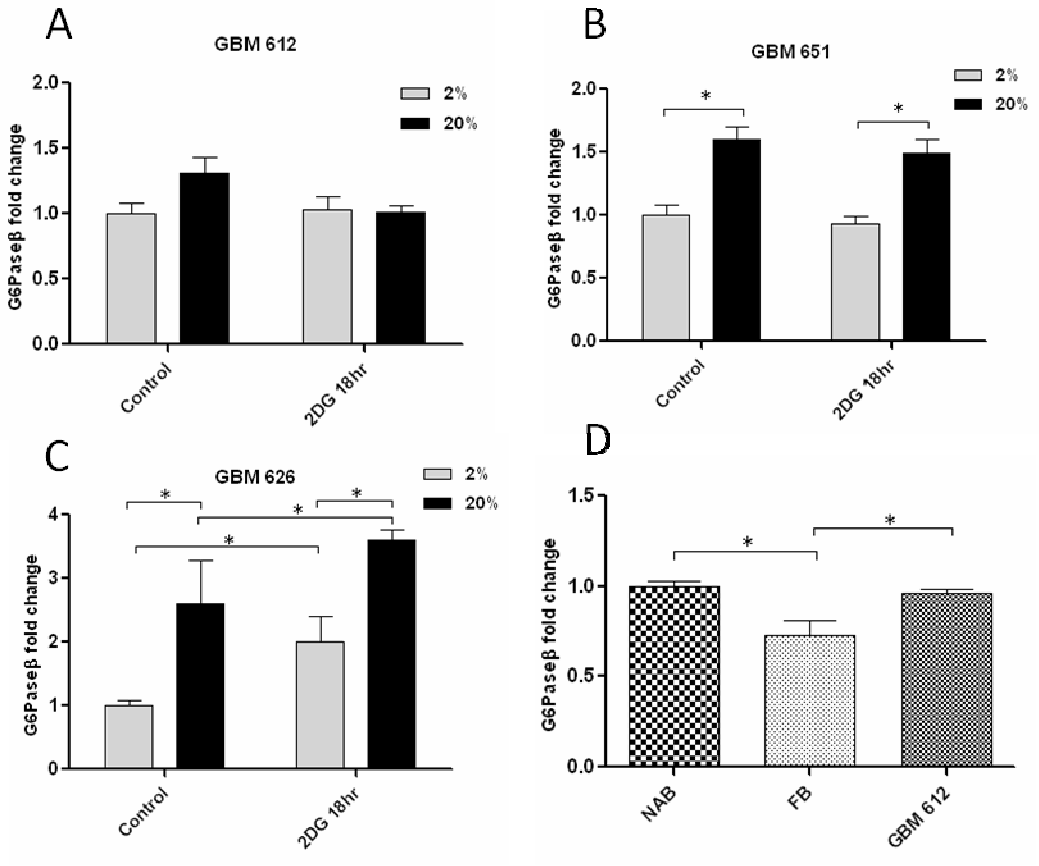

Figure 26. Quantitative RT-PCR analysis for Glucose-6-Phosphatase-β (G6PC3). (A-C) mRNA expression of G6Pase beta, measured by real-time RT-PCR in GBM612, 651 and 626. Data are represented as fold change in gene expression normalized to GAPDH and then calibrated to control 2% oxygen. (D) mRNA expression level, of G6Pase beta in Normal adult brain, fetal brain and GBM612. Data are represented as fold change in gene expression normalized to GAPDH and then calibrated to normal adult brain. Results are expressed as mean ± SEM. *< p 0.05

When we looked at the expression level of G6PC, the isoform which is found predominant in tissues like liver and kidney, alike G6PC3, we found that GBM cells exposed to 20% oxygen were characterized by a higher G6PC expression level (Fig. 27A-C, control). Moreover, a significant increase in G6PC expression level in both GBM612 and 626 occurred following addition of 2-DG (Fig. 27A-C). G6PC isoform had a very high expression level when we compared GBM612 to normal adult brain and fetal brain (Fig. 27E). Surprisingly, when cells

were allowed to recover for 72hr, after the addition of 2-DG, G6PC expression level did not decrease, eventually becoming even higher than the control level (Fig. 27D). This suggests a possible role of this enzyme in promoting a mechanism of survival from the glycolytic inhibition induced by 2-DG. Simply withdrawing glucose from the medium did not induce a significant increase of G6PC (Fig. 27F), suggesting a specific role of 2-DG in modulating G6PC expression.

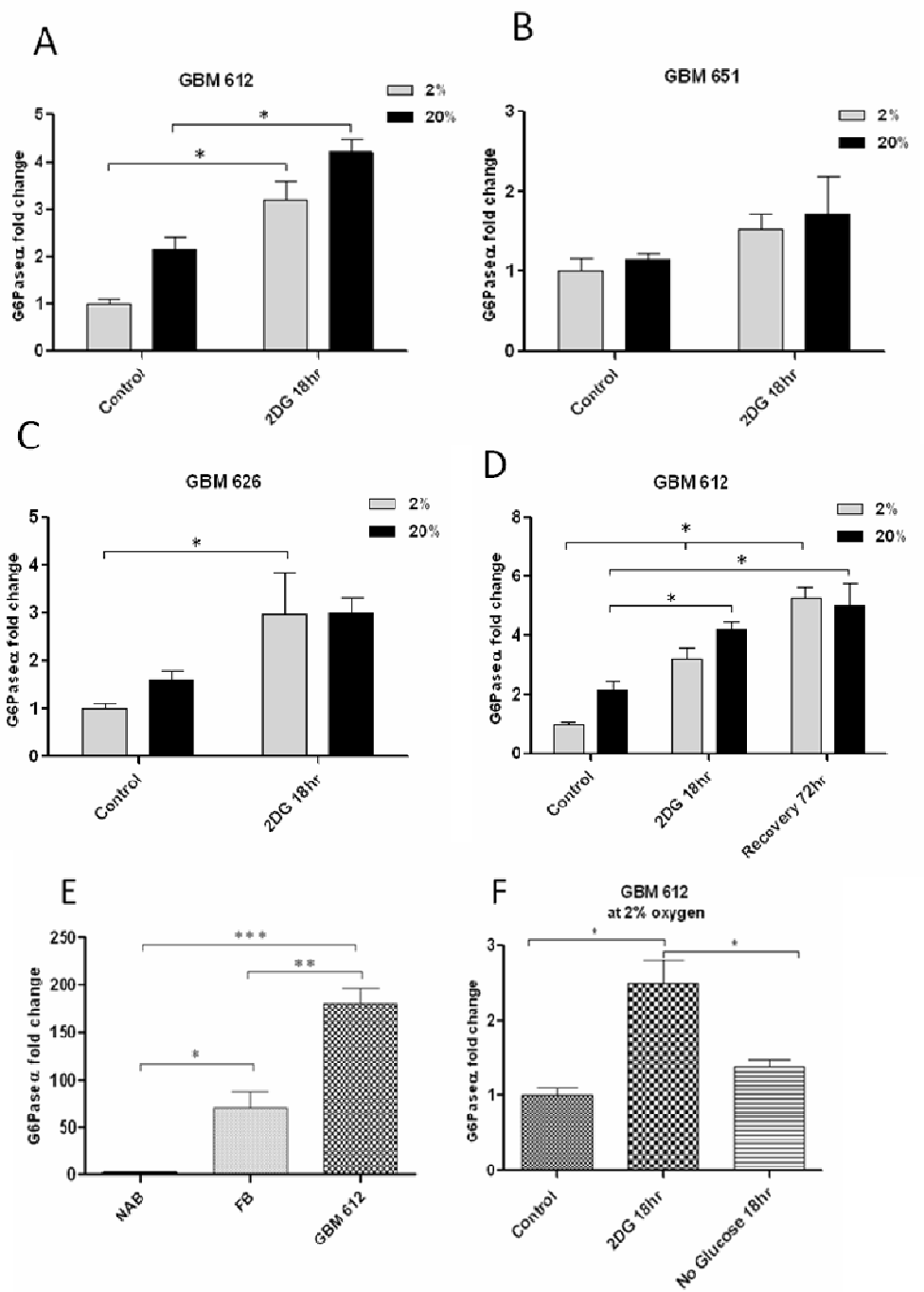

Figure 27. Quantitative RT-PCR Analysis for Glucose-6-Phosphatase-α. (A-C) mRNA expression of G6Pase alpha, measured by real-time RT-PCR in GBM612, 651 and 626. Data are represented as fold change in gene expression normalized to GAPDH and then calibrated to control 2% oxygen. (D) mRNA expression level of G6Pase alpha in control, 2-DG treated cells and 72hr recovery from 2-DG in GBM612. Data are represented as fold change in gene expression normalized to GAPDH and then calibrated to control 2% oxygen. (E) mRNA expression level of G6Pase alpha in normal adult brain, fetal brain and GBM612. Data are represented as fold change in gene expression normalized to GAPDH and then calibrated to normal adult brain. Results are expressed as mean ± SEM. *< p 0.05

We hypothesized that glucose-6-phosphatase might play a pivotal role in the pro-survival mechanism activated by GBM cells following addition of 2-DG and later recovery. In order to investigate the role of this enzyme, we treated GBM cells with Chlorogenic acid (CHL), a natural polyphenol found in tea which have been attributed possible cancer chemopreventive properties [97]. CHL inhibits endoplasmic reticulum (ER) glucose-6-phosphate (G6P) transport, and hence microsomal glucose-6-phosphatase (G6Pase) activity both in isolated microsomes [98] and *in vivo* [99]. Moreover, CHL reduces the invasion and secretion of proMMP-2 in GBM cells [64]. Our preliminary results on GBM612 showed that the addition of CHL to the recovery group decreased proliferation rate of these cells when compared to the recovery group without CHL (Fig. 28A). This result supports our hypothesis that this enzyme might be involved in the observed increase proliferation and pro-survival mechanism activated by GBM cells recovered after addition of 2-DG.

Looking at G6PC protein level , we observed that addition of 2-DG under hypoxia, while increasing G6PC mRNA level (Fig. 27A-C), , did not induce an increase also of protein level (Fig. 28B), which was slightly reduced. After 72hr of recovery, even in the presence of CHL, the protein level of G6PC was comparable to the control group (Fig. 28B). This is just a preliminary data, but it suggests that post-transcriptional modifications of G6PC mRNA might occur, whereas mRNA to protein translation is a tightly controlled process that involves different phases, each of which require a particular set of conditions and factors [100]. The identification of the involved factors will require future experimentation.

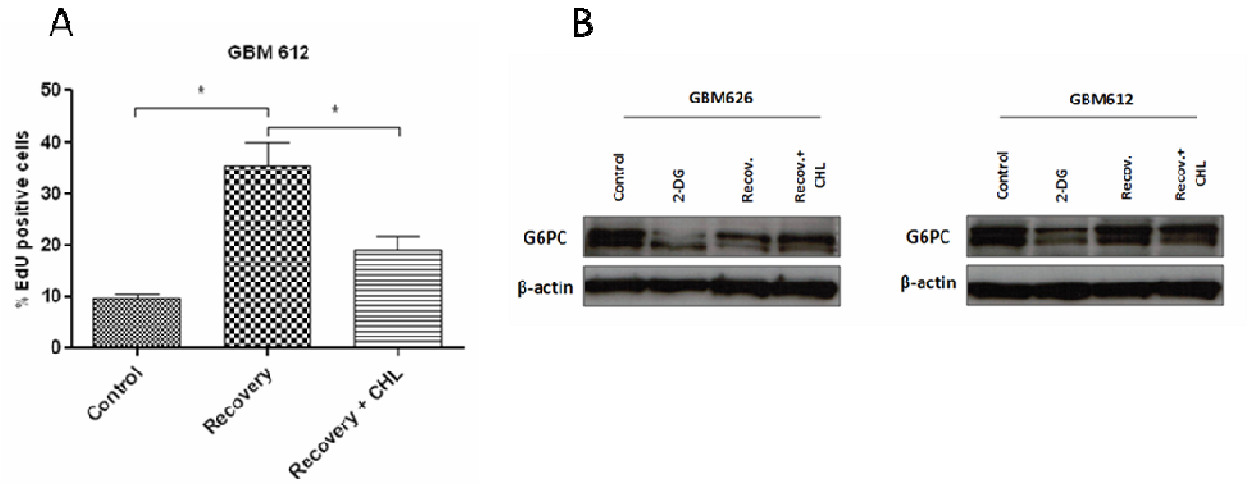

Figure 28. Inhibition of Glucose-6-Phosphatase-α by CHL inhibits pro-survival mechanism activated during the recovery phase. (A) GBM612 cells were cultured at 2% oxygen. After the addition of 2-DG for 18h cells were allowed to recover for 72hr by changing the media with 2-DG to 25mM glucose supplemented media or 25mM glucose plus 100µM CHL respectively. Results are expressed as mean ± SEM. *< p 0.05 respective to control at 2%. (B) Representative western blot images showing GBM cells cultured as described in A. Addition of 2-DG, under hypoxia, induced a decrease in G6PC protein level. After 72hr of recovery, even in the presence of CHL, the protein level of G6PC was comparable to the control group.

1.11. Addition of 2-DG decreases GBM cell migration.

A hallmark of malignant tumor cells is an increase in cell migration and invasion, promoting metastasis. These features are a result of a reduced cell–cell adhesion and an increase in the turnover of ECM. Multiple mechanisms could play a fundamental role in promoting cell migration and invasion, such as, redistribution of focal adhesion component proteins [101, 102], altered regulation of integrin signaling and decreased deposition of ECM proteins [103, 104].

To test the role that 2-DG could play in cell migration, the migratory behavior of our GBM cells was analyzed through a novel assay utilizing nano-grooves of 350 nm in width, 500 nm in depth, and evenly-spaced 350 nm apart. Prior to plating cells, nano-patterned substrata were coated with poly-D-lysine (5 µg/cm^2) for 15 minutes, followed by laminin (5 µg/cm^2) for 1 hour. The topography of the nano-patterned substrata caused cells to align and migrate parallel to the nano-grooves (Fig. 29A). Long-term observation of cell migration was performed using time-lapse microscopy, provided with a temperature/gas-regulated environmental chamber to maintain cells at 37˚C and 5% CO_2 for the duration of the experiment. Phase-contrast images were automatically recorded every 20 minutes, for 15 hours, under a 10X objective. Our preliminary results showed that the addition of 2-DG strongly decreased the ability of cells to migrate (Fig.

29B). Moreover, the recovery group had a higher capacity to migrate compared to 2DG group. In GBM626, the recovery group speed was even significantly higher than the control group. Interestingly, in all cell lines the addition of CHL decreased the speed of the recovery group (Fig. 29B).

Altogether these results suggest that the microsomal glucose-6-phosphatase (G6Pase) might play a crucial role in controlling the survival and consequentially also the migratory behavior of GBM cells following exposure to 2-DG.

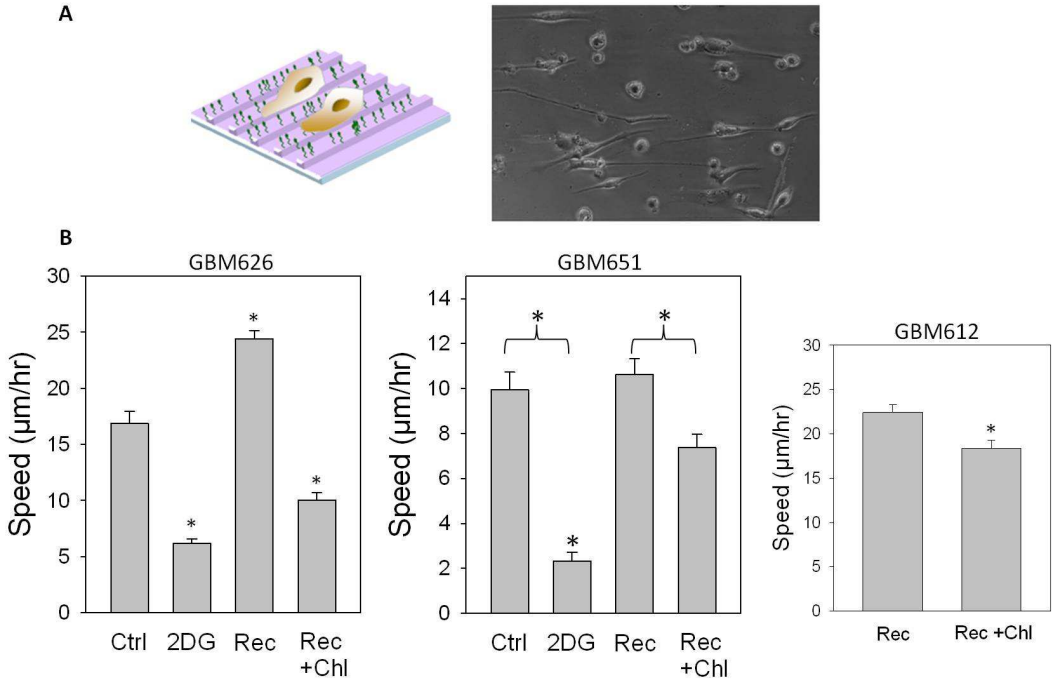

Figure 29. Addition of 2-DG decreases GBM cell migration. (A) Representative image of GBM626 cells aligned on the nano-pattern. (B) Bar graphs showing the migratory behavior of GBM626, GBM651 and GBM612. Results are expressed as mean ± SEM. *< p 0.05.

1.12. 2-DG reduces proliferative capacity of xeno-transplated GBM cells.

We next sought to investigate the migratory and invasive capacity of tumor cells in an *in vivo* model, since such abilities are critical for the lethal outcome of GBMs. We also evaluated the effects of glycolysis inhibition by 2-DG, on the growth of brain tumor cells *in vivo*, thus a survival experiment was performed. Briefly, 1.5 x10^5 cells of GBM612 were stereotactically injected into the right striatum of 20 male athymic nude mice *nu/nu*, approximately 5–6 weeks of age and weighing approximately 30g. Mice were randomized into four groups (5 animals/group).

Two groups received 2-DG pretreated cells and two groups received control cells. The next day we started daily intraperitoneal injection of 2-DG or saline solution (Table 1).

	Animals	Intraperitoneal injection
Control	10	➢ 5 animals received saline solution. ➢ 5 animals received 2-DG.
2-DG	10	➢ 5 animals received saline solution. ➢ 5 animals received 2-DG.

Table1. Experimental design

At week nine, one animal of each group was sacrificed, and coronal brain sections were stained for human specific nestin and proliferation-specific human Ki-67 (Fig. 30). All four xenograft tumor groups were associated with a big number of highly infiltrating nestin positive cells, a characteristic feature of GBM tumors, suggesting that the GBM612 cell line contains stem-like cells with a self-renewing ability (Fig. 30A).

In the adult brain, new neurons are produced in the SVZ of the lateral ventricles and the subgranular zone (SGZ) in the hippocampal [105]. From the SVZ newly generated neuroblasts migrate through a complex network of chains that merge into the rostral migratory stream (RMS) that leads into the olfactory bulb (OB). There they differentiate giving rise to a multiple types of interneurons [105]. The self-renewal, fate-choice, proliferation, migration, and differentiation of neural stem cells in the neurogenic niches are regulated by many factors such as, cell -cell interaction, diffusible signals and intimate association with endothelia cells [106, 107]. Staining for human nestin and Ki-67 revealed a large number of nestin^{+}/Ki-67^{+} cells surrounding the neurogenic niche of the right SVZ in the saline receiving mice (Fig. 30B,C). Importantly, the 2-DG receiving mice had a decrease in the number of nestin^{+}/Ki-67^{+} cells when compared to the mice receiving saline (Fig. 30D,E).

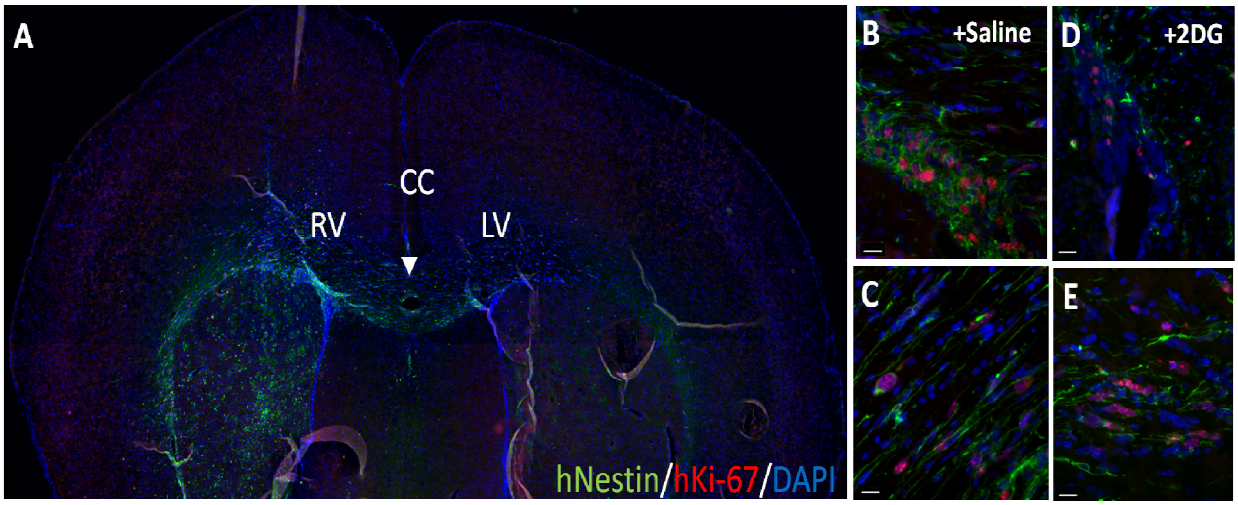

Figure 30. 2-DG reduces proliferative capacity of xeno-transplated GBM cells found both in corpus callosum and in the right ventricle. (A) Representative image of xenotransplantation of GBM612 cell line showing a large number of nestin positive cells with a highly infiltrative behavior (arrow). (B) Highly proliferative GBM cells, detected by Ki-67, were found surrounding the right ventricle of mice receiving saline via ip. (C) Proliferative GBM cells migrating through the corpus callosum of mice receiving saline via ip. (D) Decreased proliferation of GBM cells, in the right ventricle, of mice receiving 2-DG via ip. (E) Proliferative GBM cells migrating through the corpus callosum of mice receiving 2-DG via ip. Scale bar = 10 µm. Original magnification, 4x (A), 20x for (B-E). Abbreviations: (CC) Corpus callosum, (RV) Right ventricle, (LV) Left ventricle.

Moreover, nestin^{+}/Ki-67^{+} cells were also found surrounding the right RMS in the saline receiving mice (Fig.31A,C). The 2-DG receiving mice had a decrease in the number of nestin^{+}/Ki-67^{+} cells when compared to the mice receiving saline (Fig.31B,D).

The presence of GBM cells contiguous to the neurogenic niche of the SVZ and surrounding the RMS suggest that these tumor cell may utilizes important diffusible factors such as, Notch, Wnt and bone morphogenetic protein (BMP) signaling, as well as classical neurotransmitters glutamate, GABA, dopamine, and serotonin involved in supporting the lifelong self-renewal of stem cells and their production of differentiated cells [106] for their own advantage and for the maintenance of the CSC population.

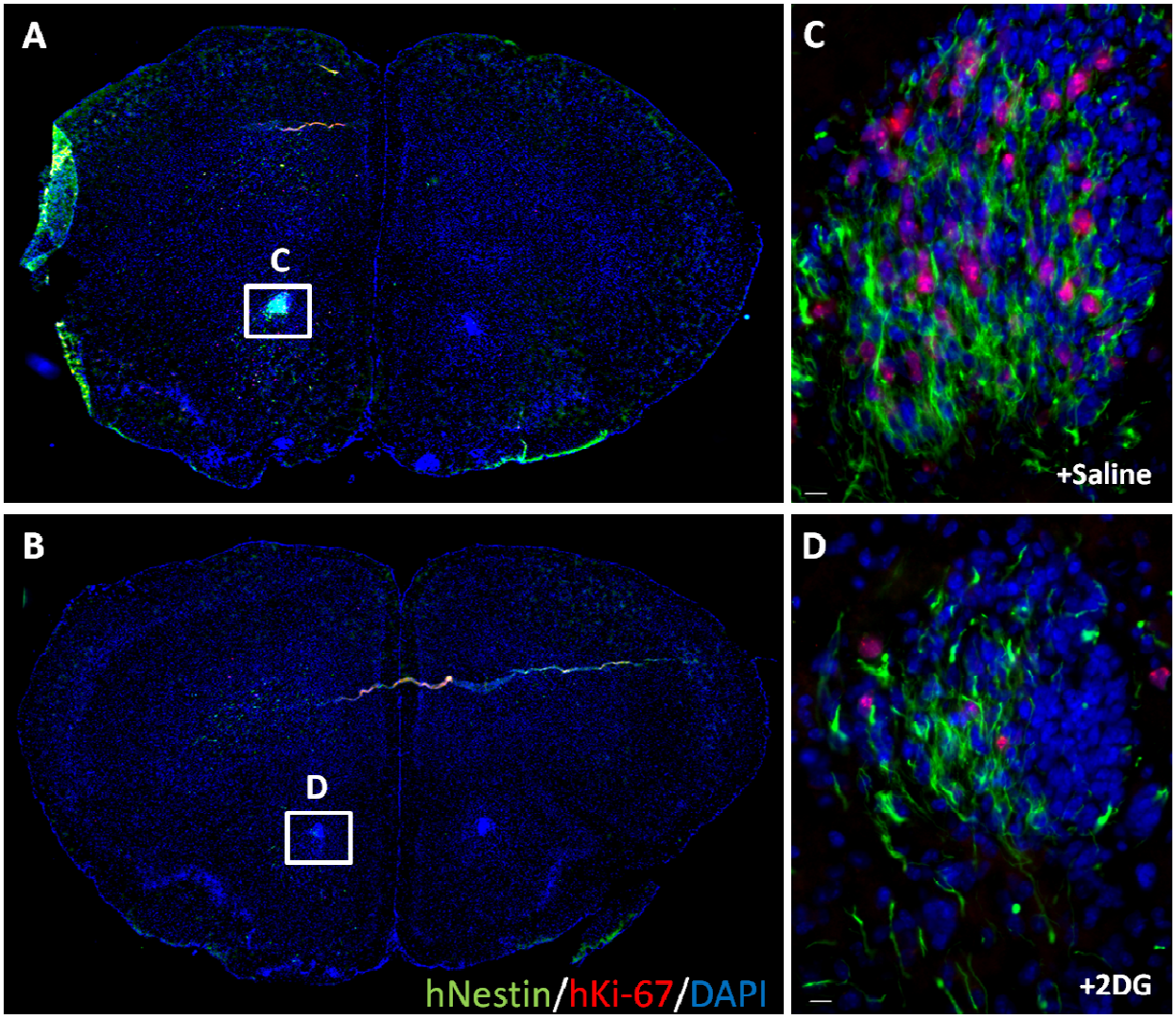

Figure 31. 2-DG reduces proliferative capacity of xeno-transplated GBM cells found the right RMS. (A) Representative image of a coronal section of xenotransplantation of GBM612 cell line showing a large number of nestin positive cells surrounding the right RMS in mice receiving saline via ip. (B). Representative image of a coronal section of xenotransplantation of GBM612 cell line showing a decrease in the number of nestin positive cells surrounding the right RMS in mice receiving 2-DG via ip. (C) Insert showing a high number of proliferative GBM cells, detected by Ki-67 surrounding the right RMS of mice receiving saline via ip. (D) Insert showing decreased proliferation of GBM cells, in the right RMS, of mice receiving 2-DG via ip. Scale bar = 10 µm. Original magnification, 4x (for A, B). Insert magnification 20x (for C and D).

We next looked at the expression of the microtubule binding protein doublecortin (DCX) which is associated with migration of neuroblasts [108]. Neuronal precursor cells begin to express DCX while actively dividing, and their neuronal daughter cells continue to express DCX for 2–3 weeks as the cells mature into neurons [108]. In the adult brain, the expression of DCX remains high within certain areas. These areas are mainly the dentate gyrus and the lateral ventricle wall

in conjunction with the rostral migratory stream and olfactory bulb [108]. Moreover, it has been shown that endogenous neural precursors have a strong tropism for GBM *in vitro* and *in vivo* and this is associated with improved survival [109]. Our preliminary results showed that GBM cells were indeed in close contact with DCX^+ mouse neuronal precursor cells , surrounding both the right ventricle and the right RMS (Fig. 32). We also found the presence of few GBM cells, migrating through the corpus callosum, which resulted to be $nestin^+/DCX^+$ (Fig. 33).

These preliminary results suggest a possible role of 2-DG in decreasing cell proliferation and hence tumor growth *in vivo*. Further *in vivo* experiments will be performed to confirm these results and to confirm the role of G6P-ase in promoting GBM cell proliferation following 2-DG treatment and consequentially grafted animals survival.

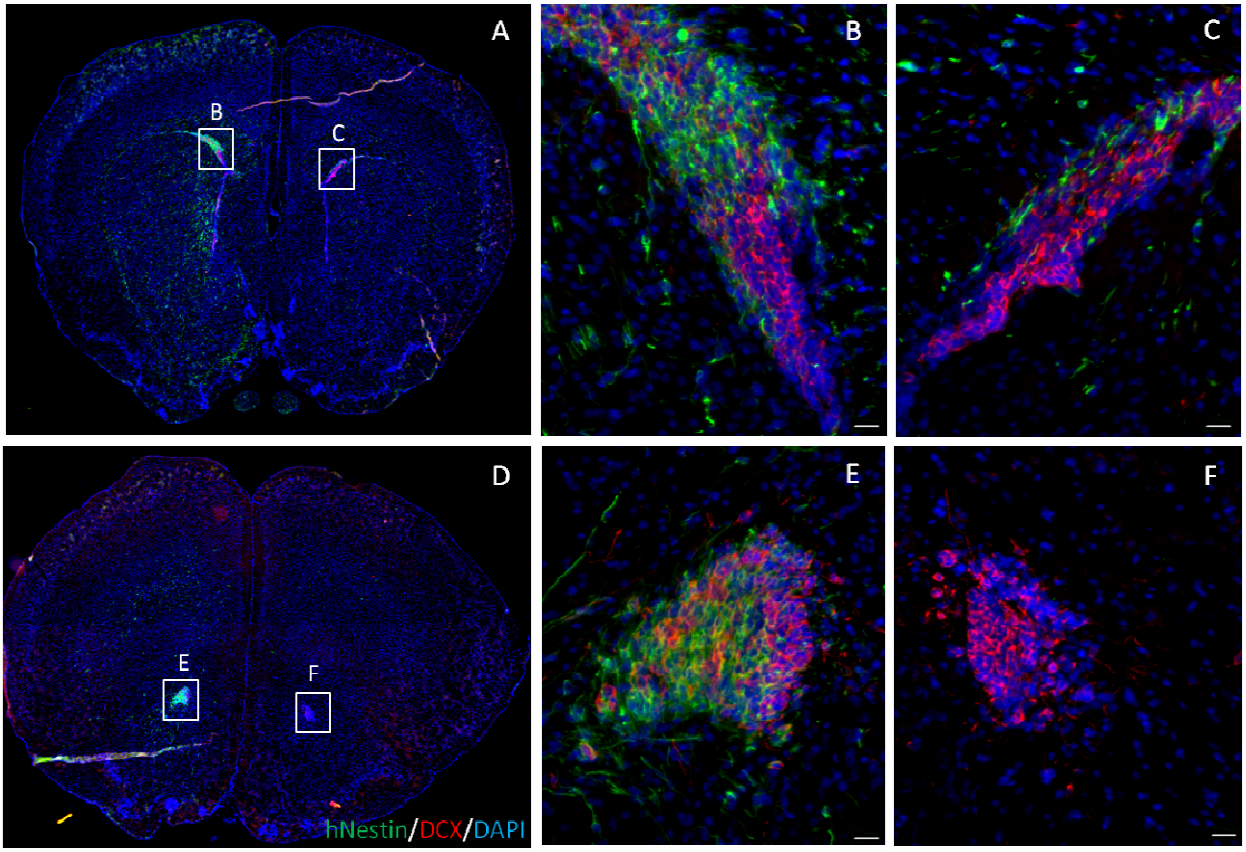

Figure 32. Xenotrasplnated GBM $nestin^+$ cells closely interact with murine DCX^+ cells. (A) Representative image of a coronal section of xenotransplantation of GBM612 cell line showing a large number of $nestin^+$ cells surrounding the right SVZ in mice receiving saline via ip. (B) Insert showing a high number of $nestin^+$ cells surrounding the right SVZ and in close relation to the mouse DCX^+ cells of mice receiving saline via ip. (C) Insert showing a few number of nestin positive cells reaching the left SVZ of mice receiving saline via ip. (D) Representative image of a coronal section of xenotransplantation of GBM612 cell line showing a large number of $nestin^+$ cells surrounding the right RMS in mice receiving saline via ip. (E) Insert showing a high number of $nestin^+$ cells surrounding the right RMS and in close relation to the mouse DCX+ cells of mice receiving saline via ip. (F) Insert showing the mouse DCX+ cells surrounding the left RMS with no nestin+ cells of mice receiving saline via ip. Scale bar = 10 µm. Original magnification, 4x (for A, D). Insert magnification 20x (for B, C, E and F).

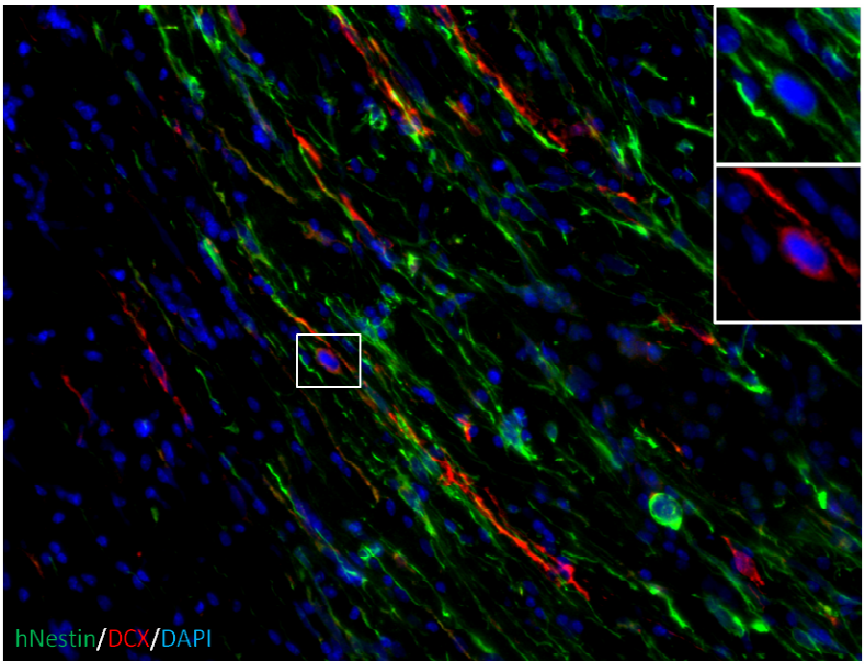

Figure 33. **Some xenotranplanted GBM cells are nestin+/DCX+.** Insert GBM cell migrating through the corpus callosum double positive for nestin+/DCX+. Magnification 20x.

RESULTS (PART II)

2.

2.1. GBM Stem Cells Are Mainly Localized in the Inner Core and in the Intermediate Layer of the Tumor Mass.

We previously reported that primary GBM-derived cells are maintained in a less committed state by hypoxia [36, 37], which preserves tumor cells under an uncommitted phenotype by inhibiting the activation of pro-differentiation signalling pathways, such as BMP and Stat3. Previous studies on primary cultures of tumor-derived cells have been performed on brain tumor samples randomly derived from tumor biopsies. To evaluate whether in the GBM tumor mass there were regional specific features, we collected specific samples from nine tumor biopsies defined through radiological imaging and image guided surgery (Fig. 34A–34C). We identified three layers, the internal core, intermediate and peripheral layers, based on the distance from the anoxic central core, to define their molecular and phenotypic features in correlation to the hypoxic concentric gradient. The intermediate portion is a thin transition area between the partially necrotic core and the peripheral area, which is defined by the presence of tumor angiogenesis (Fig. 34C).

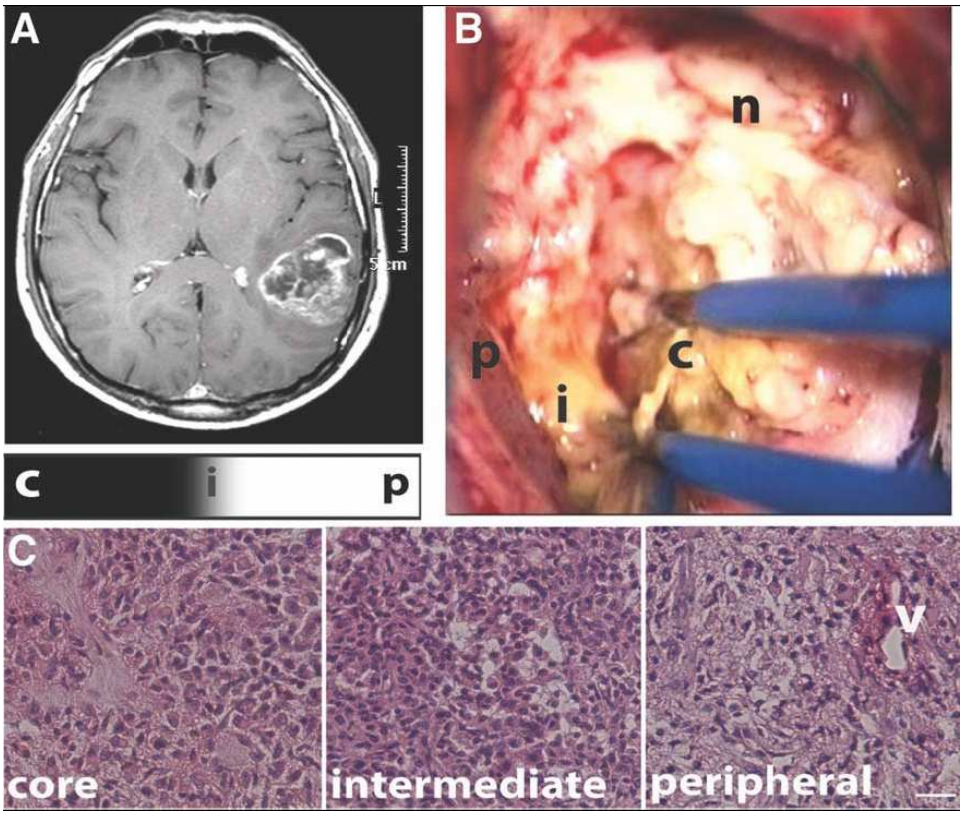

Figure 34. MRI findings and intraoperative features of a glioblastoma multiforme affected patient. (A): MRI (after gadolinium administration T1-weighted image) shows the characteristic ring enhancing lesion (HuTuP51): a hypointensive core (in black) surrounded by a hyperintensive contrast enhancing peripheral area (in white) characterized by neoangiogenesis. Below: rectangle showing a schematic representation of the three layers. (B): Surgical intraoperative image in which the three concentric layers are detectable: c, core; i, intermediate zone; p, peripheral and hypervascularized tumor layer. n, Normal brain parenchyma (HuTuP51). (C): H&E staining of the three tumor layers; v, vessels are visible in the peripheral layer. Original magnification, x20; bar = 40 µm.

Immunohistological analyses revealed that both the core and the intermediate layer were characterized by high level of HIF-1α expression (Fig. 35A) which is coexpressed with VEGF (Fig. 36A). Nevertheless, VEGF highly expressing cells, characterized by poor HIF-1 α expression, were found in the peripheral and more vascularized area of the tumor mass (Fig. 35A). To confirm the existence of a hypoxic gradient along the three tumor layers, we analyzed the expression of two well-known HIF-1α downstream target genes, the glucose transporter Glut1 [110] and the CAIX [111]. The expression of both Glut1 and CAIX was higher in the core, progressively undetectable at the periphery of the tumor (Fig. 35B,C). Also HIF-2α has been described as a major proto-oncogene in CSCs [71], nevertheless we did not find differences in HIF-2α expression among the three GBM layers (data not shown). To evaluate vascularization

distribution, we analyzed the expression of CD34, antigen constitutively expressed on endothelial cells, and we found that the peripheral area was highly enriched in CD34+ vessels (Fig. 35D), which were surrounded by GFAP+ astrocytes (Fig. 36B).

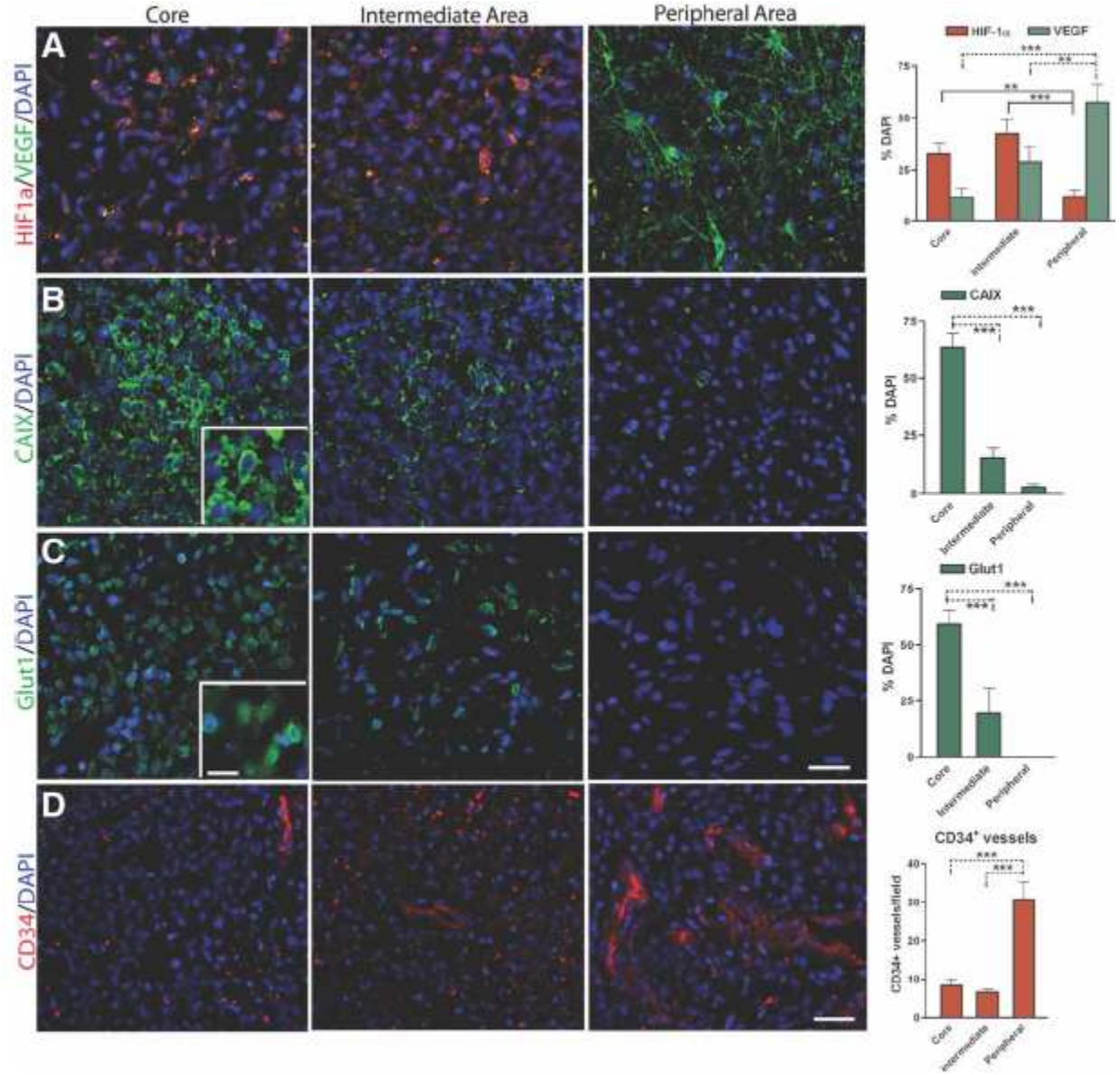

Figure 35. Presence of a hypoxic gradient within the glioblastoma multiforme (GBM) tumor mass. Representative immunohistochemical images (HuTuP55) of (A) HIF-1α (red)/VEGF (green), (B) CAIX (green), (C) Glut1 (green), and (D) CD34 (red) staining of the three GBM layers and bar graphs reporting relative quantification based on percentage of DAPI+ cells. The graphs report mean of six tumors 6 SEM, n = 1 for each tumor. Original magnification, x20; bar = 40 µm; insets magnification, x60; bar = 20 µm. Abbreviations: CAIX, carbonic anhydrase IX; DAPI, 40,6-diamidino-2-phenylindole; HIF-α hypoxia inducible factor-1α; PI, propidium iodide; VEGF, vascular endothelial growth factor.

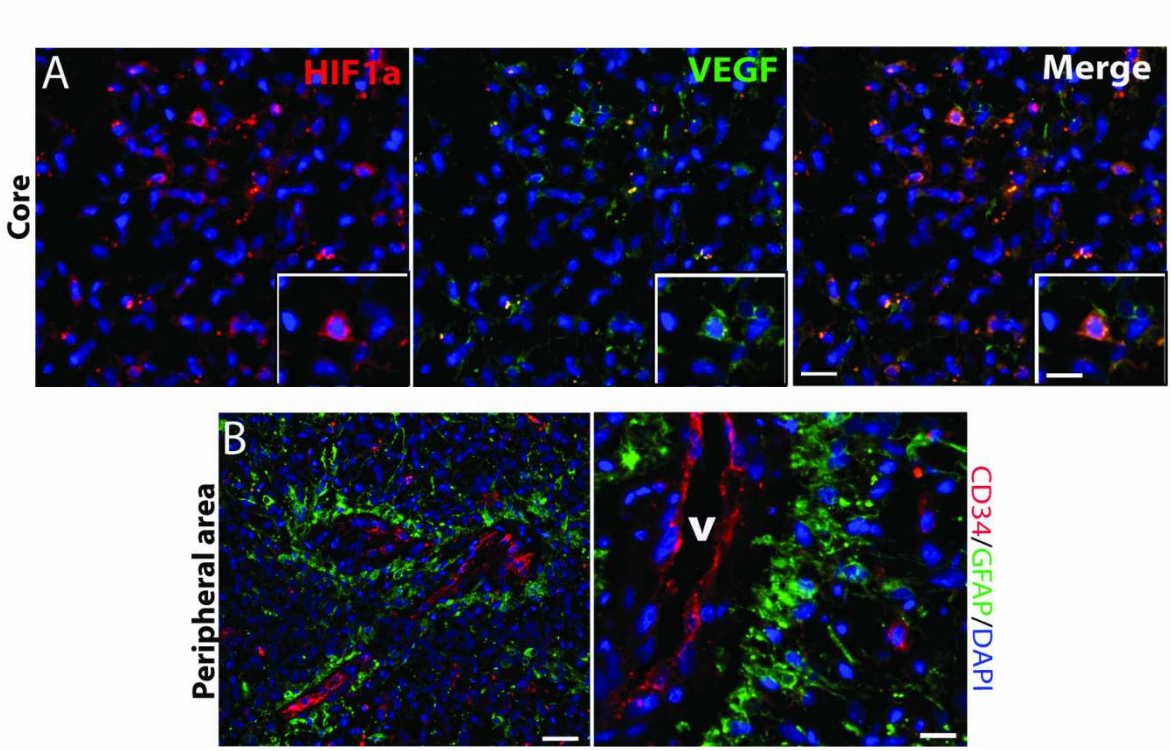

Figure 36. (A) Representative immunohistochemical images (HuTuP55) of HIF-1¤ (red) and VEGF (green) in GBM core tissue. Co-localization of both the proteins are shown. 20X magnification, bar = 40 µm; insets, 60X magnification, bar = 20 µm. (B) Representative immunohistochemical images of CD34+ vessels (v) (red) surrounded by GFAP+ astrocytes (green) in the peripheral layer (HuTuP53). Left panel, 20X magnification, bar = 40 µm; right panel, 60X magnification, bar = 20 µm.

Indeed, committed astrocytes (GFAP+; Fig. 37A) and also neurons (ß-III-Tubulin+; Fig. 37B) were mainly distributed along the peripheral layer. It has been shown that GFAP+ astrocytes, which are highly present at the tumor/normal brain interface [112], are characterized by upregulation of VEGF [113]. As we found VEGF highly expressed along the peripheral layer (Fig. 35A), we hypothesize that GFAP+ cells may be more differentiated tumor cells expressing also VEGF, especially considering VEGF distribution pattern, which mirrors GFAP+ cells morphology. Analysis of cell cycle marker Ki67 indicated that the inner core and, particularly, the intermediate-hypoxic area had the highest proliferation rate, whereas in the peripheral area, Ki67 expression was very low (Fig. 37B). Opposite to astrocytes and neurons distribution, we found that both the core and the intermediate area contained the highest level of immature nestin+ cells (Fig. 37C). These results indicate that the tumor GBM mass is characterized by a phenotypically immature anoxic core surrounded by a proliferating hypoxic layer, whereas the more vascularized and more oxygenated peripheral area is characterized by the presence of more differentiated cell types, with astroglial cells expressing pro-angiogenic signalling.

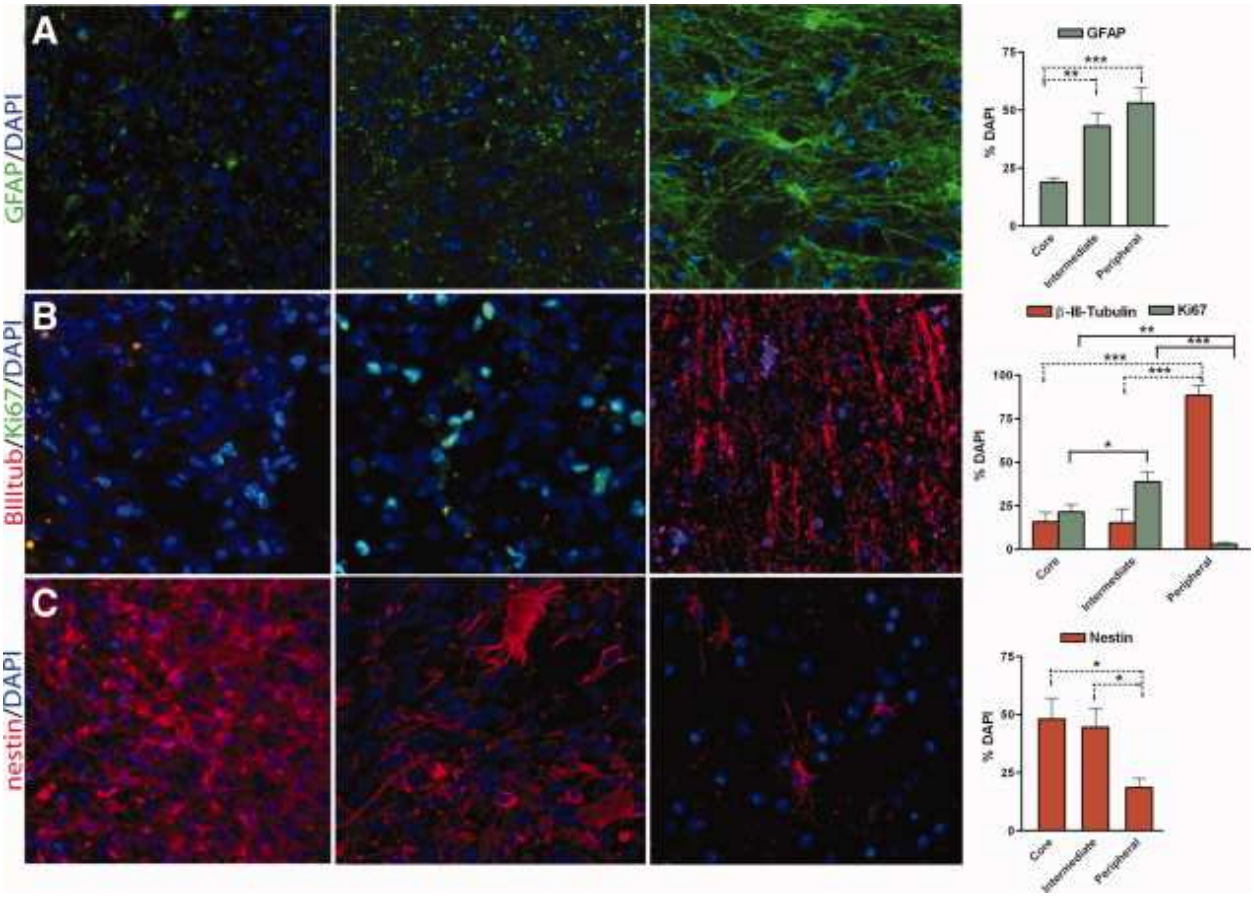

Figure 37. The three glioblastoma multiforme (GBM) layers bear phenotypic differences. Representative immunohistochemical images (HuTuP53) of (A) GFAP (green), (B) b-III-tubulin (red)/Ki67 (green), and (C) nestin (red) staining of the three GBM layers and bar graphs reporting relative quantification based on percentage of DAPI+ cells. Mean of five tumors 6 SEM, n = 1 for each tumor. Original magnification, x20; bar=40µm. Abbreviations: DAPI, 4',6-diamidino-2-phenylindole; GFAP, glial fibrillary acidic protein; PI, propidium iodide.

2.2. BMP and Akt/mTOR Signaling Result More Activated in the Peripheral Region of the Tumor.

We recently showed that pro-gliogenic BMP signaling, as seen by Smad1/5/8 activation, results to be less activated in GBM-derived cells maintained under hypoxia [36]. We also recently reported that Akt/mTOR pathway and the mTOR downstream molecule Stat3, which is correlated to BMP in promoting astrogliogenesis [114], are down-modulated in GBM cells maintained under hypoxia, and we showed that HIF-1α expression is directly implicated in this hypoxic pro-inhibitory effect [37]. Histochemical analyses of phosphorylated Smad1/ 5/8 (Fig. 38A), Akt (Fig. 38B), mTOR (Fig. 38C), and Stat3 (Fig. 38D) showed that all these pro-

differentiating signaling molecules were strongly activated mainly in the peripheral layer of the tumor mass, being barely detectable in the core and intermediate area. This confirms specific molecular signaling differences among the three concentric layers which may be causative of the observed differential phenotypic identities.

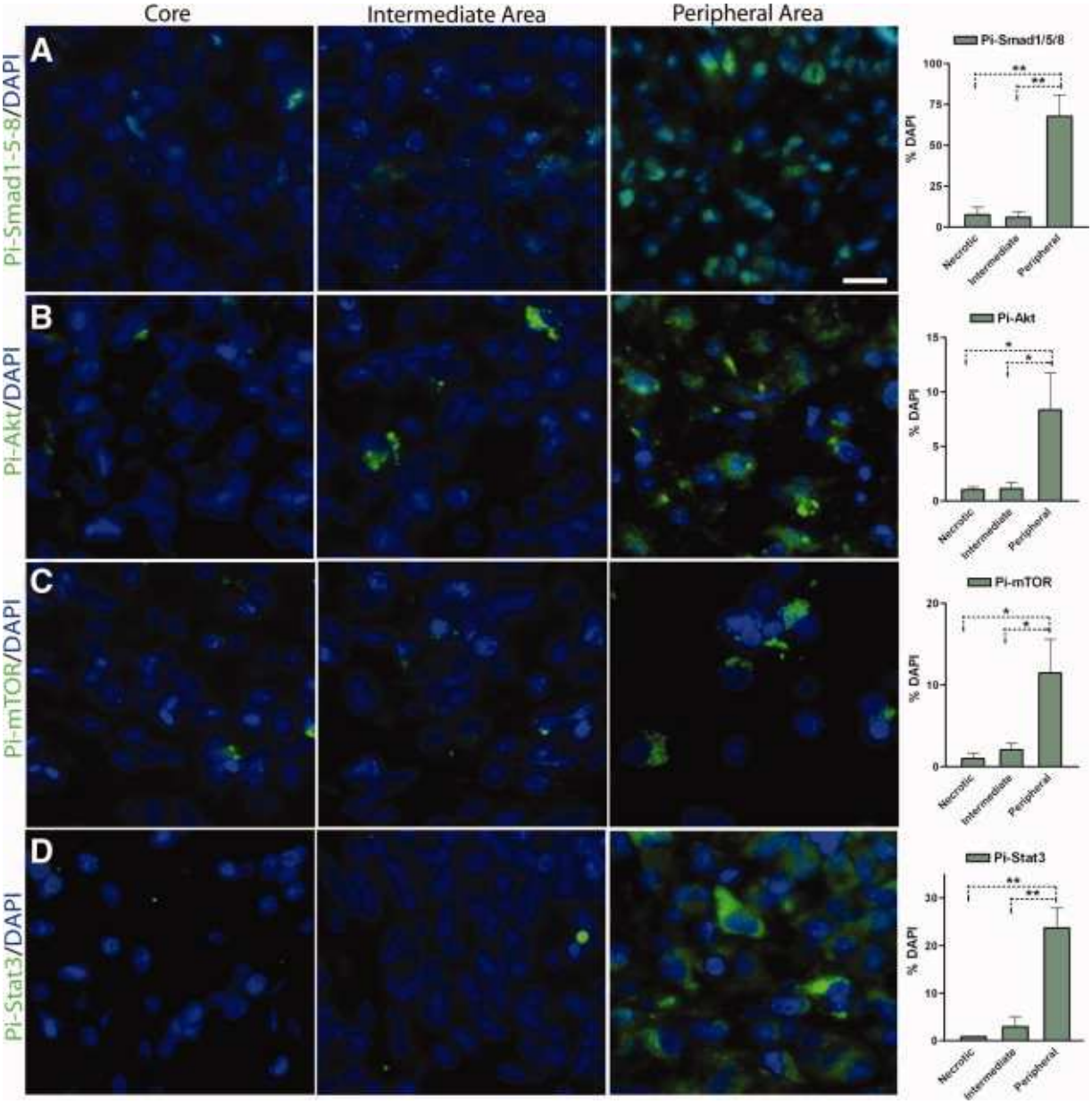

Figure 38. The three glioblastoma multiforme (GBM) layers bear differences in molecular signaling activation. Representative immunohistochemical images (HuTuP53) of (A) Phospho-Smad1 (S463/465)/Smad5 (S463/465)/Smad8 (S426/428), (B) Phospho-Akt (T308), (C) Phospho-mTOR (S2448), and (D) Phospho-Stat3 (S727) staining of the three GBM layers and bar graphs reporting relative quantification based on percentage of

$DAPI^+$ cells. Mean of five tumors ± SEM, n = 1 for each tumor. Original magnification, ×60; bar = 20 μm. Abbreviations: DAPI, 4′,6-diamidino-2-phenylindole; PI, propidium iodide.

2.3. The Majority of CD133+ Cells in the Tumor Core Expresses MGMT.

CD133 (prominin-1) expression is correlated to GBM stemness and CD133+ cells are known to recapitulate GBM tumor formation in vivo [6, 115, 116]. Moreover, CSCs seem to be the cell fraction inside the tumor bulk which is less targeted by standard treatments [5, 117, 118]. We sought to investigate CD133+ cells distribution in the three tumor areas. According to nestin+ cells localization, we found that CD133+ cells were more highly present in the inner core of the GBM mass (Fig. 39A,D). Costaining of nestin and CD133 indicate that nestin+ cells generally do not coexpress CD133 (Fig. 40). Alike CD133+ cells distribution, MGMT, a protein that confers resistance to alkylating agents, such as TMZ [67, 68], was more expressed in the inner tumor mass being barely detectable in the peripheral layer (Fig. 39B,E), where more committed cells were found (Fig. 37A,B). A recent work showed that CD133+ CSCs display strong capability on tumor's resistance to chemotherapy, as shown by the high level of MGMT and BCRP1 mRNA expression [5]. Accordingly, we found that the majority of CD133+ cells express MGMT (Fig. 39C,F). This suggests that the tumor hypoxic niche may preserve GBM stem cell identity and may regulate GBM stem cell chemoresistance.

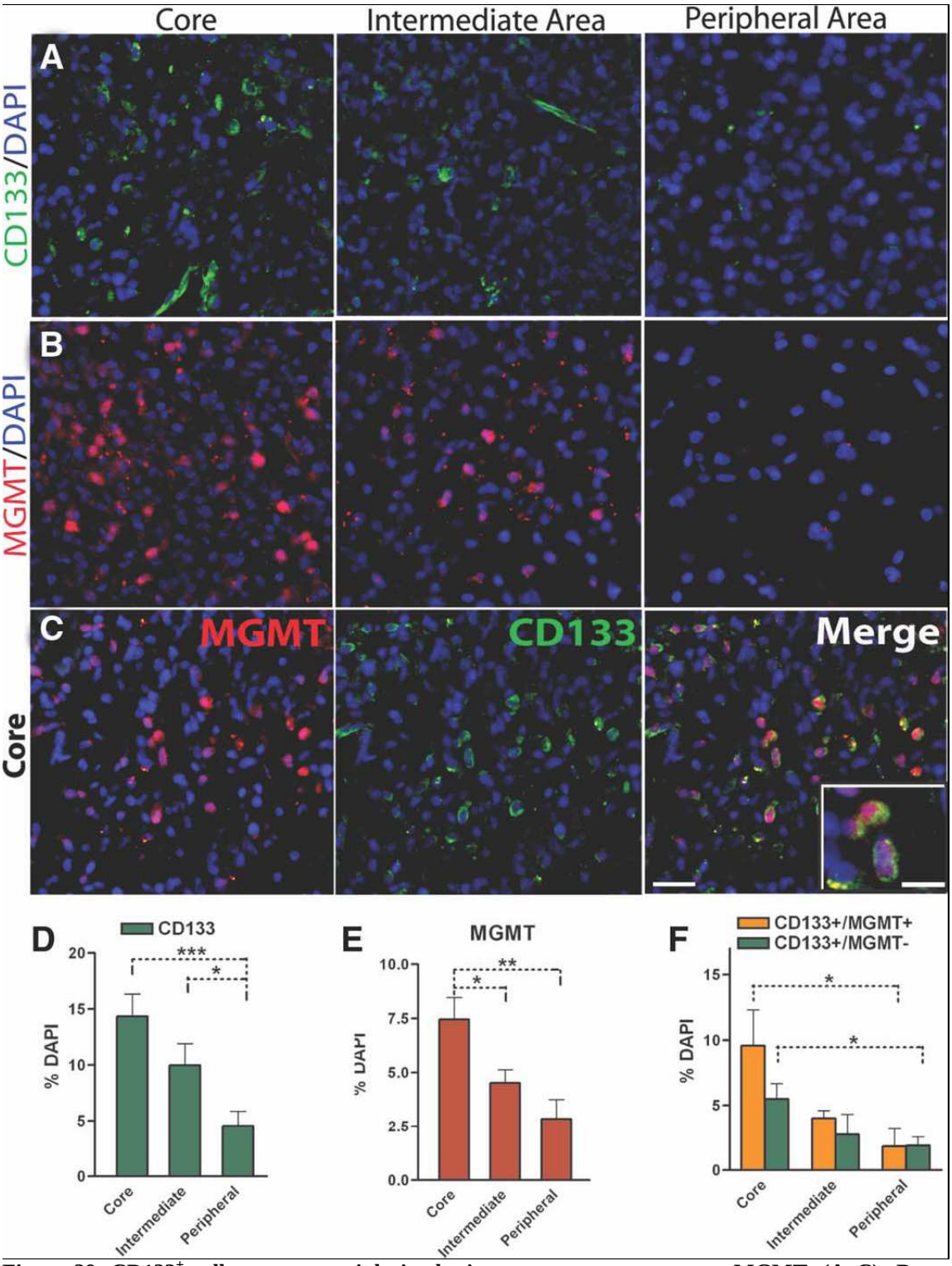

Figure 39. **CD133$^+$ cells, present mainly in the inner tumor mass, express MGMT. (A–C): Representative immunohistochemical images (HuTuP55) of (A)** CD133, **(B)** MGMT of the three glioblastoma multiforme layers, and **(C)** CD133 (green)/MGMT (red) staining in the core. **(D–F):** Bar graphs reporting relative quantification based on percentage of DAPI$^+$ cells. Mean of three tumors ± SEM, n = 2 for each tumor. Original magnification, ×20, bar = 40 μm (for **A,B,C**), inset in **C**, original magnification, ×60; bar = 20 μm. Abbreviations: DAPI, 4′,6-diamidino-2-phenylindole; MGMT, O6-methylguanine-DNA-methyltransferase; PI, propidium iodide.

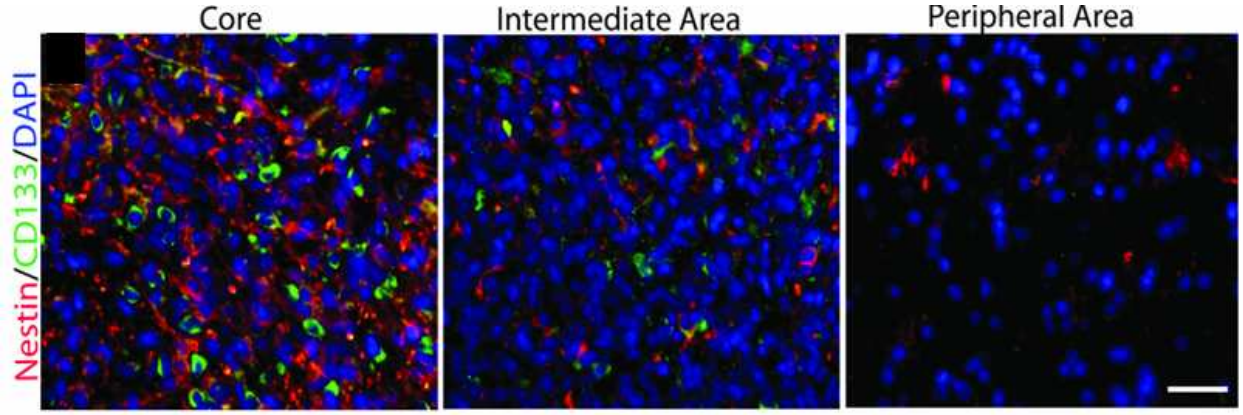

Figure 40. **Representative immunohistochemical images (HuTuP67) of CD133 (green)/nestin (red) staining of the three GBM layers**. The analysis has been confirmed on 2 additional tumors. 20X magnification, bar = 40 μm.

2.4. The Three GBM Layers Retain Phenotypic Identity and Molecular Signaling Activation Even After Single Cell Dissociation.

We sought to investigate whether GBM cells, obtained from the dissociation of the three tissue types, maintained their specific phenotypic and molecular features in our hypoxic (1.5% O2) in vitro culturing conditions. Tumor cells derived from the intermediate area tended to form neurospheres (Fig. 41A) and displayed the highest proliferation rate (Fig. 41B), confirmed also by Ki67 expression (Fig. 3B), compared with cells from the core and from the peripheral area (Fig. 41B). Conversely, cells from the peripheral area appeared more morphologically differentiated (Fig. 41A). Moreover, cells recovered from the intermediate layer resulted to form the highest number of big size neurospheres, whereas cells from the inner core formed small size neurospheres; oppositely, cells derived from the peripheral area did not generate neurospheres but rapidly differentiated (Fig. 41A,C). These results support the assumption that stem cells, which we found to be mainly located within the inner core, are characterized by a lower proliferation rate compared with committed precursors [6]. Flow cytometric analyses of CD133 and CD24, the latter indicative of neuronal commitment [119], and immunocytochemistry analyses of nestin, GFAP, and ß-III-tubulin revealed that GBM cells derived from the core and from the intermediate layer retained an immature phenotype, whereas the peripheral area contained the highest percentage of committed cells, particularly, $CD133^{-}$/CD24+ and GFAP+ cells (Fig. 41D,E). Moreover, total protein analyses showed that cells derived from the peripheral area had the highest level of activated Smad1/5/8, Akt, mTOR, and Stat3 (Fig. 41F). Conversely, total Akt, total mTOR, total Stat3, and total Smad1/5/ 8 resulted to be stable when expressed

comparing the three layers (Fig. 42), suggesting that the differences among the three cell types were more related to diverse protein activation state. These molecular signalling activations are indicative of cell commitment, as confirmed also by a higher expression of $p21^{cip1}$, involved in cell cycle arrest and induction of differentiation (Fig. 41F). Conversely, cells from the inner core, similar to the original tumor tissue, retained the highest MGMT protein level (Fig. 41F) compared to the other cell types. Together these results indicate that the three tumor cell areas maintain their phenotypic and molecular identity even after cell dissociation and appropriate in vitro culturing.

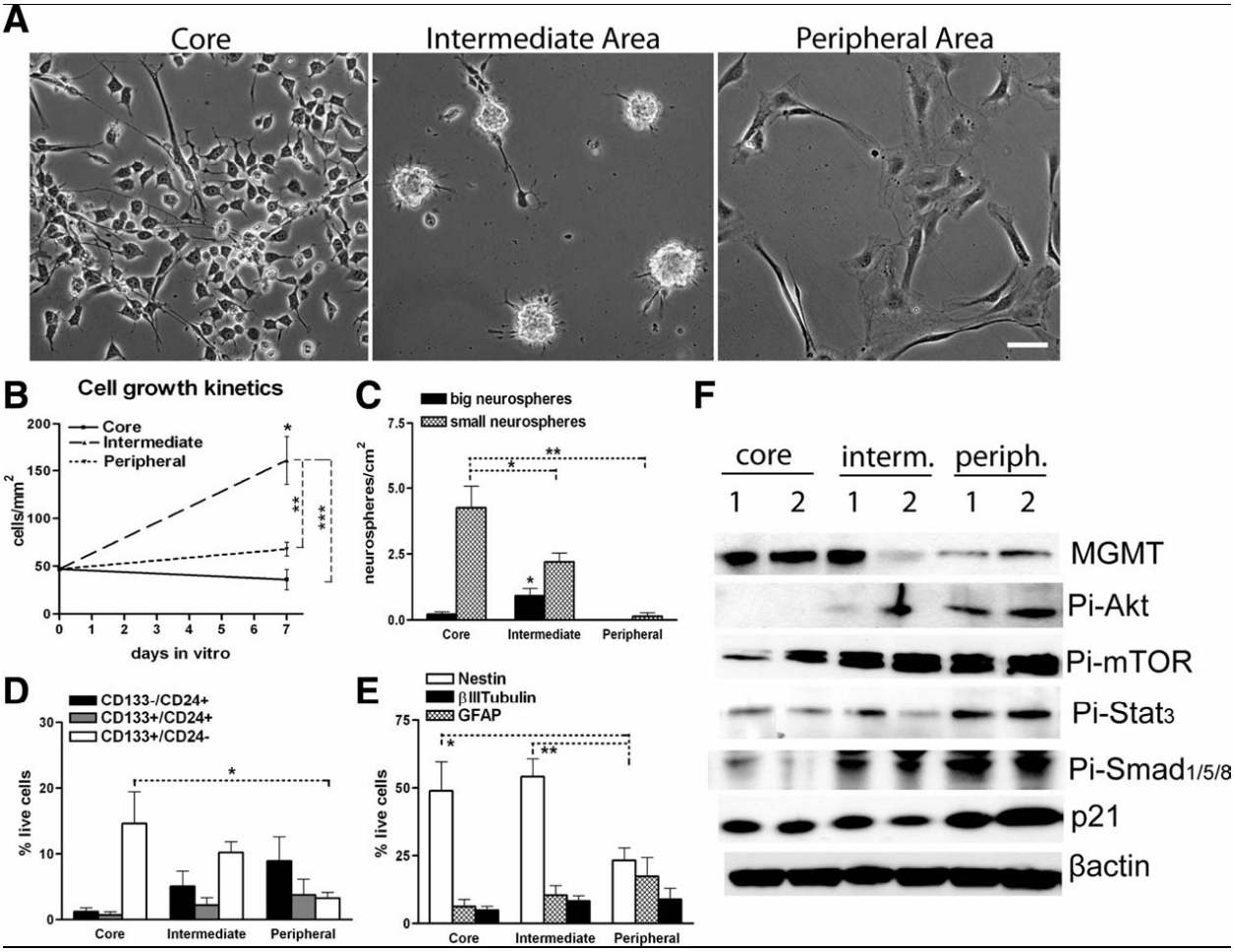

Figure 41. Phenotypic identity and molecular signaling activation state of tumor cells derived from the dissociation of the three glioblastoma multiforme (GBM) layers. (A): Representative pictures of GBM cells (HuTuP56) derived from the dissociation of the core, the intermediate, and the peripheral area. GBM cells were plated at medium density (T0 = 47 cells per millimeter squared) at 1.5% O_2. Pictures were taken after seven days in expanding culture conditions. Original magnification, ×20; bar = 40 μm. **(B):** Cell growth kinetics: GBM cells plated at medium density (T0 = 47 cells per millimeter squared) and after 7 days the cells were collected and counted by using trypan blue staining. Mean of 7 tumors ± SEM, *n* = 3 for each tumor. **(C):** Neurospheres forming assay: cells were plated a clonal density (35 cells per centimeter squared) and let grow for 7 days before

neurospheres counting; neurospheres were classified as small and big size. **(D):** Histogram showing percentages of $CD133^{+}/CD24^{-}$, $CD133^{-}/CD24^{+}$, and $CD133^{+}/CD24^{+}$ subpopulations, based on expression of cell surface antigens CD133 and CD24 in live gated cells (based on physical parameters, side scatter, and forward scatter). Mean of seven tumors ± SEM, $n = 2$ for each tumor. **(E):** Immunocytochemistry: histogram showing respectively nestin, β-III-tubulin, and GFAP quantitations relative to total live $DAPI^{+}$ cells. Cells were plated at medium density (47 cells per millimeter squared), expanded 3-day in 1.5% O_2. Mean of seven tumors ± SEM, $n = 2$ for each tumor. **(F):** Representative western blot analyses (HuTuP56) of MGMT, Pi-Smad1/5/8, Pi-Akt, Pi-mTOR, Pi-Stat3, $p21^{cip1}$ along with β-actin to control for protein loading, in GBM cells derived from two samples (one and two) of the same tumor representative of each tumor layers (core, intermediate, and peripheral). The analysis has been confirmed on five additional tumors. Abbreviations: GFAP, glial fibrillary acidic protein; MGMT, O6-methylguanine-DNA-methyltransferase.

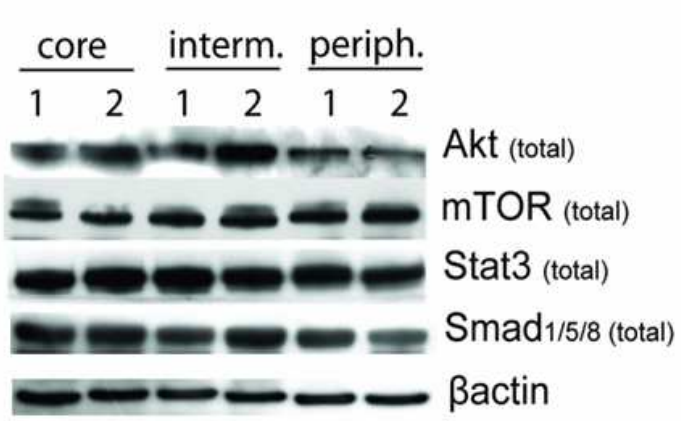

Figure 42. Total Akt, mTOR, Stat3 and Smad do not change among the three tumor layers. Representative western blot analyses (HuTuP56) of total Smad1/5/8, total Akt, total mTOR, total Stat3, along with β-actin to control for protein loading, in GBM cells derived from two samples (1 and 2) representative of each tumor layers (core, intermediate, peripheral). The analysis has been confirmed on 3 additional tumors.

2.5. GBM Cells Derived From the Inner Core and From the Intermediate Layer Are Resistant to TMZ.

Given the differential expression of MGMT within the tumor mass and retained even after tumor tissue dissociation, we sought to evaluate whether TMZ treatment (48 hours) was differentially affecting GBM cells derived from the three layers. We found that cells recovered from the peripheral area were the most responsive to TMZ (Fig. 43A,B), undergoing a significant increase of apoptosis, as shown by the higher percentage of annexin V+/PI^{-} cells, representative of early apoptotic cells. Oppositely, cells derived from the core and the intermediate layers poorly responded to treatment (Fig. 43A,B). By extending the time of TMZ treatment (72 hours), the differences in TMZ resistance among the three layers were unchanged (data not shown).

Induction of apoptosis is often followed by disruption of mitochondrial membrane potential (Dψmt), which can be analyzed by using the fluoresecent probe JC-1. We found that Dψmt

reduction was occurring specifically in cells obtained from the peripheral layer (Fig. 43C; Fig. 44), confirming the specific TMZ effect on these cell types.

To confirm the role of MGMT in determining resistance to TMZ, we treated GBM cells from the core and from the intermediate layer with 6-BG (50 μM) for 48 hours, used alone and combined with TMZ. 6-BG concentration has been based on previous report [4]. 6-BG is a nontoxic pseudosubstrate inhibitor of MGMT, already used in several studies and clinical trials either alone [120] or in combination with the maximum-tolerated dose of chemotherapy [121]. 6-BG used alone did not affect cell viability (Fig. 43D,E); by using 6-BG combined with TMZ, the sensibility to TMZ in cells derived from both core (Fig. 43D,E and Fig. 44B) and intermediate area (not shown) was significantly improved. Moreover, particularly CD133+ cells from the core (Fig. 43F), which are the ones characterized by the highest expression of MGMT, and CD133+ cells from the intermediate layer (not shown) underwent apoptosis following co-treatment with 6-BG and TMZ, being insensitive to TMZ alone (Fig. 43F). Together these data confirm the role of MGMT in determining unresponsiveness to TMZ, especially in GBM stem cells from the inner portions of the tumor mass.

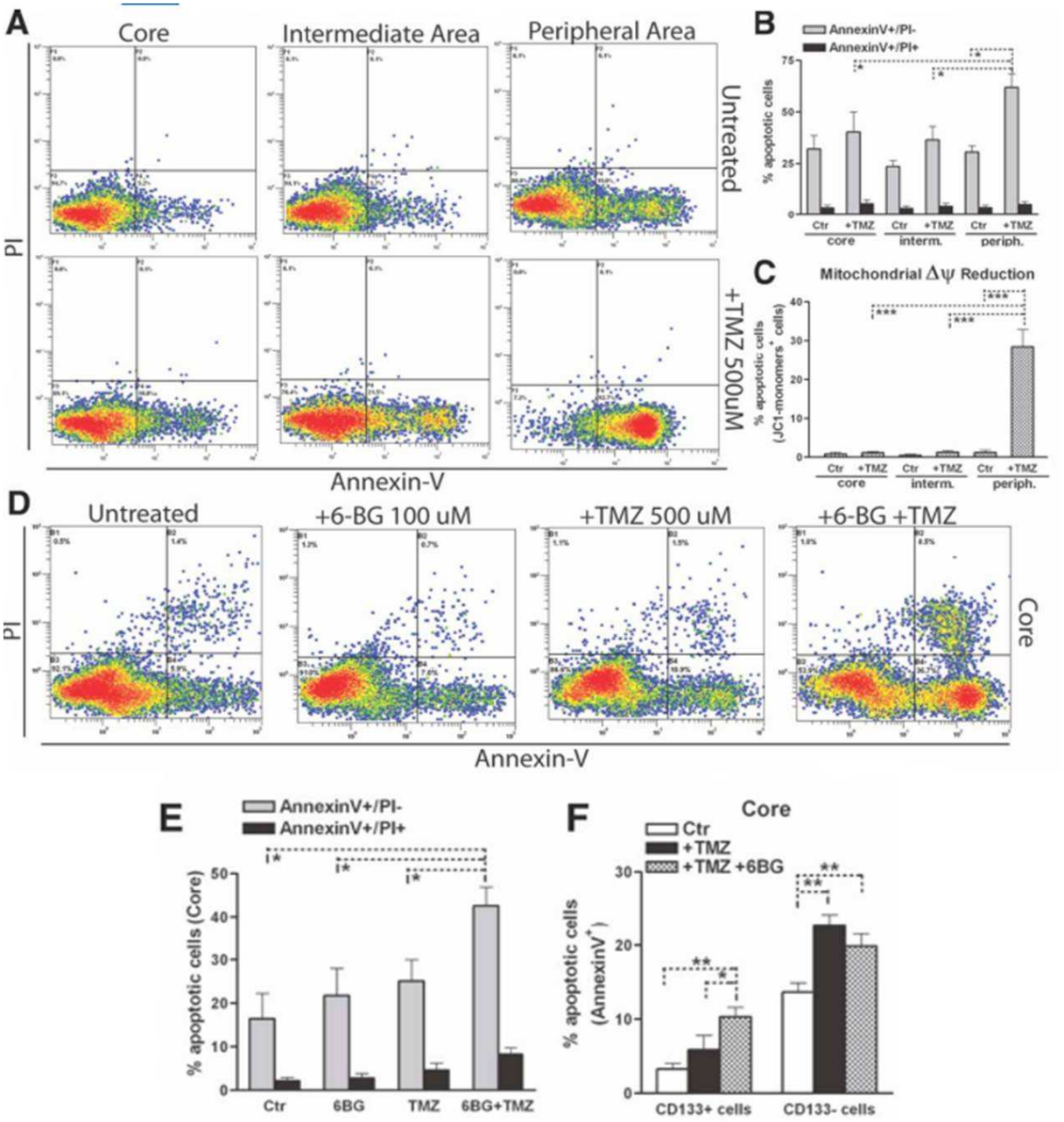

Figure 43. GBM cells derived from the inner core and from the intermediate layer are insensitive to TMZ. (A): Representative analysis of Annexin-V/PI staining (HuTuP52) comparing cells derived from the three GBM areas that have been treated with TMZ (500 μM, 48 hours) or left untreated. **(B):** Bar graph showing quantification of early apoptotic cells (Annexin-V^+/PI^-) and late apoptotic cells (Annexin-V^+/PI^+). **(C):** Bar graph showing percentage of GBM cells containing JC-1 monomers, indicative of reduced Δψmt (i.e., apoptotic cells). For both analyses, mean of three tumors ± SEM, $n = 3$ for each tumor. **(D):** Representative analysis of Annexin-V/PI staining (HuTuP64) comparing cells derived from the core that have been left untreated, treated with 6-BG (50 μM) alone, TMZ alone, or both TMZ and 6-BG. **(E):** Bar graph showing quantification of early apoptotic cells and late apoptotic cells comparing the four conditions described in **D**. **(F):** Bar graph showing percentage of Annexin-$V^+/CD133^+$ and Annexin-$V^+/CD133^-$ in cells derived from the core that have been treated as described in **D** (6-BG alone not shown). For these analyses, mean of three tumors ± SEM, $n = 3$ for each tumor. Abbreviations: 6-BG, (6)-benzylguanine; c, core; DAPI, 4′,6-diamidino-2-phenylindole; GFAP, glial fibrillary acidic protein; HIF-1α, hypoxia inducible factor-1α; i, intermediate layer; MGMT, O6-methylguanine-DNA-methyltransferase; p, peripheral-vascularized area; PI, propidium iodide; TMZ, temozolomide; VEGF, vascular endothelial growth factor.

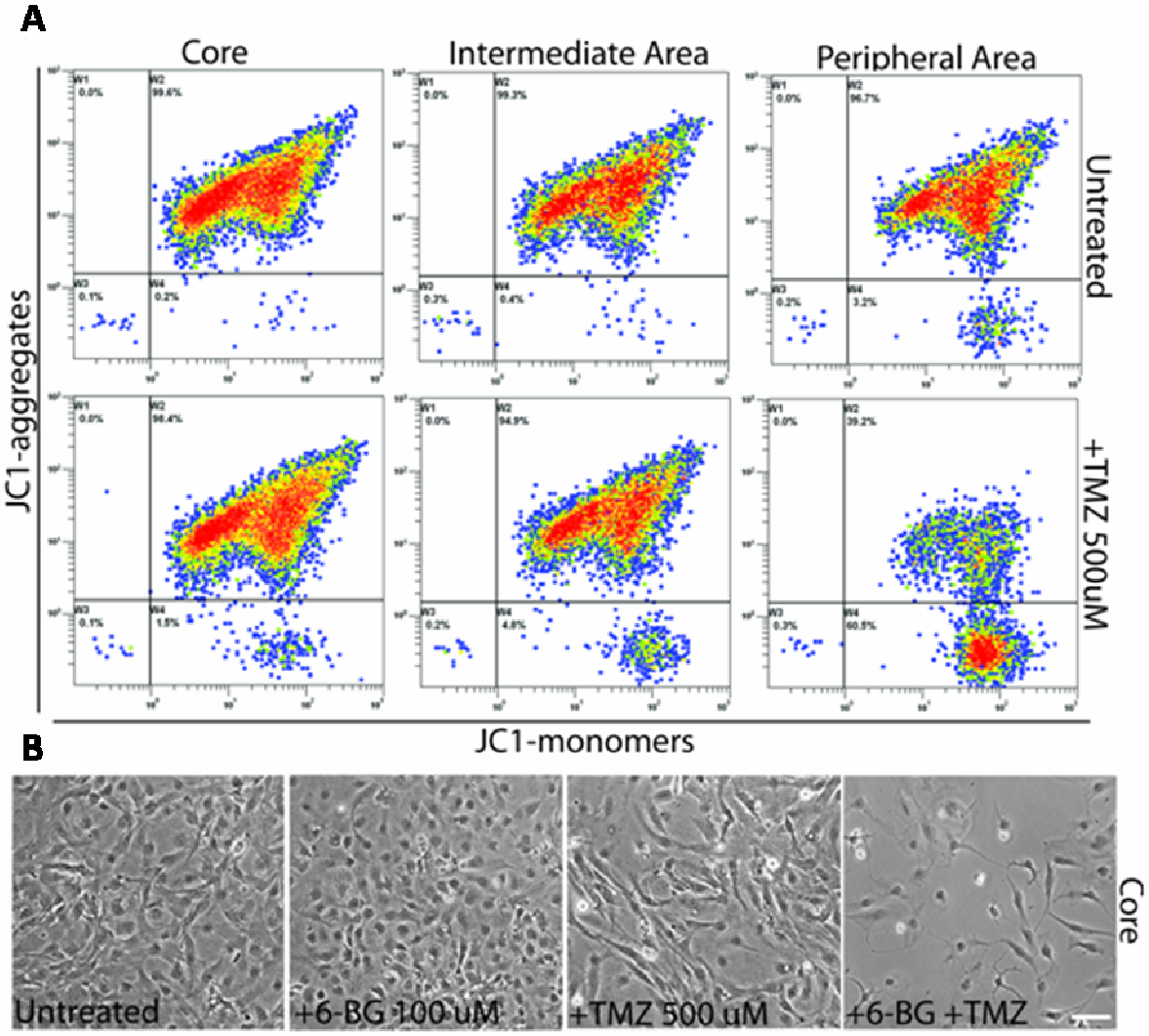

Figure 44. (A) Representative citofluorimetic analysis (HuTuP52) of Δψmt by using the fluorescent probe JC-1. (B) Representative pictures of GBM cells (HuTuP64) derived from the dissociation of the core, cells were plated at medium density (T0 = 47 cells/mm2) at 1.5% O2. Pictures were taken after 48 hr treatment with 6-BG alone, TMZ alone and both TMZ and 6-BG, compared to untreated cells. 20X magnification, bar = 40 μm.

To evaluate whether TMZ treatment affected normal (non tumor) cells, we tested TMZ on normal postnatal SVZ-derived cells, already used to perform comparison experiments with GBM [37]. We found that SVZ cells were not significantly affected by TMZ, and addition of 6-BG did not raise TMZ sensitivity (Fig. 45A–C).

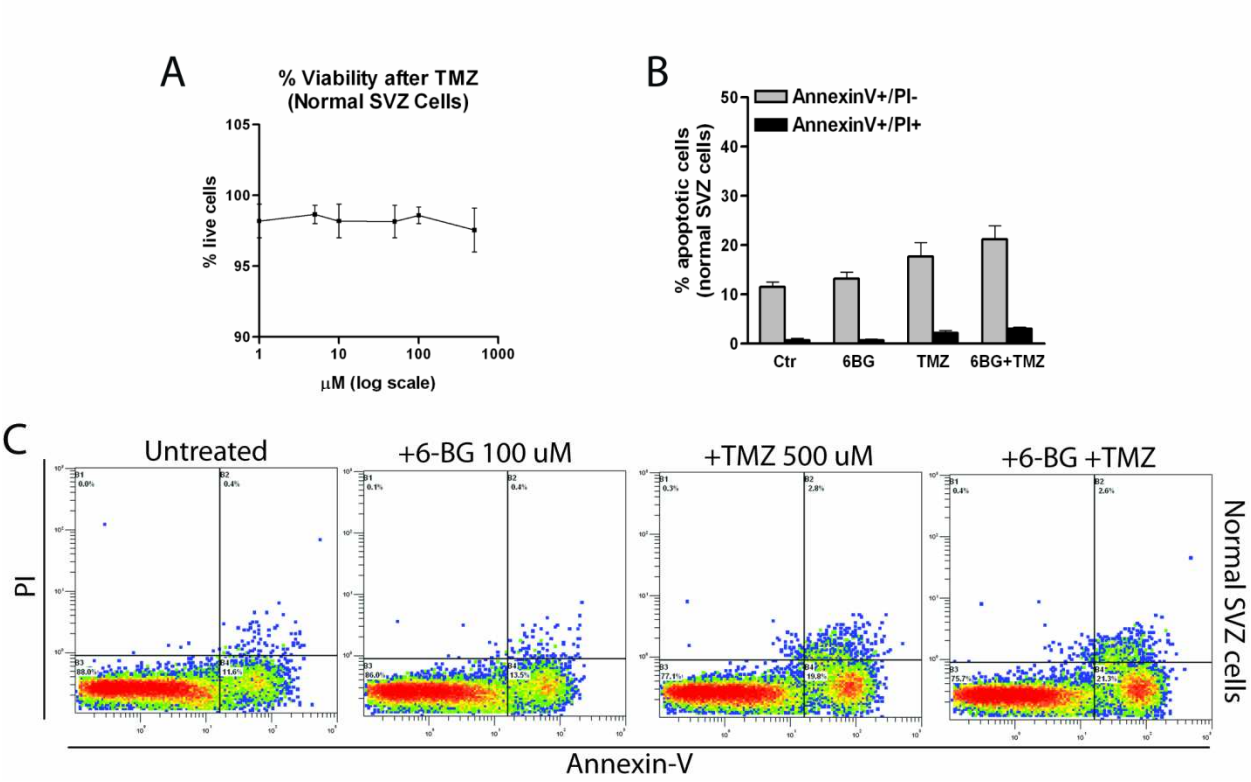

Figure 45. SVZ derived cells do not respond to TMZ treatment. (A) Dose response analysis of TMZ treatment on SVZ cells. Percentage of viable cells has been counted by trypan blue exclusion. The same doses of TMZ described in Suppl. Fig. 3A have been tested. Mean of 2 normal cell cultures ± S.E.M., n = 1. (B) Bar graph showing quantification of early apoptotic cells and late apoptotic cells comparing SVZ-derived cells that have been left untreated or treated with TMZ (500 µM, 48 hr), 6-BG (50 µM, 48 hr) or a combination of both. Mean of 2 different normal cell cultures (HuSC23 and HuSC30) ± S.E.M., n = 2. (C) Representative analysis of Annexin-V/PI staining (HuSC23) comparing the four conditions described in B.

In conclusion, our data show that intratumoral hypoxia maintains a reservoir of CD133+ stem cells in an anatomically well-defined GBM tumor area (Fig. 46). Importantly, cells derived from the inner GBM core are resistant to TMZ; this tumor fraction is enriched in CSCs, characterized by a high MGMT expression, which is causative of chemoresistance. Oppositely, GBM cells obtained from the more vascularized and differentiated region of the tumor mass result to be highly affected by TMZ.

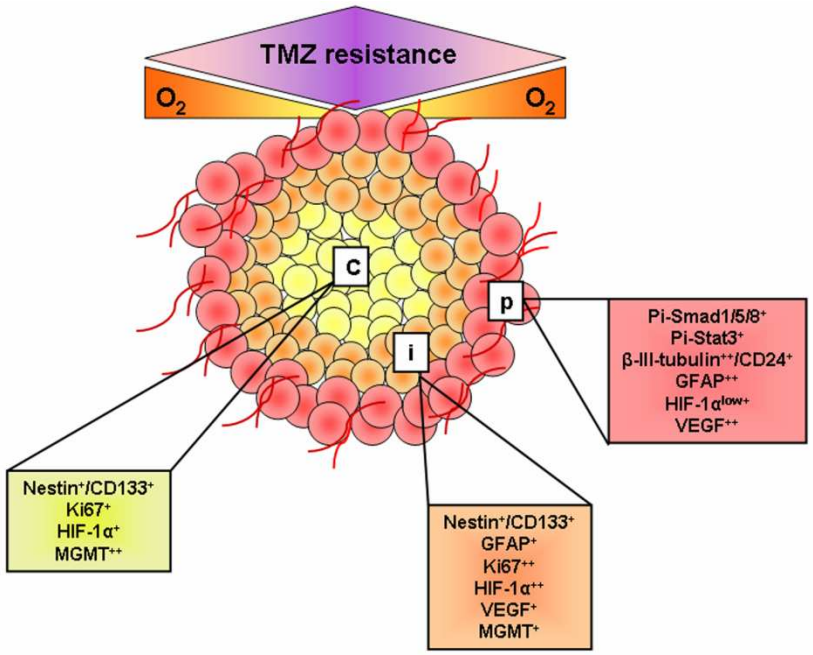

Figure 46. Graphic representation summarizing the phenotypic and molecular characteristics of the three layers constituting the GBM tumor mass.

DISCUSSION

There have been increasing efforts to characterize the solid tumor microenvironment and to define which signaling molecules and metabolic responses may be disrupted in tumor cells. As the most primitive tumor cells share characteristics with non tumor stem cells [122], the microenvironment that regulates stem cell self-renewal and differentiation may also play a role in the proliferation and fate of tumor cells. In particular, there is evidence that hypoxia plays a key role in normal homeostasis of stem cells [38] and in the initiation, development and aggressiveness of gliomas [123]. Accordingly, our recent report confirmed that intratumoral hypoxia drives GBM stem cells distribution [124]. Hypoxia could be crucial to recruit cancer stem-like cells, deregulating their differentiation [30, 31, 36] and altering their metabolism, by increasing tumor glycolytic response and reducing mitochondrial metabolism. Particularly, among mitochondrial dehydrogenases, SDH has been found inactive in some solid tumors, and this has been described as a key event leading to the accumulation of intra-cytoplasmic succinate and ROS causative of the ‘‘pseudo-hypoxic’’ effect. This is a major tumor-related hallmark, characterized by the activation of HIF even in the absence of hypoxia [42, 43]. Moreover, recent reports indicate that the gene encoding isocitrate dehydrogenase-1 (IDH1), one of the enzyme of citric acid cycle which is related to HIF-1 pathway, is mutated in 80% of certain types of GBM [125-127], thus linking mitochondrial dysfunction to tumorigenesis. 2-DG, a glucose analogue that reduces intracellular utilization of glucose, inhibits glycolysis, through competitive inhibition of some glycolytic enzymes. 2-DG can affect the growth of some tumors in vivo and it has been shown to be cytotoxic in vitro [128]. In a recent work HIF-1α has been shown to mediate resistance specifically to glycolytic inhibitors [129], however, the molecular mechanisms by which hypoxia may counteract 2-DG effects in brain tumor has not been so far fully elucidated. A decrease in provision of glucose (from 25 mM to 2,5 mM) and also of oxygen (2%) can be found in the internal perinecrotic/hypoxic region of the solid tumor mass compared to peripheral, relatively well nourished regions of the tumor [130]. Thus, in our study we set our control maintaining GBM-derived cells at 2% oxygen and in presence of high glucose concentration. In the first part of this study we showed that inhibiting glycolysis by addition of 2-DG, induces a decrease in cell proliferation and late apoptosis in primary GBM-derived cells

acutely exposed to 20% oxygen, while these effects are partially inhibited by hypoxia, condition in which 2-DG addition causes GBM cell differentiation and HIF-1α level reduction. Importantly, normal SVZ-derived cells are not affected by addition of 2-DG. Degradation of HIF-1α by 2-DG has been described in a previous report [81], nevertheless a molecular explanation for this effect has not been so far fully provided. Here we show that 2-DG increases SDH activity, reducing ROS levels and these are reliably causative of the observed HIF-1α degradation, consequentially to increased PHD2 activity. Indeed, HIF-1α is known to be chemically stabilized also by hypoxia independent factors, such as ROS [82], $CoCl_2$, Fe^{2+} [83] and cytoplasmic succinate [42]. Earlier studies have suggested that ROS produced by mitochondria are required for proper induction of HIF-1α under hypoxic conditions [131, 132]. It has been well established, that Fe^{2+} is an important cofactor for PHDs [83], andimportantlyH_2O_2, produced by mitochondria, is known to destabilize PHDs activity, either by converting Fe^{2+} in Fe^{3+} or by induction of post-transcriptional modifications of PHD2 [131]. Besides ROS acting as second messengers, impaired SDH activity and consequential intracytoplasmic succinate accumulation are associated to HIF-1α stabilization in several cancer types [42].We found that addition of succinate reverts 2-DG effects, promoting recovery of HIF-1α protein level and transcriptional activity (i.e. HRE-luciferase), as well as increase of ROS levels. Besides succinate, PHDs have been shown to be regulated also by other glycolytic and citric acid cycle metabolites, such as pyruvate and oxaloacetate, which could independently modify the oxygen-sensing abilities of cells [133]. While we found that PHD2 protein level is raised by addition of 2- DG, PHD2 transcription is decreased, and this is related to the observed degradation of HIF-1α, known to control PHD2 transcription [134]. Additionally, HIF-2a has been found highly expressed in glioma stem cells [83], but we did not find change of HIF-2a protein level following neither stimulus with 2-DG, nor addition of succinate. Importantly, HIF-1α is related to maintenance of an undifferentiated cell state and inhibition of cell differentiation [36, 40]. Particularly, HIF-1α contributes to a differentiation defect in malignant gliomas [34], even following exogenous BMP2 treatment [36, 37], shedding new light on the differentiation therapy of solid tumors by HIF-1α targeting. Therefore, HIF-1α has become in recent years an attractive, although challenging, therapeutic target [135]. Here, we found that after addition of 2-DG, a decrease of $CD133^+$ and $nestin^+$ cells and induction of neuronal differentiation occur under hypoxia, condition in which GBM cells are maintained in a less committed state [36, 124].

Oppositely, addition of succinate increases GBM cell undifferentiated state, preventing the prodifferentiating effects evoked by 2-DG. Previous reports describe that highly de-differentiated and fast growing tumors compared to slow-growing tumors or non-tumor cells are characterized by faster glycolysis and slower oxidative phosphorylation [136-139]. Here we found that diverse mechanisms may control GBM cell phenotype: on one side addition of 2-DG and raised oxygen tension induce GBM cell commitment and eventually cell death; oppositely to these, succinate and hypoxia promote GBM immature cells maintenance (Fig. 47). In conclusion, we show that reducing glycolysis in GBM tumor cells destabilizes cell functional and metabolic status, forcing cancer cells into a mitochondrial metabolism, as demonstrated by the activation of PDH and SDH, and promoting GBM cell differentiation. These findings improve the knowledge of GBM tumor intra and extracellular microenvironment and the mechanisms by which GBM cells respond to an alteration of their metabolic state.

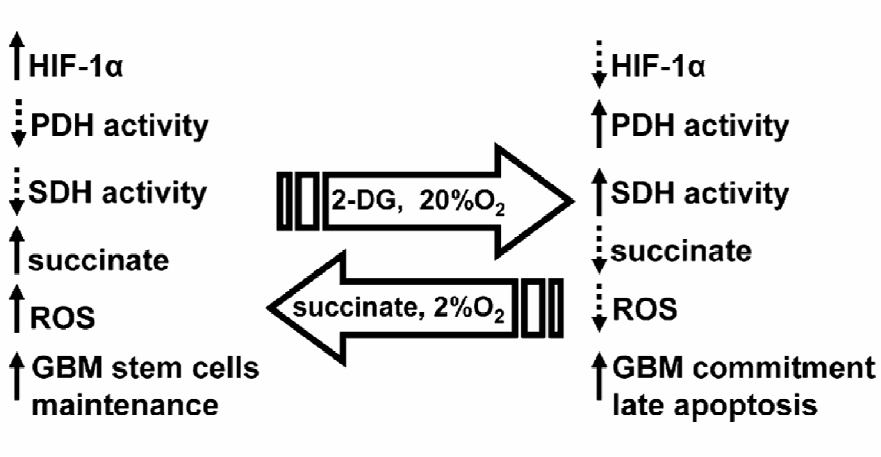

Figure 47. Summary of the principal effects elicited by 2-DG, succinate and oxygen tension in GBM cells. (Left part) Under hypoxia GBM cells display high anaerobic glycolysis, low PDH (i.e. phosphorylated PDH) and low SDH activity, the latter causative of intra-cytoplasmic accumulation of succinate and consequentially also of ROS. Both ROS and succinate have been described as inhibitors of PHDs activation, causing the stabilization of HIF-1α . Addition of succinate elicits analogous effects, as shown by HIF-1α stabilization and increased number of GBM stem cells. (Right part) Addition of 2-DG associate to exposure to 20% O2 increase PDH activity (i.e. de-phosphorylated PDH) and consequentially SDH activity, thus intracellular succinate and mitochondrial ROS release are reduced, according to literature. As a consequence PHD2 activity increases, HIF-1α is poly-ubiquitylated and consequentially degraded, which correlates with the acquisition of a more committed phenotype, according to previous works. Under these circumstances GBM cells undergo more rapidly apoptosis. Importantly, all these effects are mitigated by the hypoxia and by addition of succinate, which prevent SDH activity and tumor cell differentiation induced by 2-DG.

GBM are currently treated by surgical removal, followed by radiotherapy and frequently alkylating agents based chemotherapy, although the survival rate for GBM patients remains low. Indeed, the genetic instability of GBM tumor during time, after surgery and current chemotherapy, or eventually consequential to chemotherapy, could potentially prevent a complete control of the disease. Recent findings support novel biological hypotheses [6, 7, 9, 29, 31] that might lead to reconsider the traditional therapeutic approaches. Particularly, the discovery of a stem cell population within the tumor mass (CSCs) has changed the knowledge of tumor cell biology, leading to the definition of a cell hierarchy within the tumor [6, 7]. Importantly, CSCs seem to persist in tumors as a distinct population and may be responsible of relapse and resistance to treatments following surgical resection [70]. Thus, there is intratumoral heterogeneity that has to be taken into account for designing effective treatments. Moreover, the role of the tumor niche has been extensively investigated in the last years, and the oxygen tension gradient within the tumor mass may play a crucial role in the definition of cell phenotype. Indeed, we recently reported that pro-differentiating signaling pathways, such as BMP and Akt/ mTOR/Stat3, are inhibited in GBM-derived cells cultured under lowered oxygen tension, becoming progressively activated following acute high oxygen exposure [36, 37]. In the second part of this study we aimed to investigate whether these findings had physiological relevance and correlation with the stem cells distribution throughout the GBM mass. By sampling multiple intratumoral areas through radiological imaging and image guided surgery, we unravel a GBM phenotypic correlation to the hypoxic gradient, defining a tumor stem cell concentric model niche (Fig. 46). Here we describe a model that is constituted by three layers: the inner, highly hypoxic/anoxic core, characterized by stem cells with low proliferation index, an intermediate, mildly hypoxic layer, lining the anoxic core, with immature and proliferating tumor precursor cells, and the peripheral, more vascularized and more oxygenated area containing predominantly committed/ differentiated cells. Particularly, we found a high VEGF expression along the peripheral area of the tumor mass. As Perrin et al. described that VEGF upregulation occurs in astrocytes [113], which had been found along the tumor/normal tissue interface [112], we hypothesize that the $GFAP^+$ cells, present mainly in the peripheral layer of the tumor, may actually be tumor cells expressing VEGF. Moreover, we speculate that the hypoxic signature is crucial in determining the epigenetic activation (HIF-1α, Glut1, CAIX) and/or inhibition (BMP, Akt/mTOR/Stat3) of signaling pathways involved in the maintenance of

the tumor stem cells pool, which seems to be the more resistant to therapies. In this regard, we found that the majority of $CD133^+$ cells are characterized by high expression of MGMT, enzyme related to resistance to alkylating chemotherapies [67, 68]. This indicates that intratumoral hypoxia preserves a pool of tumor stem cells which very likely represent the tumor population resistant to treatments. Analogously, recent works have shown that within brain tumors CSCs reside in two niches, a perivascular location and the surrounding necrotic and/or less vascularized (i.e., hypoxic) tissue [21, 22, 73, 140]. According to our data, it has been reported that restricted oxygen conditions increase the CSC fraction and promote acquisition of a stem-like state [22, 140]. Current studies on MGMT expression are conducted on analysis of promoter methylation, but we did not find correlation between the methylation state of MGMT promoter (not shown) and MGMT protein expression profile, in accordance with previous report [69]. Importantly, the differences in MGMT expression observed among the three layers are causative of a strong diverse sensitivity to TMZ, the most used oral alkylating agent for the treatment of GBM. Indeed, GBM cells derived from the peripheral layer respond to TMZ by undergoing apoptosis, whereas GBM cells and, particularly, $CD133^+$ cells derived from the inner portions of the tumor mass are more resistant to this chemotherapic. Controversial data indicate that TMZ seems to induce a dose- and time-dependent decline of $CD133^+$ stem cell subpopulation in vitro, substantially reducing tumorigenicity in vivo [4], whereas other works indicate that TMZ does not seem to affect $CD133^+$ cells [5], generally considered the most chemoresistant tumor cell fraction [6-9]. In accordance with these latters, we found that $CD133^+$ cells particularly from the inner core are not sensitive to TMZ, and their sensitivity is increased by 6-BG, inhibitor of MGMT, which has already been used in some clinical trials either alone [120] or in combination with the maximum-tolerated dose of chemotherapy [121] to improve sensibility to TMZ. We hypothesize that the resistance to TMZ displayed by the tumor cells derived from the inner core and determined also by MGMT upregulation may be driven by the hypoxic microenvironment characteristic of the internal portions of the tumor mass. Indeed, hypoxia induces either directly or indirectly (through the activation of transcription factors) changes in the biology of tumor and its microenvironment leading to increased chemo- and radio-therapy resistance [70, 141]. Considering that hypoxia, through HIF-α, controls the expressions of several downstream targets [140], MGMT is probably not the only molecule responsible of GBM resistance to chemotherapy. The concentric distribution of GBM cells within the tumor mass here described

may have important implications in the management of GBM since both diagnostic and therapeutic methods could be improved. In fact, surgical needle biopsy should take into account the stem cell niche distribution to define a more accurate diagnosis. Current surgery normally aims to perform a gross total or a subtotal removal of the tumor, however, relapse occurs. As we found that cells derived from the inner portion of the GBM mass, which is enriched in stem cells, are insensitive to TMZ, we hypothesize that infiltrating and resistant GBM stem cells intraoperatively may escape from the surgical exeresis thus causing relapse. Importantly, we found a small percentage of $CD133^{+}/MGMT^{+}$ cells also in the peripheral layer of the tumor (Fig. 39F) suggesting that these might be GBM stem cells migrating from the inner core toward the periphery of the tumor in the effort to get nutrients and oxygen from the tumor vasculature.

MATERIALS AND METHODS

Under institutional-approved protocols, tissue samples were collected from patients and neonates after written informed consent. Neonatal brain subventricular zone (SVZ) tissue was obtained at the Children's Hospital of Orange County, USA, under the auspices of the protocol for the National Human Neural Stem Cell Resource (NHNSCR). Adult GBM samples were obtained at the Padova Academic Hospital, under the auspices of the protocol for the acquisition of human brain tissues obtained from the Ethical Committee board of the University of Padova. Tumor and non tumor patient characteristics are described in Table 2.

Brain tumors were acquired directly from surgery, two samples from each of the three concentric layers were obtained and part of the tissues was enzymatically dissociated. Single cells were cultured at 1.5% O_2. Patient ages listed in years (y). Non tumor tissue was from premature infants, listed in gestational weeks (gw), which died shortly after birth; periventricular zone tissue from the head of the caudate nucleus was isolated and initially characterized by [142]; no gross or microscopic abnormalities were observed at this time.

Code	Tumor Type	Age	Gender
HuTuP01	Glioblastoma	64	Male
HuTuP10	Glioblastoma	75	Female
HuTuP13	Glioblastoma	67	Male
HuTuP15	Glioblastoma	76	Female
HuTuP36	Glioblastoma	49	Female
HuTuP51	Glioblastoma	57	Male
HuTuP52	Glioblastoma	53	Male
HuTuP53	Glioblastoma	70	Male
HuTuP55	Glioblastoma	58	Male
HuTuP56	Glioblastoma	46	Male
HuTuP60	Glioblastoma	58	Male
HuTuP61	Glioblastoma	70	Female
HuTuP64	Glioblastoma	61	Male
HuTuP67	Glioblastoma	49	Male
GBM612	Glioblastoma	56	Male
GBM626	Glioblastoma	53	Male
GBM651	Glioblastoma	49	Male
Post-mortem review of non-tumor tissue source			
HuSC23	Premature polycythemic twin (of a twin-to-twin transfusion) who died on the day after birth	23 gw	Male
HuSC30	Premature fraternal twin who died on the day after birth, product of in vitro fertilization	25 gw	Male

Atmosphere-Controlled Incubation

For culture in 20% oxygen, cells were incubated in a Heraeus BBD 6220 incubator; CO_2 was added to maintain a 20% O_2, 5% CO_2 75% N_2 balance. For 2% oxygen culturing, cells were incubated in a customized system (Ruskinn C300, Ruskinn Technology Ltd., Bridgend, UK). The system maintains a constant 2% O_2, 5% CO_2, 93% N_2 balance [36].

Expansion of human CNS SVZ precursors

Normal neural precursor cells were derived from brain subventricular zone (SVZ) tissue of a premature neonate that died shortly after birth from pulmonary failure; the continuous culture from this tissue is denoted SC30 [142]. For the present experiments, cells were cultured on fibronectin-coated dishes in DMEM/F12 (Irvine Scientific, Irvine, CA) supplemented with BIT9500 (1% Bovine Serum Albumin, 10 μg/mL rh Insulin, 200 μg/mL Human Transferrin, Stem Cell Technologies, CA), 20 ng/ml basic fibroblast growth factor, (bFGF) and 10 ng/ml epidermal growth factor (EGF, both from R&D Systems, Minneapolis, MN). For continuous expansion, one-half of this medium was replaced every day and cultures were passaged every seventh day using TrypLE (Invitrogen, Gibco).

Isolation Expansion and Differentiation of human CNS Tumor Cells from Biopsies

In the present study, we dissociated and cultured cells as previously described [36]. Briefly, cells were cultured in control medium consisted of HAM'SF12/ DME with 25 mM glucose, (Irvine Scientific, Santa Ana, CA, USA), BIT9500, 10%, as serum substitute (Stem Cell Technologies, Milano, Italy). For continuous expansion, one-half of the medium was replaced every day and cells were passaged every 7–10 days using TrypLE (Invitrogen, Carlsbad, CA, USA) to dissociate them. Cells were not cultured for more than 8 passages in vitro in order to avoid long-term culture-related effects. Cell viability was evaluated by trypan blue exclusion. For low glucose experiments, cells were cultured in DMEM/F12, glucose-free, (Gibco BRL, Milano, Italy) with BIT9500 (10%), for a final glucose concentration of 2.5 mM. Two different glucose concentrations were established by adding D-glucose (12.5 and 25 mM final concentration). In experimental that required the addition of 2-deoxyglucose (2-DG) (Sigma, Milano, Italy) it was added to a final concentration of 12.5 or 25 mM as reported in literature [24,25]. In some experiments, esterificated diethyl-succinate (5 mM, Sigma– Aldrich, Milano, Italy) or pyruvate

(1 mM, Sigma–Aldrich, Milano, Italy) was added for 18 h. Pyruvate, the physiological substrate of pyruvate dehydrogenase (PDH), was used to confirm specificity of antibody specific for PDH E1a. Precursor cell differentiation was induced by culturing cells in DMEM/F12/BIT9500 in the absence of mitogens. After 2 weeks post-mitogen withdrawal, cells were fixed in cold 4% paraformaldehyde for 15 min, rinsed and stored prior to analysis.

Immunocytochemistry (ICC)

Cells were fixed in cold 4% paraformaldehyde for 15 min, rinsed and stored prior to analysis. Primary antibody staining was performed for nestin (mouse, 1:200, Millipore, Billerica, MA, USA), glial fibrillary acidic protein (GFAP, mouse, 1:1000, Sigma–Aldrich, Milano, Italy), ß-III-tubulin (mouse, monoclonal Tuj-1, 1:1000, Covance, Milano, Italy). After incubation, cells were washed and incubated with species-specific secondary antibodies conjugated to Alexa dyes (1:2000, Invitrogen, Milano, Italy). Cells were counterstained with DAPI (1:10,000, Sigma–Aldrich, Milano, Italy) to measure total cell number. Staining was visualized by epifluorescence (Nikon Eclipse 80i, Melville, NY, USA) and images compiled for figures using Adobe Illustrator (Adobe, San Jose, CA, USA).

Immunohistochemestry (IHC)

Tumor biopsies were paraffin-embedded and cut in 5-lmthick sections. Part of the sections have been used for H&E staining, others for immunohistochemical analyses. For this purpose, sections were rehydrated and then antigen retrieval was performed by incubation with citrate buffer 0.01 M pH 6 at 95^{o}C for 200. After saturation with 5% bovine serum albumin (BSA), slides were incubated with anti-Pi-Smad1/5/8 (rabbit; 1:100), anti-Pi-Stat3 (rabbit; 1:100), anti-Pi-Akt (rabbit; 1:50), anti-Pi-mTOR (rabbit; 1:100; all from Cell Signaling Technology, Beverly, MA, http://www.cellsignal.com), anti-glial fibrillary acidic protein (GFAP; rabbit; 1:500; Dako, Glostrup, Denmark, http://www.dako.com), anti-nestin (mouse; 1:200; Chemicon, Temecula, CA, http://www.chemicon. com), anti-ß-III-tubulin (mouse; 1:500; Covance, Princeton, NJ, http://www.covance.com), anti-Ki67 (mouse; 1:100; Dako, Glostrup, Denmark, http://www.dako.com), anti-HIF-1α (mouse; 1:50; BD Biosciences, San Diego, http://www.bdbiosciences. com), anti-CD34 (mouse; 1:50; Novocastra Ltd., Newcastle upon Tyne, U.K., http://www.novocastra.co.uk), anti-vascular endothelial growth factor (VEGF;

rabbit; 1:50; Santa Cruz Biotechnology Inc., Santa Cruz, CA, http://www.scbt.com), anti-CD133 (rabbit; 1:100; Abcam, Cambridge, U.K., http://www.abcam. com), anti-MGMT (mouse; 1:2,000; Novus Biologicals, Milano, Italy, http://www.novusbio.com), anti-Glut1 (rabbit; 1:100; Santa Cruz Biotechnology Inc., Santa Cruz, CA, http://www.scbt.com), anti-CAIX (rabbit; 1:1,000; Novus Biologicals, Milano, Italy, http://www.novusbio.com) and anti-doublecortin (DCX) (rabbit, 1:1,000, Millipore, Billerica, MA, USA). After incubation, sections were washed and incubated with species-specific secondary antibodies conjugated to Alexa dyes (Invitrogen, Carlsbad, CA, http:// www.invitrogen.com). Tissues were counterstained with 40,6-diamidino-2-phenylindole (DAPI) (1:1,0000; Sigma-Aldrich, Milano, Italy, http://www.sigmaaldrich.com) to measure total cell number. Staining was visualized by epifluorescence (Vico, Nikon Instruments, Inc., Melville, NY, http://www.microscopyu. com) and images compiled for figures using Adobe Illustrator (Adobe Systems Inc., San Jose, CA, http://www.adobe.com). The specificity of each staining procedure was confirmed by replacing the primary antibodies with phosphate buffered saline (PBS).

CD133, CD90, cell cycle and annexin-V/propidium iodide analyses

Cells (2 x 10^5 cells per milliliter) were incubated with antihuman CD133 (clone AC133/2-PE, as directed; Miltenyi Biotec, Bergisch Gladbach, Germany, http://www.miltenyibiotec. com), anti-human CD24 (mouse; PC5 conjugated; 1:25; Immunotech a.s., Praha, Czech Republic, http://www. immunotech.cz), and anti-human CD90 (clone 5E10, FITC conjugated, BioLegend, Milano, Italy) as previously described [36, 37, 119]. Viability was assessed by adding 7-amino-actinomycin-D (7-AAD, 50 ng/ml; BD Biosciences, San Diego, http://www.bdbiosciences. com) before analysis. Cells were analyzed on a Cytomics FC500 flow cytometer (Beckman Coulter, Fullerton, CA, http://www.beckmancoulter.com). Relative percentages of different subpopulations were calculated based on live gated cells (as indicated by physical parameters, side scatter, and forward scatter). Unlabeled cells and cells incubated with appropriate isotypic control antibodies were first acquired to ensure labeling specificity. Analysis of apoptosis was performed as recommended by using the Annexin Fluo kit (Roche Diagnostics, Basel, Switzerland, http://www.rocheapplied- science.com). For cell cycle phase analysis, cells were incubated with BrdU (1 mM, BD, Milano, Italy) for 45 min then washed and prepared for analysis as directed (BrdU Flow Kit Staining Protocol, BD, Milano, Italy).

Western blot and densitometric analyses

After culturing cells under lower or atmospheric oxygen tension total protein extracts were rapidly collected in order to minimize Hif1α protein degradation. As Hif1α turnover is rapid, with a progressive decrease in protein levels occurring after only 4-16 min of re-oxygenation [143], total protein extraction was performed by scrapering the cells from the culture dishes and cellular protein extracts were isolated by using a specific protein lyses buffer, containing TPER Reagent (Pierce), 300 mM NaCl, 1 mM orthovanadate, 200 mM PEFABLOC (AEBSF) (Roche), 1 μg/mL Aprotinin (Sigma), 5 μg/mL Pepstatin A (Sigma), 1 μg/mL Leupeptin (Sigma). This buffer is particularly indicated to preserve protein phosphorylated residues. Equal amounts of protein (10–20 μg) were resolved using a SDS-PAGE gels (at different percentage of acrylamide depending on the protein analyzed) and transferred to PVDF Hybond-p membrane (GE Healthcare). Membranes were blocked with I-blockTM Blocking (Tropix, Applied Biosystem, Monza, Italy) for at least 2 h under rotation at room temperature. Membranes were then incubated with primary antibodies against HIF-1α (mouse, 1:250, BD Biosciences, Milano, Italy), HIF-2α (mouse, 1:250, Novus Biologicals, Milano, Italy), PHD2 (goat, 1:300, Santa Cruz, Santa Cruz, CA, USA), p21cip1 (mouse, 1:1000, Sigma–Aldrich, Milano, Italy), Bcl-2, Bcl-XL, PARP, (all rabbit, 1:1000, Cell Signaling, Milano, Italy), phosphorylated PDH E1a serine 293 (rabbit, 1:5000, Novus Biologicals, Milano, Italy), total PDH E1a subunit (1:1000, Invitrogen, Carlsbad, CA, USA), MGMT (mouse; 1:1,000; Novus Biologicals), G6PC (rabbit, 1:1000, Abcam, Cambridge, MA, USA), Akt, mTOR, Stat3, Pi- Smad1/5/8 (S463/465; S463/465; S426/428), Pi-Stat3 (S727), Pi-Akt (T308), Pi-mTOR (S2448; all rabbit; 1:1,000; Cell Signaling Technology, Beverly, MA, http:// www.cellsignal.com), Smad1/5/8 (rabbit; 1:300; Santa Cruz Biotechnology Inc., Santa Cruz, CA, http://www.scbt.com), or ß-actin (mouse, 1:10,000, Sigma–Aldrich, Milano, Italy) for 2 h. Membranes were next incubated with peroxidase-labeled goat anti-rabbit IgG (1:100,000, Sigma–Aldrich, Milano, Italy), peroxidase-labeled goat anti-mouse IgG (1:100,000, Sigma–Aldrich, Milano, Italy) or peroxidase-labeled donkey anti-goat IgG (1:100,000, Santa Cruz, Santa Cruz, CA, USA) for 60 min. All membranes were visualized using ECL Advance (GE Healthcare, Catania, Italy) and exposed to Hyperfilm MP (GE Healthcare, Catania, Italy).

Mitochondrial membrane potential, reactive oxygen species (ROS) and GSH analyses

The mitochondrial membrane potential was measured with the lipophilic cation 5,5',6,6',-tetrachlo-1,1',3,3'-tetraethylbenzimidazol- carbocyanine (JC-1, Invitrogen, Milano, Italy), as described in [144], a fluorescent probe known to selectively enter into the mitochondria and used to measure changes in mitochondrial membrane potential ($\Delta\psi_{mt}$). JC-1 forms aggregates (red color) at higher potential and monomers (green color) at low membrane potential. To ensure JC-1 effectiveness GBM-derived cells have been pretreated with valinomycin (1 μM, Sigma–Aldrich, Milano, Italy), facilitating mitochondrial membrane potential depolarization (not shown). The production of ROS was measured by flow cytometry using hydrohethidine (HE) (Invitrogen, Milano, Italy) [144]. Analysis of total GSH level was measured by using monobromobimane (mBrB), (Invitrogen, Milano, Italy) (50 μM) [145, 146] and chloromethyl-dichlorofluorescein diacetate (CMDCFDA) (5 μM, Invitrogen, Milano Italy), preincubating cells for 15 and 30 min, respectively, at 37^{o}C prior to analysis.

Lactate assay

Extracellular lactate measurement was performed using the Lactate Assay Kit, (BioVision, Torino, Italy) kindly provided by Dr. Alberto Burlina (University of Padova), following the manufacturer instructions.

Succinate dehydrogenase activity

To evaluate aerobic metabolism succinate dehydrogenase (SDH) activity has been measured, since enzyme activity is considered an indicator of tricarboxylic acid (TCA) cycle activity. To measure SDH activity, we used the methods described by Levine et al. with little modifications [147]. Briefly, cell monolayers (not fixed) were snap-frozen at -80 ^{o}C for at least 1 h and were incubated for 20 min in the dark at 37 ^{o}C in a reaction buffer containing 12.3 mM diethyl-succinate (Sigma, Milano, Italy), 0.2 mM 1-methoxy-5-methylphenazine methyl sulphate (Sigma– Aldrich, Milano, Italy), 1.2 mM nitro blue tetrazolium (NBT, Sigma–Aldrich, Milano, Italy) in 50 mM Tris–HCl, pH 7.6. We used 12.3 mM malonate (Sigma, Milano, Italy) to test aspecific reactions, and 3-nitropropionic acid (3-NPA, 500 μM, Sigma–Aldrich, Milano, Italy), to irreversibly inactivate SDH, as negative control. The enzyme activity is determined by measuring the formation of nitro blue diformazan (NBT-dfz) due to NBT reduction and the end

product (i.e. blue cells) is visible by bright field microscopy or measured at 570 nm, by absorption spectroscopy.

ATP assay

Cells were cultured with 2-DG for 18 or 24 h at either 2% or 20% oxygen, collected and counted. The ATP content per 100,000 cells was determined using the CellTiter-Glo luminescent assay (Promega, Milano, Italy) according to manufacturer instruction, using a Victor3TM luminometer (PerkinElmer, Milano, Italy). Data were normalized to ATP content in cells cultured with glucose at 2% O2.

MTT assay

Individual wells of a 96-well tissue culture microtiter plate (Falcon, BD, Milano, Italy) were inoculated with 100 μl of medium containing 5 x 10^3 of GBM cells. The plates were incubated overnight prior to the analyses. After medium removal, 2-DG was added and cells were incubated for 18 or 24 h at either 2% or 20% oxygen. Cell viability was assayed by the MTT [(3-(4,5- dimethylthiazol-2-yl)-2,5 diphenyl tetrazolium bromide)] test as previously described [148].

Real-time PCR analysis

RNA was isolated from cells using Trizol (Invitrogen, Milano, Italy) and 1 mg of total RNA reverse-transcribed using SuperScript RNAse H-Reverse Transcriptase (Invitrogen, Milano, Italy). Quantitative RT-PCR reactions were run in triplicate using Brilliant1 SYBR1 Green QPCR Core Reagent Kit (Stratagene, La Jolla, CA, USA). Fluorescent emission was recorded in real-time (Sequence Detection System 7900HT, Applied Biosystems, Foster City, CA, USA). Gene expression profiling was completed using the comparative Ct method of relative quantification. PCR amplification conditions consisted of 50 cycles with primers annealing at 60^{o}C. These set of primers were used: PHD2, F: 5'-GGGACATTCATTGCCTCACT- 3', R: 5'-ACACATGTGGTGCTTGCTGT-3'; HIF-1α, F: 5'-CGTTCCTTCGATCAGTTGTC-3', R: 5'-TCAGTGGTGGCAGTGGTAGT- 3'; G6Pase-β, F: 5'-ATAGCCGAGGCGCTACAGAA-3', R: 5'- GGCCTGTCTCCAAAAAGAAACC-3', G6Pase-α, F: 5'- GTGTCCGTGATCGCAGACC-

3', R:5'- GACGAGGTTGAGCCAGTCTC-3', beta-glucuronidase (GUSB), F: 5'-GAAAATACGTGGTTGGAGAGCTCATT- 3', R: 5'-CCGAGTGAAGATCCCCTTTTTA-3'. Primers have been designed by using the software Primer 3 (http:// frodo.wi.mit.edu/primer3/input.htm) and the specificity of the primers for GUSB, HIF-1α and PHD2 sequences has been evaluated by using the software Human BLAT Search (http://genome. ucsc.edu/cgi-bin/hgBlat?command=start). PCR amplicons had been previously evaluated on agarose gel, and during SYBR green analyses primers dissociation curves have been checked in each run to ensure primers specificity. Relative RNA quantities were normalized to GUSB as a housekeeping gene and 2% oxygen T0 was used as the calibrating condition (ΔΔCt Method).

Hypoxia responsive element (HRE)-luciferase reporter assay

GBM cells were transfected using a Promega Corporation (Madison WI, USA) protocol for transient transfection of adherent cells using Effectene reagent (Qiagen, Milano, Italy). HRE-luciferase reporter construct used (wHRE) was kindly provided by Dr. Stefano Indraccolo (Istituto Oncologico Veneto—IRCCS, Padova, Italy). It consists of a trimerized 24-mer containing 18 bp of sequence from the PGK promoter including the HRE (5'-TGTCACGTCCTGCACGACTCTAGT, HRE) and an 8-bp linker sequence followed by a 50- bp minimal tyrosine kinase promoter in a pGL2-firefly luciferase basic Vector backbone (Promega, Madison, WI, USA) [149]. The mutant HRE (mHRE) construct, used to evaluate aspecific effects, has the ACG of the HIF-1 binding site mutated to CAT, abolishing binding, as well as a point mutation that abolished a BsgI restriction site for diagnostic purposes. GBM cells were transfected either with a wHRE or with a mHRE. Along with these vectors, also a Renilla luciferase vector has been transfected in order to normalize luciferase detection (Promega, Madison, WI, USA). 12 h after transfection, total medium change was done and cells were treated with 25 mM 2-DG, succinate 5 mM or a combination of both for 8 h. Finally, cells were processed and analysis of HREluciferase activity was performed as described (Dual-Luciferase Reporter Assay System, Promega, Madison, WI, USA) by using a plate-reading luminometer (Victor^{3TM}, PerkinElmer, Milano, Italy).

In vitro invasion assay

For assessing tumor cell invasion we utilized the Boyden transwell chamber system (BD Biosciences Clontech, Palo Alto, CA, USA) following the manufacturer's protocol. Each condition was done in triplicate. Briefly, the plate was allowed to thaw for 20 minutes at room temperature. Prior to plating the membrane was rehydrated by adding 500µl of media to the upper well and 750 µl to the lower well and incubated at 37^{o}C for 60 minutes. Next, 50,000 cells were plated on the top well and allowed to invade for 18hr. After incubation, the noninvasive cells were removed with a cotton swab. The cells that had migrated through the membrane and stuck to the lower surface of the membrane were fixed with methanol and stained with hematoxylin. For quantification, the cells were counted under a microscope in ten predetermined fields.

Cell migration assay

Migratory behavior of GBM cells was analyzed through a novel assay utilizing nano-grooves of 350 nm in width, 500 nm in depth, and evenly-spaced 350 nm apart. This 'nano-patterned' substratum was constructed of transparent poly(urethane acrylate) (PUA), and fabricated by UV-assisted capillary lithography [150]. Tissue culture glass was covered with anano-patterned substratum, and subsequently attached to the bottom surface of a custom-made Mattek dish (P35G-20-C). Prior to plating cells, nano-patterned substrata were coated with poly-D-lysine (5µg/cm^2) for 15 minutes, followed by laminin (5µg/cm^2) for 1 hour. The topography of the nano-patterned substrat caused cells to align and migrate parallel to the nano-grooves. Long-term observation of cell migration was performed using time-lapse microscopy. A custom Mattek dish, modified with the attached nano-patterned substratum, was mounted onto the stage of a motorized inverted microscope (Olympus IX81), equipped with a Cascade 512B II CCD camera. A temperature/gas-regulated environmental chamber was used to maintain cells at 37˚C and 5% CO_2 for the duration of the experiment. Phase-contrast images were automatically recorded every 20 minutes, for 15 hours, under a 10X objective (NA = 0.30) using the Slidebook 4.1 (Intelligent Imaging Innovations, Denver, CO). Quantitative analysis of cell migration. A custom-designed MATLAB (Mathworks) program was used to identify cell boundaries, centroid, and nucleus positions from phase-contrast images. Movements of cell centroid and nucleus positions were manually tracked through each frame of time-lapse videos. Average cell speeds

were calculated from individual cell trajectories and the duration of image acquisition. To avoid the effects of cell-cell contact on migration, cells were plated at low density (~40k cells/mL), allowing isolated movements. For each condition, over 75 cells were quantified in total. Mann-Whitney rank-sum test was used to evaluate the statistical significance where indicated.

Statistical analysis

Graphs and statistical analyses were prepared using Prism 3.03 (Graph Pad, La Jolla, CA, USA). All values were presented as mean ±standard error of the mean (S.E.M.). Statistical significance was measured by one-way ANOVA with post hoc Newman–Keul's test, *$p < 0.05$, **$p < 0.01$, ***$p < 0.001$. For all graphs, an asterisk over a bracket indicates a significant difference with a variable as indicated, an asterisk over a bar indicates a significant difference between the 2% and 20% oxygen at either a particular time point or culture condition.

In Vivo Grafting of brain tumor derived cells for survival experiment

Recapitulation of tumor has been obtained by orthotopic grafting of GBM cells into the right striatum of 6 weeks male athymic nude mice. Mice were anesthetized by intraperitoneal injection (i.p.) of ketamine/xylazine (300 mg ketamine combined with 20 mg xylazine in a 4 ml volume of HBSS vehicle; 0.2 ml per 20 g mouse) as previously described [151]. 1.5 $x10^5$ tumor derived cells were stereotactically injected in the right striatum. The mouse head was maintained within a stereotactic frame, allowing a precise and reproducible injection site, using the intersection of the coronal and sagittal sutures (bregma) [152]. The coordinates used were 0.5 mm anterior and 2.5 mm lateral from the bregma and at a depth of 3 mm. Using a Hamilton syringe, 2 µl of the cell suspension was injected at a rate of 1 µl/minute. After surgery, the skin was closed with Nexaban Liquid (a surgical glue). After injection, mice were i.p injected with a recovery solution (Yohimbine (0.02 mg/ml final, 0.2 ml per 20 g mouse), allowed to recover on a warm heating pad and then returned to the cage. The next day mice started receiving 2-DG or saline, via i.p. injection, 500 mg/kg/day of 2-DG (75 mg/ml, dissolved in saline, for the duration of the experiment as previously described [3, 59]. Mice were sacrificed when they became lethargic, hunched or manifested any sign of distress, indicative of illness or discomfort. Cardiac perfusion of saline solution followed by 15 min of 4% paraformaldehyde perfusion was performed and the whole mouse grafted brain was recovered, overnight fixed at 4C in 4% paraformaldehyde, then

frozen in OCT liquid and immunohistochemically analyzed. Human grafted cells were distinguished from murine brain cells by using human specific antibodies.

PERSONAL SCIENTIFIC EDUCATION DURING THE THREE YEARS OF DOCTORATE

POSTERS PRESENTED AT NATIONAL AND INTERNATIONAL CONGRESSES

2008. Poster presented at the National Congress XXXV AIEOP, Ancona, 26-28 october 2008. Francesca Pistollato; **Sara Abbadi**; Elena Rampazzo; David M. Panchision; Giuseppe Basso. Hypoxia represses the differentiative effects of BMPs in high grade glioma.

2008. Poster presented at the 3rd European Conference on Tumor Angiogenesis and Antiangiogenic Therapy, ECTA 2008, Padova, November 6-7-8 2008. Francesca Pistollato, **Sara Abbadi**, Elena Rampazzo, Alessandro Della Puppa, Giuseppe Basso. Hypoxia confers High Grade Glioma cells protection from glycolysis inhibition.

2009 Poster presented at the International Congress ISSCR. 7Th ISSCR Annual Meeting, Barcelona, Spain, July 8-11, 2009. **Sara Abbadi,** Francesca Pistollato, Elena Rampazzo, Alessandro Della Puppa, Giampietro Viola and Giuseppe Basso. Hypoxia confers Glioblastoma cells resistance to glycolysis inhibition.

2009 Poster presented at the International Congress ISSCR. 7Th ISSCR Annual Meeting, Barcelona, Spain, July 8-11, 2009. Francesca Pistollato, **Sara Abbadi**, Elena Rampazzo, Alessandro Della Puppa, Giampietro Viola Lucia Cavallini, David M. Panchision and Giuseppe Basso. Glioblastoma derived cells, under hypoxia, undergo HIF-1α degradation and cell commitment following glycolysis block.

2009. Oral presentation at the 14th National Congress A.I.N.O, Padova, 4-7 october 2009.

NATIONAL AND INTERNATIONAL CONGRESSES

2008. Attended the International Congress ISSCR. 6Th ISSCR Annual Meeting, Philadelphia, USA, June 11-14, 2008.

2008. Attended the 3rd European Conference on Tumor Angiogenesis and Antiangiogenic Therapy, ECTA 2008, Padova, November 6-7-8 2008.

2009 Attended the International Congress ISSCR. 7Th ISSCR Annual Meeting, Barcelona, Spain, July 8-11, 2009.

2009 Attended the 14th National Congress A.I.N.O, Padova, 4-7 october 2009.

PUBLICATION

1. Pistollato F, Rampazzo E, **Abbadi S**, Della Puppa A, Scienza R, D'Avella D, Denaro L, Te Kronnie G, Panchision DM, Basso G. Molecular mechanisms of HIF-1alpha modulation induced by oxygen tension and BMP2 in glioblastoma derived cells. PLoS One. 2009 Jul 9;4(7):e6206.
2. Pistollato F, **Abbadi S**, Rampazzo E, Persano L, Della Puppa A, Frasson C, Sarto E, Scienza R, D'avella D, Basso G. Intratumoral hypoxic gradient drives stem cells distribution and MGMT expression in glioblastoma. Stem Cells. 2010 May;28(5):851-62.
3. Pistollato F, **Abbadi S**, Rampazzo E, Viola G, Della Puppa A, Cavallini L, Frasson C, Persano L, Panchision DM, Basso G. Hypoxia and succinate antagonize 2-deoxyglucose effects on glioblastoma. Biochem Pharmacol. 2010 Nov 15;80(10):1517-27. Epub 2010 Aug 10.
4. Pistollato F, Rampazzo E, Persano L, **Abbadi S**, Frasson C, Denaro L, D'Avella D, Panchision DM, Della Puppa A, Scienza R, Basso G. Interaction of hypoxia-inducible factor-1α and Notch signaling regulates medulloblastoma precursor proliferation and fate. Stem Cells. 2010 Nov;28(11):1918-29. doi: 10.1002/stem.518.

REFERENCES

1. Krakstad, C. and M. Chekenya, *Survival signalling and apoptosis resistance in glioblastomas: opportunities for targeted therapeutics.* Mol Cancer, 2010. **9**: p. 135.
2. Laks, D.R., K. Visnyei, and H.I. Kornblum, *Brain tumor stem cells as therapeutic targets in models of glioma.* Yonsei Med J, 2010. **51**(5): p. 633-40.
3. Maschek, G., et al., *2-deoxy-D-glucose increases the efficacy of adriamycin and paclitaxel in human osteosarcoma and non-small cell lung cancers in vivo.* Cancer Res, 2004. **64**(1): p. 31-4.
4. Beier, D., et al., *Temozolomide preferentially depletes cancer stem cells in glioblastoma.* Cancer Res, 2008. **68**(14): p. 5706-15.
5. Liu, G., et al., *Analysis of gene expression and chemoresistance of CD133+ cancer stem cells in glioblastoma.* Mol Cancer, 2006. **5**: p. 67.
6. Altaner, C., *Glioblastoma and stem cells.* Neoplasma, 2008. **55**(5): p. 369-74.
7. Sanchez-Martin, M., *Brain tumour stem cells: implications for cancer therapy and regenerative medicine.* Curr Stem Cell Res Ther, 2008. **3**(3): p. 197-207.
8. Murat, A., et al., *Stem cell-related "self-renewal" signature and high epidermal growth factor receptor expression associated with resistance to concomitant chemoradiotherapy in glioblastoma.* J Clin Oncol, 2008. **26**(18): p. 3015-24.
9. Higa, G.M. and J. Abraham, *Biological mechanisms of bevacizumab-associated adverse events.* Expert Rev Anticancer Ther, 2009. **9**(7): p. 999-1007.
10. Gatenby, R.A. and R.J. Gillies, *Why do cancers have high aerobic glycolysis?* Nat Rev Cancer, 2004. **4**(11): p. 891-9.
11. Hsu, P.P. and D.M. Sabatini, *Cancer cell metabolism: Warburg and beyond.* Cell, 2008. **134**(5): p. 703-7.
12. Hawkins, R.A. and M.E. Phelps, *PET in clinical oncology.* Cancer Metastasis Rev, 1988. **7**(2): p. 119-42.
13. Weber, W.A., N. Avril, and M. Schwaiger, *Relevance of positron emission tomography (PET) in oncology.* Strahlenther Onkol, 1999. **175**(8): p. 356-73.
14. Gambhir, S.S., *Molecular imaging of cancer with positron emission tomography.* Nat Rev Cancer, 2002. **2**(9): p. 683-93.
15. Rivenzon-Segal, D., et al., *Glycolysis and glucose transporter 1 as markers of response to hormonal therapy in breast cancer.* Int J Cancer, 2003. **107**(2): p. 177-82.
16. Artemov, D., et al., *Two-compartment model for determination of glycolytic rates of solid tumors by in vivo 13C NMR spectroscopy.* NMR Biomed, 1998. **11**(8): p. 395-404.
17. Mathupala, S.P., A. Rempel, and P.L. Pedersen, *Aberrant glycolytic metabolism of cancer cells: a remarkable coordination of genetic, transcriptional, post-translational, and mutational events that lead to a critical role for type II hexokinase.* J Bioenerg Biomembr, 1997. **29**(4): p. 339-43.
18. Schilling, C.H., et al., *Metabolic pathway analysis: basic concepts and scientific applications in the post-genomic era.* Biotechnol Prog, 1999. **15**(3): p. 296-303.
19. Dang, C.V., et al., *Oncogenes in tumor metabolism, tumorigenesis, and apoptosis.* J Bioenerg Biomembr, 1997. **29**(4): p. 345-54.

20. Schornack, P.A. and R.J. Gillies, *Contributions of cell metabolism and H+ diffusion to the acidic pH of tumors.* Neoplasia, 2003. **5**(2): p. 135-45.
21. Gilbertson, R.J. and J.N. Rich, *Making a tumour's bed: glioblastoma stem cells and the vascular niche.* Nat Rev Cancer, 2007. **7**(10): p. 733-6.
22. Heddleston, J.M., et al., *Hypoxia inducible factors in cancer stem cells.* Br J Cancer, 2010. **102**(5): p. 789-95.
23. Dewhirst, M.W., *Relationships between cycling hypoxia, HIF-1, angiogenesis and oxidative stress.* Radiat Res, 2009. **172**(6): p. 653-65.
24. Cairns, R.A., T. Kalliomaki, and R.P. Hill, *Acute (cyclic) hypoxia enhances spontaneous metastasis of KHT murine tumors.* Cancer Res, 2001. **61**(24): p. 8903-8.
25. Brahimi-Horn, C. and J. Pouyssegur, *The role of the hypoxia-inducible factor in tumor metabolism growth and invasion.* Bull Cancer, 2006. **93**(8): p. E73-80.
26. Louis, D.N., et al., *The 2007 WHO classification of tumours of the central nervous system.* Acta Neuropathol, 2007. **114**(2): p. 97-109.
27. Brahimi-Horn, M.C. and J. Pouyssegur, *Oxygen, a source of life and stress.* FEBS Lett, 2007. **581**(19): p. 3582-91.
28. Mohyeldin, A., T. Garzon-Muvdi, and A. Quinones-Hinojosa, *Oxygen in stem cell biology: a critical component of the stem cell niche.* Cell Stem Cell, 2010. **7**(2): p. 150-61.
29. Azuma, Y., et al., *Hypoxia and differentiation in squamous cell carcinomas of the uterine cervix: pimonidazole and involucrin.* Clin Cancer Res, 2003. **9**(13): p. 4944-52.
30. Helczynska, K., et al., *Hypoxia promotes a dedifferentiated phenotype in ductal breast carcinoma in situ.* Cancer Res, 2003. **63**(7): p. 1441-4.
31. Jogi, A., et al., *Hypoxia alters gene expression in human neuroblastoma cells toward an immature and neural crest-like phenotype.* Proc Natl Acad Sci U S A, 2002. **99**(10): p. 7021-6.
32. Smith, K., et al., *Silencing of epidermal growth factor receptor suppresses hypoxia-inducible factor-2-driven VHL-/- renal cancer.* Cancer Res, 2005. **65**(12): p. 5221-30.
33. Ke, Q. and M. Costa, *Hypoxia-inducible factor-1 (HIF-1).* Mol Pharmacol, 2006. **70**(5): p. 1469-80.
34. Lu, H., et al., *Hypoxia-inducible factor-1alpha blocks differentiation of malignant gliomas.* Febs J, 2009. **276**(24): p. 7291-304.
35. Piccirillo, S.G., et al., *Bone morphogenetic proteins inhibit the tumorigenic potential of human brain tumour-initiating cells.* Nature, 2006. **444**(7120): p. 761-5.
36. Pistollato, F., et al., *Hypoxia and HIF1alpha repress the differentiative effects of BMPs in high-grade glioma.* Stem Cells, 2009. **27**(1): p. 7-17.
37. Pistollato, F., et al., *Molecular mechanisms of HIF-1alpha modulation induced by oxygen tension and BMP2 in glioblastoma derived cells.* PLoS One, 2009. **4**(7): p. e6206.
38. Pardal, R., et al., *Glia-like stem cells sustain physiologic neurogenesis in the adult mammalian carotid body.* Cell, 2007. **131**(2): p. 364-77.
39. Wong, E.T. and S. Brem, *Antiangiogenesis treatment for glioblastoma multiforme: challenges and opportunities.* J Natl Compr Canc Netw, 2008. **6**(5): p. 515-22.
40. Gustafsson, M.V., et al., *Hypoxia requires notch signaling to maintain the undifferentiated cell state.* Dev Cell, 2005. **9**(5): p. 617-28.
41. Dang, C.V. and G.L. Semenza, *Oncogenic alterations of metabolism.* Trends Biochem Sci, 1999. **24**(2): p. 68-72.

42. King, A., M.A. Selak, and E. Gottlieb, *Succinate dehydrogenase and fumarate hydratase: linking mitochondrial dysfunction and cancer.* Oncogene, 2006. **25**(34): p. 4675-82.
43. MacKenzie, E.D., et al., *Cell-permeating alpha-ketoglutarate derivatives alleviate pseudohypoxia in succinate dehydrogenase-deficient cells.* Mol Cell Biol, 2007. **27**(9): p. 3282-9.
44. Jin, S., et al., *Metabolic catastrophe as a means to cancer cell death.* J Cell Sci, 2007. **120**(Pt 3): p. 379-83.
45. Zhu, Z., et al., *2-Deoxyglucose as an energy restriction mimetic agent: effects on mammary carcinogenesis and on mammary tumor cell growth in vitro.* Cancer Res, 2005. **65**(15): p. 7023-30.
46. Michels, K.B. and A. Ekbom, *Caloric restriction and incidence of breast cancer.* Jama, 2004. **291**(10): p. 1226-30.
47. Vander Heiden, M.G., L.C. Cantley, and C.B. Thompson, *Understanding the Warburg effect: the metabolic requirements of cell proliferation.* Science, 2009. **324**(5930): p. 1029-33.
48. Kim, J.W. and C.V. Dang, *Multifaceted roles of glycolytic enzymes.* Trends Biochem Sci, 2005. **30**(3): p. 142-50.
49. Bonnet, S., et al., *A mitochondria-K+ channel axis is suppressed in cancer and its normalization promotes apoptosis and inhibits cancer growth.* Cancer Cell, 2007. **11**(1): p. 37-51.
50. Cori, C.F. and G.T. Cori, *The carbohydrate metabolism of tumors: I. The free sugar, lactic acid, and glycogen content of malignant tumors.* J Biol Chem, 1925. **64**: p. 11-22.
51. Cori, C.F. and G.T. Cori, *The carbohydrate metabolism of tumors: II. Changes in the sugar, lactic acid, and co-combing power of blood passing through a tumor* J Biol Chem, 1925. **65**: p. 397-405.
52. Jope, R.S., C.J. Yuskaitis, and E. Beurel, *Glycogen synthase kinase-3 (GSK3): inflammation, diseases, and therapeutics.* Neurochem Res, 2007. **32**(4-5): p. 577-95.
53. Rodriguez-Enriquez, S., M.E. Torres-Marquez, and R. Moreno-Sanchez, *Substrate oxidation and ATP supply in AS-30D hepatoma cells.* Arch Biochem Biophys, 2000. **375**(1): p. 21-30.
54. Parolin, M.L., et al., *Regulation of glycogen phosphorylase and PDH during exercise in human skeletal muscle during hypoxia.* Am J Physiol Endocrinol Metab, 2000. **278**(3): p. E522-34.
55. Fukumura, D. and R.K. Jain, *Imaging angiogenesis and the microenvironment.* Apmis, 2008. **116**(7-8): p. 695-715.
56. Tennant, D.A., R.V. Duran, and E. Gottlieb, *Targeting metabolic transformation for cancer therapy.* Nat Rev Cancer, 2010. **10**(4): p. 267-77.
57. Liu, X., et al., *Dual mechanisms for glucose 6-phosphate inhibition of human brain hexokinase.* J Biol Chem, 1999. **274**(44): p. 31155-9.
58. Nelson, C.A., et al., *The interaction among glucose transport, hexokinase, and glucose-6-phosphatase with respect to 3H-2-deoxyglucose retention in murine tumor models.* Nucl Med Biol, 1996. **23**(4): p. 533-41.
59. Ben Sahra, I., et al., *Targeting cancer cell metabolism: the combination of metformin and 2-deoxyglucose induces p53-dependent apoptosis in prostate cancer cells.* Cancer Res, 2010. **70**(6): p. 2465-75.

60. Singh, D., et al., *Optimizing cancer radiotherapy with 2-deoxy-d-glucose dose escalation studies in patients with glioblastoma multiforme.* Strahlenther Onkol, 2005. **181**(8): p. 507-14.
61. Gupta, S., et al., *Enhancement of radiation and chemotherapeutic drug responses by 2-deoxy-D-glucose in animal tumors.* J Cancer Res Ther, 2009. **5 Suppl 1**: p. S16-20.
62. Hutton, J.C. and R.M. O'Brien, *Glucose-6-phosphatase catalytic subunit gene family.* J Biol Chem, 2009. **284**(43): p. 29241-5.
63. Ghosh, A., et al., *Brain contains a functional glucose-6-phosphatase complex capable of endogenous glucose production.* J Biol Chem, 2005. **280**(12): p. 11114-9.
64. Belkaid, A., et al., *The chemopreventive properties of chlorogenic acid reveal a potential new role for the microsomal glucose-6-phosphate translocase in brain tumor progression.* Cancer Cell Int, 2006. **6**: p. 7.
65. Visted, T., et al., *Mechanisms of tumor cell invasion and angiogenesis in the central nervous system.* Front Biosci, 2003. **8**: p. e289-304.
66. Denysenko, T., et al., *Glioblastoma cancer stem cells: heterogeneity, microenvironment and related therapeutic strategies.* Cell Biochem Funct, 2010. **28**(5): p. 343-51.
67. Chinot, O.L., et al., *Correlation between O6-methylguanine-DNA methyltransferase and survival in inoperable newly diagnosed glioblastoma patients treated with neoadjuvant temozolomide.* J Clin Oncol, 2007. **25**(12): p. 1470-5.
68. Hegi, M.E., et al., *MGMT gene silencing and benefit from temozolomide in glioblastoma.* N Engl J Med, 2005. **352**(10): p. 997-1003.
69. Cao, V.T., et al., *The correlation and prognostic significance of MGMT promoter methylation and MGMT protein in glioblastomas.* Neurosurgery, 2009. **65**(5): p. 866-75; discussion 875.
70. Amberger-Murphy, V., *Hypoxia helps glioma to fight therapy.* Curr Cancer Drug Targets, 2009. **9**(3): p. 381-90.
71. Li, Z., et al., *Hypoxia-inducible factors regulate tumorigenic capacity of glioma stem cells.* Cancer Cell, 2009. **15**(6): p. 501-13.
72. Soeda, A., et al., *Hypoxia promotes expansion of the CD133-positive glioma stem cells through activation of HIF-1alpha.* Oncogene, 2009. **28**(45): p. 3949-59.
73. Calabrese, C., et al., *A perivascular niche for brain tumor stem cells.* Cancer Cell, 2007. **11**(1): p. 69-82.
74. Piccirillo, S.G., et al., *Distinct pools of cancer stem-like cells coexist within human glioblastomas and display different tumorigenicity and independent genomic evolution.* Oncogene, 2009. **28**(15): p. 1807-11.
75. Rieske, P., et al., *Arrested neural and advanced mesenchymal differentiation of glioblastoma cells-comparative study with neural progenitors.* BMC Cancer, 2009. **9**: p. 54.
76. Chaichana, K.L., et al., *Intra-operatively obtained human tissue: protocols and techniques for the study of neural stem cells.* J Neurosci Methods, 2009. **180**(1): p. 116-25.
77. Ljungkvist, A.S., et al., *Dynamics of tumor hypoxia measured with bioreductive hypoxic cell markers.* Radiat Res, 2007. **167**(2): p. 127-45.
78. Berridge, M.V. and A.S. Tan, *Characterization of the cellular reduction of 3-(4,5-dimethylthiazol-2-yl)-2,5-diphenyltetrazolium bromide (MTT): subcellular localization,*

substrate dependence, and involvement of mitochondrial electron transport in MTT reduction. Arch Biochem Biophys, 1993. **303**(2): p. 474-82.
79. McFate, T., et al., *Pyruvate dehydrogenase complex activity controls metabolic and malignant phenotype in cancer cells.* J Biol Chem, 2008. **283**(33): p. 22700-8.
80. Lenaz, G., *The mitochondrial production of reactive oxygen species: mechanisms and implications in human pathology.* IUBMB Life, 2001. **52**(3-5): p. 159-64.
81. Staab, A., et al., *Modulation of glucose metabolism inhibits hypoxic accumulation of hypoxia-inducible factor-1alpha (HIF-1alpha).* Strahlenther Onkol, 2007. **183**(7): p. 366-73.
82. Taylor, C.T., *Mitochondria and cellular oxygen sensing in the HIF pathway.* Biochem J, 2008. **409**(1): p. 19-26.
83. Kang, G.S., et al., *Effect of metal ions on HIF-1alpha and Fe homeostasis in human A549 cells.* Mutat Res, 2006. **610**(1-2): p. 48-55.
84. Xu, K., et al., *Silencing of HIF-1alpha suppresses tumorigenicity of renal cell carcinoma through induction of apoptosis.* Cancer Gene Ther, 2010. **17**(3): p. 212-22.
85. Gillespie, D.L., et al., *Silencing of hypoxia inducible factor-1alpha by RNA interference attenuates human glioma cell growth in vivo.* Clin Cancer Res, 2007. **13**(8): p. 2441-8.
86. Oliver, F.J., et al., *Importance of poly(ADP-ribose) polymerase and its cleavage in apoptosis. Lesson from an uncleavable mutant.* J Biol Chem, 1998. **273**(50): p. 33533-9.
87. Gartel, A.L., *p21(WAF1/CIP1) and cancer: a shifting paradigm?* Biofactors, 2009. **35**(2): p. 161-4.
88. Kang, M.K. and S.K. Kang, *Tumorigenesis of chemotherapeutic drug-resistant cancer stem-like cells in brain glioma.* Stem Cells Dev, 2007. **16**(5): p. 837-47.
89. Pilkington, G.J., *The paradox of neoplastic glial cell invasion of the brain and apparent metastatic failure.* Anticancer Res, 1997. **17**(6B): p. 4103-5.
90. Yong, V.W., et al., *Metalloproteinases in biology and pathology of the nervous system.* Nat Rev Neurosci, 2001. **2**(7): p. 502-11.
91. Pessin, J.E. and G.I. Bell, *Mammalian facilitative glucose transporter family: structure and molecular regulation.* Annu Rev Physiol, 1992. **54**: p. 911-30.
92. Warburg, O., *On the origin of cancer cells.* Science, 1956. **123**(3191): p. 309-14.
93. Currie, J.C., et al., *MT1-MMP down-regulates the glucose 6-phosphate transporter expression in marrow stromal cells: a molecular link between pro-MMP-2 activation, chemotaxis, and cell survival.* J Biol Chem, 2007. **282**(11): p. 8142-9.
94. Belkaid, A., et al., *Necrosis induction in glioblastoma cells reveals a new "bioswitch" function for the MT1-MMP/G6PT signaling axis in proMMP-2 activation versus cell death decision.* Neoplasia, 2007. **9**(4): p. 332-40.
95. Belkaid, A., et al., *Silencing of the human microsomal glucose-6-phosphate translocase induces glioma cell death: potential new anticancer target for curcumin.* FEBS Lett, 2006. **580**(15): p. 3746-52.
96. Lord-Dufour, S., et al., *Evidence for transcriptional regulation of the glucose-6-phosphate transporter by HIF-1alpha: Targeting G6PT with mumbaistatin analogs in hypoxic mesenchymal stromal cells.* Stem Cells, 2009. **27**(3): p. 489-97.
97. Lambert, J.D., et al., *Inhibition of carcinogenesis by polyphenols: evidence from laboratory investigations.* Am J Clin Nutr, 2005. **81**(1 Suppl): p. 284S-291S.
98. Herling, A.W., et al., *Pharmacodynamic profile of a novel inhibitor of the hepatic glucose-6-phosphatase system.* Am J Physiol, 1998. **274**(6 Pt 1): p. G1087-93.

99. van Dijk, T.H., et al., *Acute inhibition of hepatic glucose-6-phosphatase does not affect gluconeogenesis but directs gluconeogenic flux toward glycogen in fasted rats. A pharmacological study with the chlorogenic acid derivative S4048.* J Biol Chem, 2001. **276**(28): p. 25727-35.
100. Livingstone, M., et al., *Mechanisms governing the control of mRNA translation.* Phys Biol, 2010. **7**(2): p. 021001.
101. Hynes, R.O., *Integrins: versatility, modulation, and signaling in cell adhesion.* Cell, 1992. **69**(1): p. 11-25.
102. Fincham, V.J. and M.C. Frame, *The catalytic activity of Src is dispensable for translocation to focal adhesions but controls the turnover of these structures during cell motility.* Embo J, 1998. **17**(1): p. 81-92.
103. Datta, A., F. Huber, and D. Boettiger, *Phosphorylation of beta3 integrin controls ligand binding strength.* J Biol Chem, 2002. **277**(6): p. 3943-9.
104. Johansson, M.W., et al., *Altered localization and cytoplasmic domain-binding properties of tyrosine-phosphorylated beta 1 integrin.* J Cell Biol, 1994. **126**(5): p. 1299-309.
105. Merkle, F.T. and A. Alvarez-Buylla, *Neural stem cells in mammalian development.* Curr Opin Cell Biol, 2006. **18**(6): p. 704-9.
106. Riquelme, P.A., E. Drapeau, and F. Doetsch, *Brain micro-ecologies: neural stem cell niches in the adult mammalian brain.* Philos Trans R Soc Lond B Biol Sci, 2008. **363**(1489): p. 123-37.
107. Johnson, M.A., J.L. Ables, and A.J. Eisch, *Cell-intrinsic signals that regulate adult neurogenesis in vivo: insights from inducible approaches.* BMB Rep, 2009. **42**(5): p. 245-59.
108. Brown, J.P., et al., *Transient expression of doublecortin during adult neurogenesis.* J Comp Neurol, 2003. **467**(1): p. 1-10.
109. Glass, R., et al., *Glioblastoma-induced attraction of endogenous neural precursor cells is associated with improved survival.* J Neurosci, 2005. **25**(10): p. 2637-46.
110. Marin-Hernandez, A., et al., *HIF-1alpha modulates energy metabolism in cancer cells by inducing over-expression of specific glycolytic isoforms.* Mini Rev Med Chem, 2009. **9**(9): p. 1084-101.
111. Liao, S.Y., M.I. Lerman, and E.J. Stanbridge, *Expression of transmembrane carbonic anhydrases, CAIX and CAXII, in human development.* BMC Dev Biol, 2009. **9**: p. 22.
112. Rempel, S.A., et al., *SPARC: a signal of astrocytic neoplastic transformation and reactive response in human primary and xenograft gliomas.* J Neuropathol Exp Neurol, 1998. **57**(12): p. 1112-21.
113. Perrin, J.S., et al., *Glial vascular endothelial growth factor overexpression in rat brainstem under tolerable hypoxia: evidence for a central chemosensitivity.* J Neurosci Res, 2009. **87**(1): p. 79-85.
114. Nakashima, K., et al., *Astrocyte differentiation mediated by LIF in cooperation with BMP2.* FEBS Lett, 1999. **457**(1): p. 43-6.
115. Galli, R., et al., *Isolation and characterization of tumorigenic, stem-like neural precursors from human glioblastoma.* Cancer Res, 2004. **64**(19): p. 7011-21.
116. Yuan, X., et al., *Isolation of cancer stem cells from adult glioblastoma multiforme.* Oncogene, 2004. **23**(58): p. 9392-400.
117. Fu, J., et al., *Glioblastoma stem cells resistant to temozolomide-induced autophagy.* Chin Med J (Engl), 2009. **122**(11): p. 1255-9.

118. McCord, A.M., et al., *CD133+ glioblastoma stem-like cells are radiosensitive with a defective DNA damage response compared with established cell lines.* Clin Cancer Res, 2009. **15**(16): p. 5145-53.
119. Panchision, D.M., et al., *Optimized flow cytometric analysis of central nervous system tissue reveals novel functional relationships among cells expressing CD133, CD15, and CD24.* Stem Cells, 2007. **25**(6): p. 1560-70.
120. Schold, S.C., Jr., et al., *O6-benzylguanine suppression of O6-alkylguanine-DNA alkyltransferase in anaplastic gliomas.* Neuro Oncol, 2004. **6**(1): p. 28-32.
121. Spiro, T.P., et al., *O6-benzylguanine: a clinical trial establishing the biochemical modulatory dose in tumor tissue for alkyltransferase-directed DNA repair.* Cancer Res, 1999. **59**(10): p. 2402-10.
122. Singh, S.K., et al., *Identification of a cancer stem cell in human brain tumors.* Cancer Res, 2003. **63**(18): p. 5821-8.
123. Diabira, S. and X. Morandi, *Gliomagenesis and neural stem cells: Key role of hypoxia and concept of tumor "neo-niche".* Med Hypotheses, 2008. **70**(1): p. 96-104.
124. Pistollato, F., et al., *Intratumoral hypoxic gradient drives stem cells distribution and MGMT expression in glioblastoma.* Stem Cells, 2010. **28**(5): p. 851-62.
125. Parsons, D.W., et al., *An integrated genomic analysis of human glioblastoma multiforme.* Science, 2008. **321**(5897): p. 1807-12.
126. Pollard, P.J. and P.J. Ratcliffe, *Cancer. Puzzling patterns of predisposition.* Science, 2009. **324**(5924): p. 192-4.
127. Zhao, S., et al., *Glioma-derived mutations in IDH1 dominantly inhibit IDH1 catalytic activity and induce HIF-1alpha.* Science, 2009. **324**(5924): p. 261-5.
128. Aft, R.L., et al., *Enhancing targeted radiotherapy by copper(II)diacetyl- bis(N4-methylthiosemicarbazone) using 2-deoxy-D-glucose.* Cancer Res, 2003. **63**(17): p. 5496-504.
129. Maher, J.C., et al., *Hypoxia-inducible factor-1 confers resistance to the glycolytic inhibitor 2-deoxy-D-glucose.* Mol Cancer Ther, 2007. **6**(2): p. 732-41.
130. Dearling, J.L., et al., *Combining radioimmunotherapy with antihypoxia therapy 2-deoxy-D-glucose results in reduction of therapeutic efficacy.* Clin Cancer Res, 2007. **13**(6): p. 1903-10.
131. Bell, E.L., et al., *The Qo site of the mitochondrial complex III is required for the transduction of hypoxic signaling via reactive oxygen species production.* J Cell Biol, 2007. **177**(6): p. 1029-36.
132. Chandel, N.S., et al., *Reactive oxygen species generated at mitochondrial complex III stabilize hypoxia-inducible factor-1alpha during hypoxia: a mechanism of O2 sensing.* J Biol Chem, 2000. **275**(33): p. 25130-8.
133. Dalgard, C.L., et al., *Endogenous 2-oxoacids differentially regulate expression of oxygen sensors.* Biochem J, 2004. **380**(Pt 2): p. 419-24.
134. Metzen, E., et al., *Regulation of the prolyl hydroxylase domain protein 2 (phd2/egln-1) gene: identification of a functional hypoxia-responsive element.* Biochem J, 2005. **387**(Pt 3): p. 711-7.
135. Poon, E., A.L. Harris, and M. Ashcroft, *Targeting the hypoxia-inducible factor (HIF) pathway in cancer.* Expert Rev Mol Med, 2009. **11**: p. e26.
136. Krieg, R.C., et al., *Mitochondrial proteome: cancer-altered metabolism associated with cytochrome c oxidase subunit level variation.* Proteomics, 2004. **4**(9): p. 2789-95.

137. Moreno-Sanchez, R., et al., *Energy metabolism in tumor cells.* Febs J, 2007. **274**(6): p. 1393-418.
138. Pedersen, P.L., *Tumor mitochondria and the bioenergetics of cancer cells.* Prog Exp Tumor Res, 1978. **22**: p. 190-274.
139. Ristow, M., *Oxidative metabolism in cancer growth.* Curr Opin Clin Nutr Metab Care, 2006. **9**(4): p. 339-45.
140. Heddleston, J.M., et al., *The hypoxic microenvironment maintains glioblastoma stem cells and promotes reprogramming towards a cancer stem cell phenotype.* Cell Cycle, 2009. **8**(20): p. 3274-84.
141. Panchision, D.M., *The role of oxygen in regulating neural stem cells in development and disease.* J Cell Physiol, 2009. **220**(3): p. 562-8.
142. Schwartz, P.H., et al., *Isolation and characterization of neural progenitor cells from post-mortem human cortex.* J Neurosci Res, 2003. **74**(6): p. 838-51.
143. Jewell, U.R., et al., *Induction of HIF-1alpha in response to hypoxia is instantaneous.* Faseb J, 2001. **15**(7): p. 1312-4.
144. Viola, G., et al., *Induction of apoptosis by photoexcited tetracyclic compounds derivatives of benzo[b]thiophenes and pyridines.* J Photochem Photobiol B, 2006. **82**(2): p. 105-16.
145. Chow, S. and D. Hedley, *Flow cytometric determination of glutathione in clinical samples.* Cytometry, 1995. **21**(1): p. 68-71.
146. Rice, G.C., et al., *Quantitative analysis of cellular glutathione by flow cytometry utilizing monochlorobimane: some applications to radiation and drug resistance in vitro and in vivo.* Cancer Res, 1986. **46**(12 Pt 1): p. 6105-10.
147. Levine, S., et al., *Bioenergetic adaptation of individual human diaphragmatic myofibers to severe COPD.* J Appl Physiol, 2002. **92**(3): p. 1205-13.
148. Mosmann, T., *Rapid colorimetric assay for cellular growth and survival: application to proliferation and cytotoxicity assays.* J Immunol Methods, 1983. **65**(1-2): p. 55-63.
149. Arsham, A.M., et al., *Phosphatidylinositol 3-kinase/Akt signaling is neither required for hypoxic stabilization of HIF-1 alpha nor sufficient for HIF-1-dependent target gene transcription.* J Biol Chem, 2002. **277**(17): p. 15162-70.
150. Kim, D.H., et al., *Nanoscale cues regulate the structure and function of macroscopic cardiac tissue constructs.* Proc Natl Acad Sci U S A, 2010. **107**(2): p. 565-70.
151. Al-Hajj, M., et al., *Prospective identification of tumorigenic breast cancer cells.* Proc Natl Acad Sci U S A, 2003. **100**(7): p. 3983-8.
152. Rynkowski, M.A., et al., *A mouse model of intracerebral hemorrhage using autologous blood infusion.* Nat Protoc, 2008. **3**(1): p. 122-8.